Physics – Uspekhi **49** (2) 117 – 166 (2006)

REVIEWS OF TOPICAL PROBLEMS PACS numbers: **34.50. – s**, **36.40. – c**, 43.25.Cb, 79.20.Rf, **81.15. – z**

Extreme processes in clusters impacting on a solid surface

G N Makarov

DOI: 10.1070/PU2006v049n02ABEH004666

Contents

Abstract. A large high-energy cluster impacting on a solid surface (the number of particles in a cluster $N \geqslant 10^2 - 10^6$, the collision energy per particle $E_{col} \geqslant 10 - 10^3$ eV) forms for a short time ($\leqslant 50 - 500$ fs) a medium characterized by extremely high temperature ($\geqslant 10^4 - 10^5$ K), density (up to 4 to 5 times the solid state value), and pressure ($\geqslant 1 - 10$ Mbar). As this takes place, the cluster heating rate reaches the value $\geqslant 10^{15} - 10^{16}$ K s^{-1}. In these extreme conditions, physical and chemical processes that are impossible in thermal equilibrium can occur both in the cluster itself and the collision zone. In this paper, extreme processes induced in clusters as a result of their strong excitation at collisions with a solid surface are reviewed, including ionization, light and charged-particle emission, fragmentation, breaking and making of chemical bonds, microshock wave generation, nuclear fusion, and surface bombardment. Conditions for these processes to proceed are examined and models to describe them discussed. It is shown that the characteristics of the processes depend significantly on the velocity, size, and composition of the cluster, as well as the material and temperature of the surface. Cluster excitation by an impact with a surface and that by a superhigh-power ultrashort laser pulse are compared and practical applications of the above processes are discussed.

G N Makarov Institute of Spectroscopy, Russian Academy of Sciences, 142190 Troitsk, Moscow Region, Russian Federation
Tel. (7-495) 334 02 32
E-mail: gmakarov@isan.troitsk.ru

Received 29 March 2005, revised 21 June 2005
Uspekhi Fizicheskikh Nauk **176** (2) 121 – 174 (2006)
Translated by Yu V Morozov; edited by A Radzig

1. Introduction

Cluster beam studies constitute a most rapidly developing area of physical and chemical research (see, for instance, monographs and collected works [1 – 23] and reviews [24 – 69]). Clusters attract the attention of researchers most of all because they make up an intermediate link between isolated elementary particles (atoms and molecules) and bulky liquids or solids. Clusters are frequently called 'a new phase of matter' [1] since they display, due to the discrete structure of their energy levels and the large surface/volume ratio, novel characteristic properties distinguishing them from both their constituent particles and bulky matter. It is therefore expected that investigations into cluster structure and dynamics will make it possible to establish a minimal number of particles in a cluster at which the physical properties of a bulky substance begin to manifest themselves. It should be noted that in certain cases the threshold number of particles from which a cluster starts to exhibit certain characteristics of a macroscopic substance is already known. For example, it

has been shown that superfluidity in helium nanodroplets (clusters) [70] becomes apparent when the number of particles in a cluster amounts to $N \geqslant 60-100$ [65, 69, 71–76]. However, the threshold is arbitrary in the majority of cases because various properties of a liquid or a solid begin to emerge at different numbers of particles in a given cluster.

The rapid development of cluster science during the last decade has given rise to a few new interesting and practically important lines of inquiry, such as the excitation of large clusters by superhigh-power ultrashort laser pulses [77–83] and the employment of this excitation for the generation of X-rays [84–92] and neutrons [93–97]; the interaction of high-energy clusters and cluster ions between themselves [98, 99] and with solid surfaces [46], and its exploitation for nuclear fusion [100–109] and the initiation of chemical reactions [110–129], as well as the use of cluster beams for the thin-film deposition [10, 130–164], production of new materials [149–168], and surface treatment [169–187]. Studies of fullerenes, i.e., carbon clusters with a closed structure [14, 20, 34, 37, 48–51], and carbon nanotubes [19, 43, 52, 60] also have very important implications. It is worthwhile to note that a group of researchers (R E Smalley, R F Curl, and H Kroto) were awarded the Nobel Prize in Chemistry 1996 for their work on the preparation and investigation of fullerenes [48–50].

Many areas of current cluster research are highlighted in monographs and reviews (see Refs [1–69]). Some early review articles were concerned with processes of gas condensation and production of cluster beams [27–30], the structure and dynamics of small complexes weakly bound by van der Waals forces [26, 30, 31, 33, 35, 36, 39], and metal clusters [25, 32]. Paper [38] discusses the energy structure and quantum effects in large semiconducting clusters (semiconductor nanocrystals). The structure, energetics, and dynamics of clusters and cluster ions are considered in Ref. [40]. A number of reviews are devoted to fullerenes [14, 20, 34, 37, 51] (see also Refs [48–50]), carbon [14, 19, 20, 34, 37, 51] and carbon nanotube [19, 43, 52, 60] structures. Others are concerned with the employment of cluster beams (as targets) for proton-scattering experiments in high-energy physics [45]. Reference [42] (see also Refs [46, 47]) discusses the application of clusters in femtochemistry. Review papers [53–59] are devoted to problems related to cluster beam excitation by superhigh-power ultrashort laser pulses and to the use of laser excitation of clusters for the generation of X-rays and neutrons. Recent reviews [61–69] consider the structure and properties of superfluid helium nanodroplets (clusters), as well as spectroscopic studies of single molecules and clusters introduced into helium droplets [63–65, 68, 69]. The present communication is first and foremost focused on the especially interesting and important (in the author's opinion) results of studies dealing with the processes that take place during collisions of high-energy clusters and cluster ions with solid surfaces. It should be emphasized from the very beginning that the author does not pretend to comprehensively review all the results of these studies. It is practically impossible to consider and analyze in a single paper all publications on the problem of interest because their number amounts to several hundred and continues to increase rapidly.

This review deals mostly with the processes that occur when a solid surface is impinged by clusters formed with the aid of weak ($\cong 0.1-0.2$ eV) van der Waals or stronger ($\cong 0.3-0.6$ eV) hydrogen bonds. At the same time, it concerns some processes proceeding as clusters and cluster ions of metals and carbon characterized by a rather strong ($\cong 1-10$ eV) coupling hit a surface. All the aforesaid clusters differ widely in the type, structure, and strength of their bonds, as well as in their physical and chemical properties [1, 56]. A common feature of the above processes, essential in the context of the present review, is the strong heating of clusters that hit a surface with a collision energy much higher than the cluster binding energy. In accordance with the definition of clusters proposed in the monograph [1] (see Section 2.1), all the aforementioned aggregate varieties should be regarded as such.

When high-energy clusters hit a solid surface, both the clusters themselves and the material of the surface in the impact area undergo strong excitation. Such excitation is due to the transfer of the cluster translational energy to the internal degrees of freedom and surface atoms. This has the effect of inducing a number of physico-chemical processes proceeding under extreme conditions. These processes include ionization of atoms and molecules [188–197], emission of charged particles [198–215], cluster fragmentation [119, 120, 216–235], breakdown and making of chemical bonds [110–129], initiation of reactions with high energy barriers [121–129], generation of microshock waves [118, 236, 237], nuclear fusion [100–109], light emission [238], film deposition [10, 130–166], formation of nanostructures with specific properties [149–168], and surface bombardment [169–187]. It is these processes that are the focus of the present review. At the same time, the results of solid surface–cluster beam collision studies at a moderate (thermal) energy are touched on. These data provide a basis for the investigation into high-energy collisions of clusters and cluster ions with a surface and help to better understand processes that occur at high-energy collisions.

The outline of the review is as follows. Section 2 contains a brief discussion of the methods used for the production of clusters and cluster beams, such as aggregation of gases, surface erosion, sputtering of target materials, laser ablation, pulsed arc discharges, and cluster aggregation. Further attention is given to methods for producing cluster beams during supersonic expansion of gas in its outflow from the nozzle and the laser-assisted generation of metallic clusters. It is these methods of cluster beam production that are most frequently employed at present and referred to in the majority of works cited in this review. Section 3 provides a brief analysis of methods for the detection and investigation of cluster beams. They include mass spectrometry, electron impact-induced fluorescence, electron diffraction, light and particle scattering, as well as laser-bolometric and pyroelectric techniques. In other words, Sections 2 and 3 are designed to give an idea of the methods for the production and investigation of cluster beams and may be helpful in reading the subsequent sections.

Section 4 is an overview of data obtained in the studies of interactions between cluster beams and a surface at moderate (thermal) collision energies. Reviewed in this section are the results of early experiments on the reflection of cluster beams from a solid surface with special reference to cluster beam focusing. It is shown that cluster scattering from a surface is essentially different from monomer scattering. Cluster scattering data are provided depending on the velocity and cluster size, angles of cluster beam incidence on a surface, and surface temperature. Clusters reflected from a surface are shown to undergo acceleration resulting from the recoil effect due to evaporation. Cluster scattering from a heated surface is found to be similar to the Leidenfrost effect. The results of

experiments on van der Waals cluster scattering from a surface is considered along with the binary collision model proposed for the description of this process. Also, the results of studies on the evaporation of small fragments in the course of argon cluster scattering from a graphite surface and the thermokinetic model describing this scattering channel are discussed. And the results of an investigation into tangential angle scattering of large fragments and the dynamic model of zone structure, governing this scattering channel, are analyzed as well. Finally, the section deals with diffuse scattering of atoms upon collision between van der Waals clusters and a surface, and also with experiments and model calculations of the ionization of water clusters impinging upon a solid surface.

Section 5, the central one in this review, is designed to discuss the results of studies on the processes induced by high-energy cluster beam – solid surface collisions (including those of cluster ion beams). This section considers experimental findings and model calculations of electron emission, cluster fragmentation, molecular dissociation, and initiation of chemical reactions with high energy barriers, such as the 'air burning' reaction. The results of model calculations of the generation of microshock waves in clusters upon their impact on a surface at supersonic and hypersonic speeds are provided together with the results of experimental and theoretical studies on deuterium nuclear fusion and neutron generation. The section analyzes results of an investigation into light emission in the near-IR and visible spectral regions upon collisions of clusters composed of unlike atoms with a solid surface. Also presented are the data on the employment of cluster beams for the deposition of thin films, the production of new materials, and the treatment of surfaces.

Section 6 is devoted to the process of cluster excitation by superhigh-power ultrashort laser pulses. The purpose of the brief discussion included in this section is to compare the results of cluster excitation upon collision with a surface (presented in Section 5) with the data on cluster excitation by laser pulses. It is shown that the processes of cluster excitation by these two methods have much in common despite some essential differences. Finally, the concluding Section 7 summarizes the main results of the studies discussed in the present review, with special emphasis on the most important achievements and promising lines of further investigations.

2. Production of clusters and cluster beams

2.1 General remarks and brief review of methods

Under clusters are meant aggregates composed of more than one to a few millions of atoms or molecules kept together by different types of bonds with binding energies ranging from a few tenths of an electron-volt to several electron-volts [1]. Today, there are many techniques available to produce clusters. A detailed review of the methods intended for the production of clusters and cluster beams can be found, for instance, in the wonderful book by Pauly [1] and in a number of review articles [24, 30, 56, 239 – 242]. It was not our purpose to consider at length all the existing methods. Therefore, only a few general remarks are in order here concerning the currently used techniques, with a bit more detailed discussion of the methods for the production of cluster beams during gasdynamic expansion in nozzle sources and the laser-assisted generation of metallic clusters.

In the conditions of thermodynamic equilibrium, a gas or a vapor always contains a certain fraction of clusters (largely of small size) for the most part in the form of dimers. The relative number of larger clusters exponentially decreases as their size increases, provided the binding energy in the cluster is a monotonic function of its size. The simplest way to obtain cluster beams boils down to employing effusion sources because thermodynamic equilibrium of the gas remains undisturbed in effusive molecular beams (if the Knudsen condition is fulfilled [24, 30]). However, the cluster fraction in such beams is insignificant, and the size of the clusters is usually small. Meanwhile, many experiments require intense cluster beams and large-sized clusters to be used. As a result, additional methods have been developed to meet these requirements. Classification of the currently available methods for the production of cluster beams is arbitrary because a combination of various techniques is sometimes needed, depending on the purpose of the study. Nevertheless, cluster sources can be subdivided into several classes [1]. The most frequently employed methods for the production of clusters are based on using supersonic gasdynamic jets, aggregation of gases, surface erosion, sputtering, laser ablation, and pulsed arc discharges [1, 30, 56].

Gas aggregation. With this technique, a solid or liquid material is evaporated to produce a cold gas residing in a steady state or in a flux. The atoms or molecules are cooled due to collisions with the cool gas. This process results in gas condensation and cluster formation [243]. It makes the process of cluster formation analogous to the formation of smoke, clouds, or fog as they occur in nature. Gas aggregation sources are frequently called 'smoke sources' [1]. Evaporation of a condensed substance is performed either in ovens or in an arc discharge initiated in a noble gas. The latter technique was successfully employed to obtain for the first time macroscopic amounts of C_{60} molecules [244]. Pulsed discharges can also be used for the same purpose.

The process of gas aggregation usually produces clusters of a large size ($N \leqslant 10{,}000$). The size of the clusters is determined by the conditions of aggregation, such as time, gas pressure, temperature, and rate of the cooling gas flow. The cluster size varies in rather a broad range depending on the aggregation conditions. The intensities of the resulting cluster beams turn out to be significantly lower than those of supersonically produced ones. It is possible, however, to obtain clusters characterized by a rather low temperature ($T < 100$ K). A large number of collisions with the cooling gas accounts for a highly irregular translational velocity of the clusters that, in turn, is responsible for the different velocity distributions of clusters having dissimilar masses.

Surface erosion. With this method, atoms or molecules are removed from the surface of a solid or liquid as it is bombarded by heavy ions or after its exposure to intense laser radiation (laser ablation), a pulsed arc discharge, or a high-voltage electric field.

Sputtering. This method is based on the fact that heavy ions possessing a rather high energy hit a solid target that may be a gas, either solid or frozen, or a liquid. High-energy ion – surface collisions induce an ejection of atoms, molecules, or clusters from the surface [245] (see also Section 5.7). The clusters thus formed are usually of a small size and their temperature is close to the evaporation temperature of the target material. Moreover, the resultant clusters are characterized by energy distribution over a wide enough range (roughly up to 10 eV).

Laser ablation. In this method, intense radiation of a pulse laser is focused on a target and causes evaporation of several atomic layers of its material. Hot plasma produced in the laser focus expands and gives rise to the formation of clusters containing up to a few hundred particles [246]. The temperature of the clusters depends on the expansion conditions and may be roughly equal to the temperature of the source. The laser ablation technique can be easily combined with the gas aggregation method in order to improve the reproducibility of the cluster formation process, increase the size of the clusters obtained, and decrease their temperature [247].

Pulsed arc discharges. This method is based on the evaporation of particles from the surface of an electrode under the effect of a pulsed arc discharge (instead of laser radiation). It largely produces ionized clusters. Intense cluster beams can be obtained by combining this technique with gas aggregation.

Clusters can also be produced using liquid-metal ion sources [1, 30, 56] in which particles are emitted from the tip wetted in a liquid metal under the effect of an electric field. Tips are usually made of a refractory material [248].

Worthy of note are two other methods of cluster production: laser-induced pyrolysis successfully used to produce clusters of refractory materials [249, 250], and atomic diffusion through a foil [251] (see also Ref. [1]).

Aggregation of clusters. The recently developed cluster aggregation technique is based on the conversion of noble gas clusters to metal clusters by capturing atoms of a metal by large clusters of inert gases [252]. This method is successfully used at present to obtain molecular or atomic clusters inside or at the surface of superfluid helium nanodroplets (clusters) (see, for instance, publications [63 – 65, 68, 69] and references cited therein). The capture of atoms and molecules by large clusters of inert gases (the pick-up technique [253]) is also successfully employed for the production of mixed clusters (see, for instance, Refs [254, 255]).

2.2 Production of cluster beams in nozzle sources

The cluster science has its origin in the early studies of colloids, aerosols, and fogs, carried out in the second half of the 19th century [256 – 258] (see also the paper [40] and references cited therein). Extensive cluster studies began in the middle of the 20th century with the advent of molecular and cluster beams [259, 260]. In 1956, Becker, Bier and Henkes [261] reported intense condensation in supersonic jets formed during gasdynamic expansion of a gas passing through a small nozzle. Although the phenomenon of gas condensation in expanding jets had been described much earlier [262], the beginning of a new phase in cluster studies came in the year 1961 when Bentley [263] and Henkes [264] independently observed the generation of CO_2 clusters in gasdynamic jets using a mass spectrometer. Since that time, the combination of cluster beams and mass spectrometers has been playing a very important role in the investigation of clusters.

Today, the homogeneous condensation of a gas as it expands in its outflow from a nozzle is the most widespread method of cluster production [1 – 3, 24, 28 – 30]. The gas initially at rest above the nozzle at temperature T_0 and pressure p_0 expands when outflowing through the nozzle opening into a vacuum chamber. The expanding gas accelerates in the process and cools down adiabatically. Cooling causes oversaturation of the gas which, in turn, initiates cluster growth. As a result, the jet carries a mixture of clusters and the gas (uncondensed particles).

A gas flux is proportional to $p_0 d^2 T_0^{-1/2}$, where d is the diameter of the nozzle opening, and p_0 and T_0 are the gas pressure and temperature above the nozzle, respectively. Cluster-producing facilities usually have a nozzle diameter from 5 – 10 to 200 μm, and a gas pressure from 1 to 50 – 60 atmospheres. Pulsed nozzles have an opening diameter from 0.1 to 2 mm. In the ideal gas approximation, a nozzle with the opening diameter of 50 μm at $T_0 \cong 300$ K and $p_0 \cong 2$ atm provides a gas flux of approximately 4 atm cm^3 s^{-1} ($\cong 0.16$ mmol s^{-1}) [63]. To ensure the evacuation of such a gas flux, it is necessary to utilize diffusion pumps with an evacuation rate of some 10,000 l s^{-1} for helium, and $\cong 4000$ l s^{-1} for nitrogen at the ultimate operating pressure of 3×10^{-4} Torr. The molecular (cluster) beam is isolated from the expanding jet with a skimmer placed approximately 1 – 3 cm from the nozzle. The front edges of the skimmer's walls must be as thin as possible to exclude the scattering of the beam by the skimmer. Most skimmers are fabricated by means of electrophoresis sputtering and have an entrance opening diameter of 0.5 – 2 mm.

The processes of gas condensation and cluster formation in nozzle sources are known fairly well (see, for instance, Refs [265 – 268]). Hagena and Obert [265] described the conditions for the onset of cluster formation in gas jets. Both the course of cluster formation and cluster size depend on the conditions of gas expansion in the jet [265, 267]. Hagena [265, 267] proposed characterizing the cluster formation process by a dimensionless parameter (the Hagena parameter) given by the expression

$$\Gamma^* = k \, \frac{(d \tan \alpha)^{0.85} p_0}{T_0^{2.29}} \,, \qquad (2.1)$$

where d is the diameter of the nozzle opening (in microns), α is the angle equalling half of the cone angle of the divergent part of the nozzle, p_0 is the gas pressure above the nozzle (in millibars), T_0 is the gas temperature prior to expansion, and k is a constant depending on the kind of the gas ($k \approx 2900$ for Kr, 1700 for Ar, 180 for Ne, and 4 for He [269]). The results of many studies indicate that clusters begin to form in a gas when the parameter Γ^* exceeds 300. In such a case, the mean cluster size increases in (rough) proportion to $(\Gamma^*)^{2.0-2.5}$ [265, 270]. The same results suggest that large clusters ($N > 10^4$ atoms per cluster) are produced when $\Gamma^* > 5 \times 10^4$ [269]. This parameter also shows that cluster formation is more intense in such heavy inert gases as Kr and Ar than in Ne and He. For example, at a diameter of the nozzle opening of 1 mm, the gas pressure above the nozzle of about 1.5 atm is sufficient for the formation of krypton or argon clusters in a jet at room temperature. On the other hand, helium clusters begin to form at a gas pressure in excess of 10 atmospheres. It also follows from relationship (2.1) that cluster formation depends essentially on the opening angle of the divergent part of the nozzle (see Section 2.2.1). Cluster formation can be enhanced by employing supersonic nozzles as confirmed by the studies of many gases [271]. The results of these studies indicate that Ar, Kr, Xe, and N_2 are the most suitable gases for the formation of large clusters.

2.2.1 Effect of the nozzle shape. The process of cluster formation in nozzle sources depends rather strongly on the nozzle shape. This dependence was partly evaluated in experiment [265] and also by means of numerical calculations based on the method of characteristics [272]. Figure 1

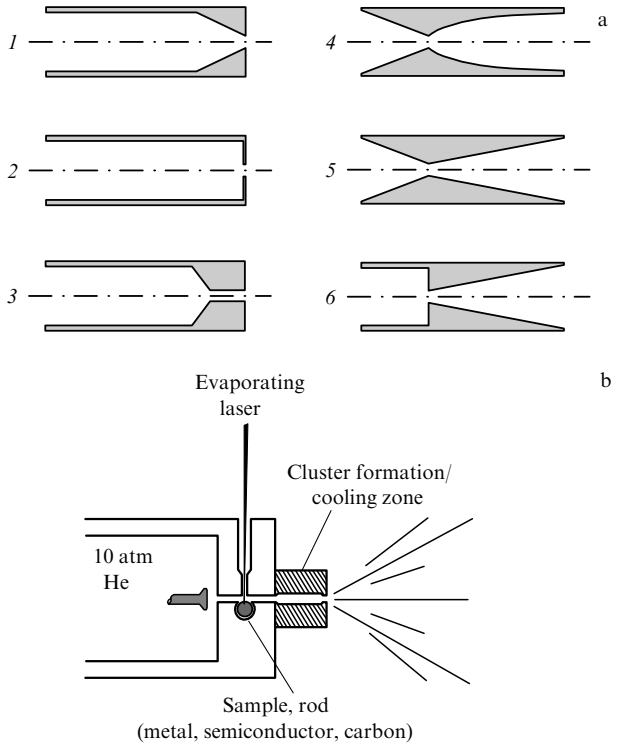

Figure 1. (a) The shapes of the nozzles utilized to produce molecular and cluster beams [1]. (b) A pulsed source for producing metallic cluster beams [290].

schematically depicts [1] variations of the nozzle shape used in different studies. Short convergent nozzles *1* are usually employed to produce free jets. Nozzles *2* and *3* have an ideal and capillary aperture, respectively. Nozzles with ideal apertures are extremely difficult to make, which accounts for a very small difference between type *2* and *3* nozzles, except for very long capillary ones. In contrast, *4*–*6* type nozzles are quite different from nozzles *1*–*3* because they have a divergent part of the nozzle that greatly facilitates cluster formation. Nozzle *4* is a Laval type nozzle, nozzle *5* also represents the convergent–divergent type, and nozzle *6* operates as a divergent one.

The probability of cluster formation in a type *2* nozzle is comparable with that in type *1* convergent nozzles; it is considerably higher in type *3* capillary nozzles because particles spend more time in the high-pressure area at the exit from the nozzle [273]. Convergent–divergent nozzles (type *5*), Laval nozzles (type *4*), and divergent nozzles (type *6*) are almost equally efficient in terms of cluster formation, as was shown in early experiments [265] and corroborated by later studies [274]. Given nozzles with identical gas pressures and opening diameters, more intense beams and larger clusters can be obtained using type *6* divergent nozzles. This can be accounted for by the fact that particles in a flux confined to the cone long remain in the expansion zone where they experience more collisions and therefore deeper cooling. The probability of cluster formation is minimal in type *1* nozzles. Such nozzles are normally used when cluster formation in a beam is undesirable [1, 30].

In order to compare cluster production in type *1* standard (sonic) nozzles or type *2* nozzles with a thin-walled aperture and that in type *5* convergent–divergent nozzles or type *6* divergent ones, the scaling parameter Γ^* needs to be taken into consideration when calculating the nozzle diameter [266]. To this end, an 'equivalent' diameter of the opening for divergent nozzles should be introduced. Under stagnation conditions being equal, a nozzle with the 'equivalent' diameter produces a flux with the same characteristics as type *1* sonic nozzles do. The equivalent diameter of the nozzle opening is given by the expression

$$d_{\mathrm{eq}} = \frac{c(\gamma)d}{\tan\alpha}\,, \tag{2.2}$$

where α is the angle equalling half the angle of the divergent part of the nozzle's cone. Constant c depends on parameter $\gamma = c_p/c_v$, i.e., the ratio between specific heats of the expanding gas. It has different values in the events of axial-symmetric and planar gas expansion. Table 1 presents a few numerical values of constant c for the case of axial-symmetric expansion. For example, the equivalent diameter of the nozzle opening at angle $\alpha = 5^\circ$ is 8.4 times the sonic nozzle opening diameter (for $\gamma = 5/3$). This means that a cone-shaped sonic nozzle provides a flux along the jet axis identical with that in a coneless nozzle under conditions when the overall gas consumption is reduced by a factor of 70 or so (because boundary effects are negligibly small).

Table 1. Constant $c(\gamma)$ values for axial-symmetric gas expansion [1].

γ	5/3	7/5	9/7
c	0.736	0.866	0.986

2.2.2 Effect of gas-carriers. The probability of cluster formation in supersonic jets can be increased by dilution of the particles under study in an inert gas-carrier. The role of atoms of the gas-carrier largely consists in cooling the growing clusters and removing the heat of condensation. In this way, the atoms protect clusters against evaporation. In case of inefficient cooling, stabilization of clusters is achieved by means of evaporation of one or several particles. Gas-carrier acts in a similar way when molecular clusters are being formed [275].

There is an optimal partial pressure of gas-carrier. At small partial pressures, the velocity of collisions between cluster's constituent particles and atoms of a gas-carrier is insufficient to ensure effective cooling of the clusters. At high partial pressures of the gas-carrier, the collision velocity between cluster's constituent particles decreases to make up for the cluster cooling effect.

Mixed clusters may form when the interaction energy between cluster's constituent particles is not significantly different from the interaction energy between cluster's constituent particles and atoms of the gas-carrier [276, 277]. It is worthwhile to note that cluster formation is also influenced by the mass of gas-carrier atoms. A heavy gas expands more slowly; hence, there is more time for aggregation. Under these conditions, formation of larger clusters is promoted (see, for instance, Refs [30, 278]).

2.3 Production of metal clusters by the laser technique

Let us consider the production of atomic and cluster beams of metals by the laser technique [279–291] which is also used to produce clusters of semiconducting materials [290, 292], carbon (including fullerenes) [49, 285, 287, 293], and cluster and atomic beams of other refractory elements [281, 292, 294], including binary cluster beams, such as $(Si_xC_{1-x})_N$ [294]. It should be recalled that this method and the physical processes

underlying it have been analyzed in much detail in a review by B M Smirnov [56]. Therefore, the fundamentals of this technique are only briefly discussed below along with the role of the most important elements of the source of a cluster beam. A few variants of pulsed laser sources are currently available for the production of cluster and atomic beams of metals and other refractory materials. All of them are based on the laser-assisted evaporation of the material of interest, followed by the formation of atomic or cluster beams from evaporated material. A sample such a material is placed in front of the nozzle channel; due to this, the atoms evaporated by laser radiation are trapped by the gas-carrier and cooled in the course of gasdynamic expansion, thus giving rise to clusters.

A source for the production of supersonic beams of metallic clusters by means of laser-assisted evaporation of the material was first developed by Smalley and colleagues [279 – 282]. Initially, it was a very simple device [282]. In the course of time, it underwent several modifications to take into account the shape of the sample chosen for material evaporation and the conditions of atomic cluster formation [49, 286, 287, 290]. Figure 1b shows a cross-sectional sketch of a pulsed source of cluster beams. In this source, high-intensity radiation of a pulsed laser is focused on a rod of the material being studied and a small amount of this substance is evaporated into the flux of an inert gas-carrier (usually helium) in which metal vapors are cooled down and condensed into clusters. The mixture thus produced is thereafter expanded into a vacuum. In this case, the heating area is confined to a small target region; hence, neither thermal shielding nor cooling is needed. Moreover, a moderately efficient pump may be used for evacuating the vacuum chamber because the gas is fed as short pulses. Sources of this type are employed in many laboratories with only slight modifications, their advantages being a simple and universal construction and the possibility of producing even clusters of a large variety of refractory materials.

In such sources, the flux of an inert gas-carrier passes through a narrow channel (usually 1 – 1.5 mm in diameter). Its pressure (in front of the valve) amounts to 10 atm, and may be as high as 1 atm within the channel. A hole drilled perpendicular to the channel serves to direct laser radiation onto the target rod. Evaporation of the sample is achieved by means of its irradiation either by eximer laser light [285, 290] or by the second harmonic of an Nd:YAG laser (at a wavelength of 532 nm) [283, 284, 287, 292, 294]. The energy of the pulse normally amounts to 30 – 50 mJ, and its duration is 5 – 50 ns. It should be recalled that the authors of Ref. [291] have demonstrated highly efficient evaporation of metallic samples (Fe, Co, Ni) irradiated by 3-μs pulses from a Ti-sapphire laser (at a wavelength of 790 nm) with an energy of 250 mJ. A laser pulse evaporates a small amount of the material ejected in the form of plasma. The plasma cloud has the following characteristics: particle velocity on the order of 10^6 cm s^{-1}, temperature $T \cong 10^4$ K, and number density $10^{18} - 10^{19}$ cm^{-3} [295]. Although a significant portion of the particle energy in the cloud is transferred to the channel walls by virtue of heat conduction through the inert gas, its quite a large part remains in the gas where it produces a relatively hot beam characterized by a sufficiently high average particle velocity. The most efficient heat insulation is normally achieved by using a long (2 – 3 cm) channel or by introducing an attachment of larger diameter placed in front of the diverging section [296, 297] (see text below).

One of the most critical elements of a source with laser-assisted evaporation of the sample is the channel connecting the source of cluster beams with the supersonic expansion area (Fig. 1b). In this channel, the plasma formed by a laser pulse recombines, hot atoms undergo thermalization and unite into clusters, and the energy released in the course of cluster formation dissipates due to collisions with the gas-carrier. Bearing in mind the importance of the shape and size of such a channel for the production of clusters, various modifications of the nozzle were tested in experiments [290].

It has been shown that the most efficient construction has an additional zone for cluster formation and cooling [49, 286, 290] (see Fig. 1b). It is frequently referred to as an integrating cup [49]. This zone is approximately 1.5 cm in length and about 0.4 cm in diameter, with the diameter of the sonic nozzle opening ranging from 0.1 to 0.25 cm. The integrating cup is usually attached at the outlet of the standard pulsed nozzle. Such a device has a number of advantages as far as cluster production is concerned. To begin with, it is a place where the portion of a helium flux containing hot plasma is mixed with the cold helium that comes to this zone from the leading part of the flux containing no hot atoms. In other words, the temperature of the gas-carrier containing metal atoms decreases in the integrating cup. Secondly, a time interval of ~ 100 μs during which this zone harbors atoms of the metal and the gas-carrier (the length of the interval being dependent on the exit diameter of the nozzle) is sufficient to maintain efficacious atomic clustering and collisions of atoms and clusters with a buffer gas. These collisions result in cooling the clusters down to room temperature. Last but not least in importance, the cluster-containing gas volume present in this zone expands each time during roughly one and the same span of time (100 – 200 μs). This makes it possible to effectively stabilize the flux pulse amplitude and substantially reduce intensity fluctuations resulting from minor changes in the velocity of the supersonic flux between successive pulses [290].

Let us now consider in more detail how such a cluster source operates (see Fig. 1b). The nozzle valve being activated, the pulsed gas flux spreads throughout a channel 1 – 1.5 mm in diameter in a time of slightly less than 1 ms and passes around the sample. At a certain instant of time that is usually in the mid-pulse of the gas flux, an evaporating laser pulse is applied and focused on the sample. The evaporated particles are entrained by the gas. In order to prevent the appearance of deep craters at the surface of the sample and ensure approximately equal conditions for substance ablation during each pulse, the sample is revolved and moved in space. It is worth noting that in certain experiments designed to obtain and study fullerenes (see, for instance, Refs [49, 286, 292, 293]), the sample was shaped as a disk rotated about the central axis. Multiphoton ionization and subsequent heating of the plasma being formed in the process limited the amount of the material evaporated during each laser pulse. A high laser pulse energy may cause plasma breakdown [56]. It is therefore necessary to use laser radiation of moderate energy. The degree of clusterization can be varied by changing the gas pressure, the instant of laser pulse feeding relative to the gas mid-pulse, and the length and geometry of the channel down the flow from the site of its evaporation; it also depends on the presence of an integrating cup.

The process of cluster formation may continue in the case of supersonic gas expansion at the exit from the nozzle to the

vacuum chamber. The temperature of gas particles in the jet falls from a value slightly higher than room temperature to a few kelvins. As the gas expands, the particles in the jet practically cease colliding with each other. Simultaneously, a narrow, sharply directed velocity distribution of particles is formed. From the jet of cold clusters being formed, a molecular (cluster) beam is extracted with the help of skimmers, to be further analyzed in a mass spectrometer.

3. Methods for the detection and investigation of cluster beams

All the above methods may be used to obtain the cluster size distributions rather than clusters of a given size. This can be attributed to the purely statistical character of the cluster formation process [1]. Clusters of a desired size are needed in both experimental studies and theoretical models, hence the importance of the development of methods for cluster beam diagnostics and cluster selection by size. At the very least, the mean cluster size in a beam and the cluster-size distribution itself must be known. The problem of separation of clusters of a given size from the beam in the general case remains to be solved despite a variety of methods available for this purpose. The most popular of them will be discussed in Section 3.5. The discussion is preceded by a review of the most widely employed methods for the diagnostics of cluster beams.

3.1 Mass-spectrometric method

The very first data on cluster-size distribution in a supersonic beam were obtained by mass-spectrometric methods [263, 264, 298–302]. This technique may be used to directly observe clusters even though it is not devoid of drawbacks. A cluster beam passes through an ion source where clusters undergo ionization either by electron impact or by photons [1]. Mass analysis of ionization products allows studying the distribution of cluster ions produced in an ion source. However, ionization is a rather complicated process. It is not confined to the parent cluster alone but also involves efficient fragmentation of clusters, depending on the energy that is added to them. As a result, the mass-spectrum displays not only peaks corresponding to the parent cluster but also those to the fragments. The latter peaks may overlap the peaks of smaller parent clusters. For this reason, the cluster-size distribution measured with the help of mass spectrometry may be substantially different from the distribution of neutral clusters in a beam.

Two factors responsible for cluster fragmentation in a beam are structural relaxation and excess energy donated to the cluster in the course of its ionization [1]. The structural relaxation takes place when the geometric structure of a given cluster in the ground state is markedly different from the geometric configuration of the corresponding cluster ion. In this situation, the cluster ion being formed has excessive vibrational energy that may be higher than its binding energy and therefore lead to its fragmentation. This mechanism plays an essential role in the fragmentation of micrometer-sized clusters regardless of the ionization mode.

Structural changes become more localized as the cluster size grows. For example, the charge of inert gas clusters is located on the dimer ion, while the energy of its formation (close to 1 eV) is released in the remaining part of the cluster via vibrational relaxation leading to the detachment of one or several atoms from the cluster [303]. In molecular clusters, the charge is initially associated with an isolated molecule in a cluster. Whether the cluster undergoes homolytic fragmentation ($M_N^+ \rightarrow M_{N-1}^+ + M$) or ion-molecular reactions depends on the energy related to structural changes in the cluster. Ionization-induced structural changes are usually unessential for clusters of metal atoms having completely delocalized conduction electrons and poorly defined geometry. This accounts for their weak fragmentation during ionization. The same is true of noble gas micrometer-sized clusters doped with aromatic molecules.

The fragmentation of large clusters for which evaporation of a small number of constituent atoms is of little consequence depends on the excess energy added to a cluster in the course of its ionization. The smaller the excess energy, the lower the fragmentation intensity. Such a reduction is, however, difficult to achieve when cluster ionization is induced by electron impact because spatial charge effects at low accelerating voltages allow only high-intensity electron beams to be obtained. Hence, there occurs strong cluster fragmentation. Nevertheless, in the event of cluster ionization by laser light, it is possible to work near the ionization threshold by selecting a proper radiation wavelength. Then, the measured cluster-size distribution corresponds (for large clusters) to the distribution in a neutral beam. As this takes place, the radiation power must be low, otherwise, intense fragmentation may be due to multiphoton processes or consecutive absorption of several photons.

3.2 Electron beam-induced fluorescence

In this method, frequently referred to as EBIF (electron beam-induced fluorescence) [304, 305], cluster molecules or atoms are excited into upper electronic states by an electron impact. The thus excited particles then fluoresce into lower electronic states. At electron energies in excess of 1 keV, the cross section for dipole interactions is much larger than that for multiplet interactions, which accounts for the predominance of dipole-allowed transitions. The information about the initial distribution of molecules over quantum states is possible to derive from the fluorescence spectrum, given that the transition probabilities to excited states, as well as the transition probabilities to lower states, are known. The electron beam-induced fluorescence technique is essentially different from laser-induced fluorescence (LIF) [306–309] in that the initial excitation is not selective with respect to the radiation wavelength. This significantly complicates the interpretation of fluorescence spectra due to the existence of several molecular excitation channels into a certain quantum state. Nonetheless, this method is successfully employed for the investigation of molecular and cluster beams (see, for instance, Refs [304, 305, 310]).

3.3 Diffraction of electrons

The electron diffraction method leans upon well-collimated electron beams (about 100 μm in diameter in the scattering plane) having an energy on the order of 50 keV, and an electron current of several microampers [1]. The electrons that cross a cluster beam at the right angles produce a diffraction pattern recorded on photographic film. In the simplest case of electron scattering from a single atom, the amplitude of the scattered signal is given (see, for instance, Ref. [311]) by the expression

$$A_s = A_0 \frac{2me^2}{\hbar^2 q^2} \left[Z - F(q) \right], \tag{3.1}$$

where m and e are the electron rest mass and charge, respectively, A_0 is the incident wave amplitude, $\hbar = h/2\pi$ is the Planck constant, Z is the nucleus charge, and $F(q)$ is the electron density form-factor that describes shielding of the nucleus by the atomic electron cloud. Quantity q can be expressed through the scattering angle:

$$q = 2k \sin \frac{\theta}{2}\,, \tag{3.2}$$

where $k = 2\pi/\lambda$ is the wave number, and λ is the de Broglie electron wavelength. By virtue of factor $1/q^4$, the differential absorption cross section

$$\frac{\mathrm{d}\sigma}{\mathrm{d}\omega} = \frac{4m^2e^2}{\hbar^4 q^4}\left[Z - F(q)\right]^2 \tag{3.3}$$

is a monotonic and rapidly decreasing function of the scattering angle.

When electrons are scattered from a large number of atoms (with the atomic number density n and scattering volume V), the differential scattering cross section (3.3) must be simply multiplied by nV provided that individual scattering processes are superimposed in a incoherent mode [1]. This condition is usually fulfilled because the atomic concentration is not too high or, to be precise, because the average distance between the atoms is usually much larger than their diameter.

On the other hand, the diffraction pattern produced by large clusters ($N \geqslant 1000$) consists of two components [1]. One is due to the scattering of electrons by cluster atoms, as described in the preceding paragraph; it is lacking in an interference structure. The other component arises due to the characteristic distances of the periodic crystalline structure. It has a well-apparent interference structure associated with the Bragg crystal planes. The situation is reminiscent of electron diffraction from a powder of small randomly oriented crystals. The interference structure can be assessed by a well-known crystallographic method [312]. The crystal structure and lattice parameters can be found from the position of interference rings, whereas the width of the interference maximum is related to the cluster size. Finally, the degree of crystallographic line damping with respect to the diffraction angle is related to the mean interatomic separation and therefore provides information about cluster temperature [313 – 316]. In the case of intermediate-sized clusters, the scattering amplitude is a superposition of the contributions from different atoms of the cluster. This makes it rather difficult to analyze the diffraction pattern. Nevertheless, the two limiting cases cited above are readily distinguishable in the studies of cluster formation processes in supersonic expanding jets [313 – 321].

3.4 Light scattering

Rayleigh light scattering has long been used to determine mean cluster radii measuring dozens of angstroms [322]. The method leans upon the Mie theory for the electromagnetic scattering. For radiation (with the wavelength λ) from homogeneous spherical particles having radius R, refraction index n, and magnetic susceptibility $\mu = 1$, in the limit

$$\frac{2\pi R}{\lambda} \ll 1 \quad \text{and} \quad n\,\frac{2\pi R}{\lambda} \ll 1 \tag{3.4}$$

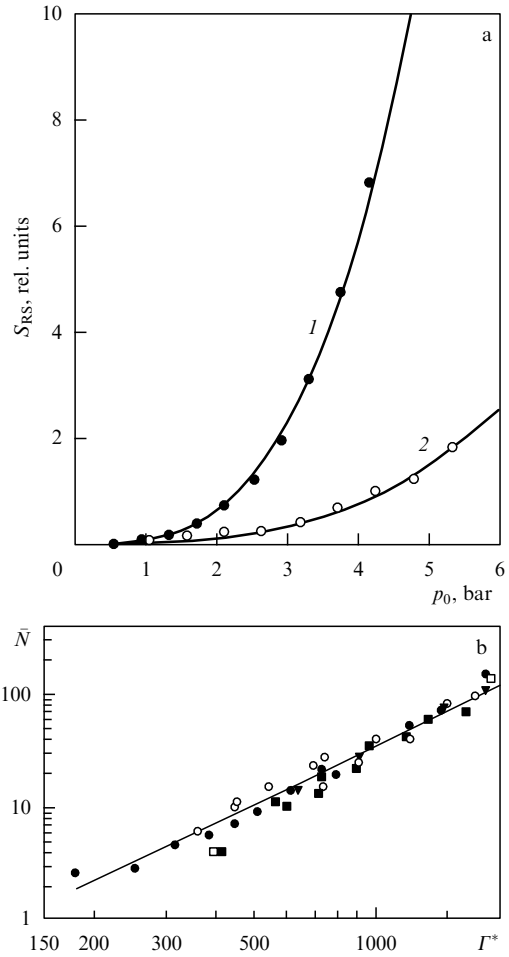

Figure 2. (a) Signal intensity of Rayleigh light scattering plotted as a function of the gas pressure above the nozzle for Xe (*1*) and Kr (*2*) beams [58, 326]. Solid lines are power-like dependences [see relationship (3.6)]. (b) Results of measuring mean cluster size depending on the scaling parameter Γ^*: ● — Xe_N, ■ — Ar_N, □ — Kr_N [328], ○ — Ar_N [329], ▼ — Ar_N [28]. (Taken from Ref. [1].)

the Mie theory gives [1] the angle-independent differential scattering cross section [323, 324]

$$\frac{\mathrm{d}\sigma}{\mathrm{d}\Omega} = \frac{8}{3}\left(\frac{2\pi R}{\lambda}\right)^4 \pi R^2 \left(\frac{n^2-1}{n^2+2}\right)^2, \tag{3.5}$$

which must be averaged over the cluster-size distribution function. It is worthwhile to note that the Rayleigh scattering is relatively small under conditions (3.4). The differential scattering cross section becomes angle-dependent when the cluster radius is comparable with the radiation wavelength.

Rayleigh scattering is not infrequently used to study the onset of condensation processes and cluster formation in expanding jets [58, 325 – 327]. By way of example, Fig. 2a depicts the dependences of scattered light intensity on the gas pressure above the nozzle for Xe and Kr beams expanding in a pulsed gasdynamic jet, obtained in Refs [58, 326]. In these experiments, radiation of the second harmonic of an Nd:YAG laser was focused on the gas expansion area at a distance equivalent to six nozzle diameters. The energy and the duration of the laser pulse were 100 μJ and 10 ns, respectively, and the wavelength 532 nm. The light scattered within an angle of 90° was detected using a photomultiplier with a narrow-band filter placed in front of it. The jet

outflowed from a convergent–divergent nozzle having an orifice diameter $d = 500$ μm and cone opening angle $\alpha = 45°$. The gas temperature above the nozzle was $T_0 = 295$ K.

The experimental results indicate that measurable clusters begin to form at a pressure of about 1000 mbar in the case of xenon, and about 2000 mbar in the case of krypton. These values correspond to the scaling parameter $\Gamma^* \approx 2400$ [see relationship (2.1)]. In addition, the experiments show that the dependence of scattered light intensity on the gas pressure above the nozzle has the power-like form

$$S_{\mathrm{RS}} \propto p_0^k \,. \tag{3.6}$$

The exponent k roughly equals 3 ($k = 3.3$ for xenon, and $k = 3.2$ for krypton). These values are consistent with simple arguments for spherical cluster scattering [1]. On the basis of measured results, and taking into account relation (3.6), the size of the cluster can be presented in the form

$$N \propto p_0^{k-1} \propto (\Gamma^*)^{k-1} \,. \tag{3.7}$$

Using the obtained experimental value of parameter k ($k \approx 3$), relationship (3.7) agrees very well with the results of other experiments [267, 269]. It should be noted that the Rayleigh scattering can be utilized for measuring only the relative size of clusters as a function of the gas pressure above the nozzle or, in general, as a function of the scaling parameter Γ^*. The absolute cluster size is found from the comparison of scattering data with the results of cluster size measurements by other methods. For example, it is possible to employ the dependence of the mean cluster size on the scaling parameters [1, 28, 328, 329] (see Fig. 2b).

3.5 Particle scattering

The scattering of a cluster beam propagating through a gas-containing chamber can also be used to obtain the average cluster size. Replacing such a gas chamber by an atomic or molecular beam intersecting the cluster beam makes it possible to determine both the mean cluster size and the cluster-size distribution (in the case of large clusters). Moreover, the scattering may be utilized for selecting microclusters by size. The gas scattering method permits studying various parameters of cluster beams. In what follows we shall consider in brief methods for measuring integral cross sections of clusters and the size distribution of clusters.

3.5.1 Measurement of the integral absorption cross section. The effective integral scattering cross section σ_{eff} is found from the measurements of cluster beam attenuation in a scattering chamber in accordance with the Beer law

$$I = I_0 \exp\left(-nL\sigma_{\mathrm{eff}}\right), \tag{3.8}$$

where I_0 and I are the intensities of the initial and scattered beams, respectively, n is the particle number density in the scattering chamber, and L is the length of the scattering chamber. After the introduction of the total absorption cross section σ_{tot} independent of the relative velocity of the particles scattered, the effective cross section may be written down in the form

$$\sigma_{\mathrm{eff}} = \sigma_{\mathrm{tot}}\, \mathrm{Fa}_0(\infty, x) \,, \tag{3.9}$$

where $x = v_{\mathrm{cl}}/v_{\mathrm{w}}$ is the ratio of the cluster velocity to the most probable velocity of the target gas particles (scattering gas), and $\mathrm{Fa}_0(\infty, x)$ is the function taking into account averaging over the Maxwellian velocity distribution in the target gas [1]. Thus, the total cross section is given by the relationship

$$\sigma_{\mathrm{tot}} = \frac{1}{nL\,\mathrm{Fa}_0(\infty, x)} \ln \frac{I_0}{I} \,. \tag{3.10}$$

When it is considered that a cluster has the form of a hard sphere, its geometric cross section may be represented in the form

$$\sigma_{\mathrm{g}} = \pi R_N^2 = \pi R_1^2 N^{2/3} \,, \qquad \text{where} \qquad R_1 = \left(\frac{3m_0}{4\pi\rho}\right)^{1/3} \tag{3.11}$$

is the effective atomic radius inside the cluster, m_0 is the mass of particles comprising the cluster, and ρ is the density of the macroscopic liquid or solid phase. Assuming that $\sigma_{\mathrm{g}} = \sigma_{\mathrm{tot}}$, the cluster size is found as

$$N = \left(\frac{\ln\left(I_0/I\right)}{nL\,\mathrm{Fa}_0(\infty, x)\,\pi R_1^2}\right)^{3/2} \,. \tag{3.12}$$

The equality $N = \overline{N}$ gives a simple estimate of the average cluster size in the beam of interest. To be precise, the total cross section contains [in conformity with formula (3.9)] the normalization function due to the size-dependent cluster detection efficiency that can be taken into account given the cluster-size distribution in the beam and size-dependent probability of detection are known [330, 331].

3.5.2 Determination of the cluster-size distribution. Cluster distribution by sizes can be assessed from the deflection of a cluster beam by an atomic or molecular beam that intersects it [1, 330, 331]. Let a monochromatic molecular beam intersect a cluster beam at an angle α. For a cluster with mass $M = Nm_0$ and velocity v_{cl} that strikes a particle of mass m and velocity v for $Nm_0 \gg m$, small deflection angles θ, and complete momentum transfer, the angle of deflection is described by the expression

$$\theta = \frac{mv}{Nm_0 v_{\mathrm{cl}}} \sin\alpha \,. \tag{3.13}$$

In such a case, the size of the cluster as a function of the deflection angle is given by the formula

$$N(\theta) = \frac{mv}{m_0 v_{\mathrm{cl}}} \frac{1}{\theta} \sin\alpha \,, \tag{3.14}$$

which leads to the following transformation of the measured angular distribution $I(\theta)$ into the cluster-size distribution:

$$f(N)\,\mathrm{d}N \propto I(\theta)\theta^2\,\mathrm{d}\theta \,. \tag{3.15}$$

Bearing in mind that the probability of cluster scattering is proportional to cluster cross section ($N^{2/3}$) and that of cluster detection is also proportional to the cross section, the transformation of the measured clusters' angular distribution into their distribution by size takes the final form [1, 330, 331]

$$f(N)\,\mathrm{d}N \propto \theta^{10/3} I(\theta)\,\mathrm{d}\theta \,. \tag{3.16}$$

This approach was successfully employed in Refs [330, 331] for examining the size distribution of nanodroplets

(clusters) of superfluid helium in a beam. The authors studied clusters of an average size ranging from $\overline{N} \cong 1000$ to $\overline{N} \cong 20{,}000$. It was found that the distribution of helium clusters by size could be described by the log-normal distribution [1, 330, 331]. This distribution had the form of a Gaussian in the coordinate system with the logarithmic abscissa axis. It is worth noting that, in recent studies [332, 333], the scattering of a cluster beam (nanodroplets of superfluid helium) from the intersecting atomic beam was proposed to use for the laser-assisted selection of molecules embedded into the droplets in terms of isotope (component) composition. Concluding this section, we should note that the method of cluster beam scattering from the intersecting molecular beam is also successfully applied to select (deflect through different angles) small-sized clusters (dimers, trimers, and tetramers) [1, 30, 31, 35, 36].

3.6 Laser-bolometric and pyroelectric methods

The laser-bolometric method is rather extensively used in cluster and molecular beam research [334, 335]. In particular, it was successfully employed for studying van der Waals complexes [26, 31, 33, 63, 65, 69]. In this method, the molecules or clusters present in a beam are excited by laser radiation and the beam particle energy is measured with a bolometer. It should be emphasized that in the case of molecular excitation in the beam the bolometer detects a rise in the molecular beam energy attributable to the absorption of laser radiation energy by the molecules. In cluster beams, on the contrary, a bolometer most frequently records a decrease in the beam energy because, under these conditions, the absorption of laser radiation as a rule leads to the dissociation of clusters and subsequent scattering of the resulting fragments from the beam [26, 31, 33]. As a result, the beam is impoverished (depleted), and the total energy detectable by the bolometer decreases. This method has been successfully used in recent spectroscopic studies of molecules and clusters inside nanodroplets of superfluid helium (see Refs [63, 65, 69] and references cited therein).

The pyroelectric method [336 – 338], which is in essence very similar to the laser-bolometric technique, is also frequently employed for detecting molecular and cluster beams. The employment of uncooled pyroelectric receivers built around the polycrystalline organic films [337, 339] and characterized by a rather high time resolution (around 3 – 5 μs) makes it possible to obtain time-of-flight spectra of molecular and cluster beams and also measure the internal energy of the molecules in a beam [336, 337]. Experimental procedures for detecting molecular beams with the help of uncooled pyroelectric receivers are described in detail in a few recent publications [340, 341].

4. Cluster – surface collisions at moderate energies

4.1 Early experiments. Reflection of van der Waals clusters from a solid surface. The role of surface temperature

Studies of interactions between cluster beams and solid surfaces date back to the works of Becker and his co-workers [342, 343]. In experiments with nitrogen clusters that fell on a polished stainless steel substrate, the normal component of the velocity of clusters scattered from the surface was found to be very close to zero, whereas the tangential component remained practically unaltered. Due to this, at incidence angles of $60-70^\circ$ with respect to the normal to the surface, the reflected clusters were concentrated into a very narrow beam with an angle of reflection about 88°. A rise in the flux density of the reflected particles compared with that of the incident particles suggested the possibility of collimation of cluster beams with the help of appropriately shaped reflectors.

It was shown in the same experiments that the angle of reflection increased with increasing cluster size. This opened up the possibility of obtaining clusters of different sizes by shielding different angular sections in the reflected beam [342]. Further studies along the same line included the scattering of helium [343] and hydrogen [344, 345] clusters. These studies were focused on the effect of surface temperatures of up to 300 K on the cluster reflection. Direct measurements of the cluster sizes confirmed the mass selectivity with respect to the scattering process. The results of the experiment were well described by a simple model according to which the normal component of cluster velocity varied due to the reflection of molecules from the cluster portion that was in contact with the surface. These results were obtained for clusters having an average size $\overline{N} \cong 10^5$. Later studies yielded similar results for medium-sized clusters with $\overline{N} \cong 10^6$, as they were scattered from the surface at room temperature.

The results of measuring the size, velocity, and angular distribution of reflected clusters, as well as the normal momentum and energy exchange between the clusters and the surface, allowed for the conclusion that the normal momentum of reflected clusters is negligibly small compared with that in an incident beam even in the case of its normal incidence upon the surface. A decrease in the cluster size with decreasing angle of reflection is partly due to the evaporation maintained by the energy transferred to the cluster from the surface [346].

The interaction between cluster beams and a solid surface has been examined in detail in Ref. [347]. This work was designed to study the reflection of helium, hydrogen, and nitrogen clusters from a polished plate of stainless steel at temperatures between 80 and 550 K. Clusters incident upon the surface contained on the average $N \cong 1.5 \times 10^5$ helium atoms or hydrogen and nitrogen molecules. A time-of-flight mass spectrometer was utilized to study angular distributions, average sizes, velocities, and intensities of incident and reflected cluster beams. Also, the authors developed a semiempiric model that fairly well describes the temperature dependence of the reflection angle during high-temperature cluster scattering.

The authors of the paper [347] found a similarity between the dependence of cluster reflection on the surface temperature and the dependence of scattering of monatomic gases from a metal surface on the incident energy. It is well known [348, 349] that in the latter case there are at least two scattering regimes, viz., thermal and structural. The thermal scattering regime takes place at small energies of incident atoms and is governed by thermal velocities of surface atoms. The structural or hyperthermal regime predominates at high energies of incident atoms and is conditioned by the surface roughness. Scattering through angles smaller than the angle of incidence occurs under the thermal scattering regime, whereas in the structural scattering regime and in the transitional region the scattering angles turn to be larger than the angle of incidence.

It has been shown in experiment [347] that clusters lose their mass under a high-temperature regime but their velocity increases by virtue of interaction with the reflecting surface. This observation is in conflict with the usually observed retardation of the relative motion of interacting solids due to friction. Friction is accompanied by the conversion of the kinetic energy into heat, whereas the kinetic energy of clusters undergoing high-temperature reflection increases, being supported by the surface thermal energy. It has been demonstrated that the acceleration of clusters is a recoil effect due to the rapid evaporation of those molecules in a cluster that come in contact with the reflector.

The process of cluster reflection from a surface is somewhat reminiscent of the well-known Leidenfrost effect, namely, a substantial decrease in the evaporation rate of liquid droplets on a hot plate when the plate temperature is so high that an insulating vapor layer is formed between the droplets and the surface. However, the reflection of the clusters is not accompanied by the formation of a real insulating vapor layer because the time of their interaction with the reflector is rather short and the clusters are small compared with any conceivable length of the mean free path of the molecules. Also, it has been shown in Ref. [347] that the model of recoil effect due to evaporation fairly well explains the angular dependence of the size of the reflected clusters. In accordance with this model, the incident clusters are sorted out by size due to a change in the ratio of recoil momentum to incident momentum for clusters of different sizes that depends on the surface-to-volume ratio of incident clusters.

It should be emphasized that neither the physical principles underlying collision events nor the mechanisms of energy transfer and recoil of van der Waals clusters from a surface could be comprehensively understood based on the results of early studies despite a rather large amount of available experimental data. One of the causes hindering a deeper insight into the cluster scattering process was the poor knowledge of the characteristics of cluster beams themselves. The relationship between the nozzle parameters (gas temperature and pressure, the diameter of the opening and the shape of the nozzle) and the cluster sizes was investigated in much detail in Refs [265, 266, 350]. At the same time, it remained virtually unknown how the nozzle parameters may affect the size and the structure of van der Waals clusters.

Studies of nitrogen cluster beams using the electron diffraction technique proved very helpful in this respect [351, 352], demonstrating the relation between the conditions above the nozzle (gas temperature and pressure), on the one hand, and the cluster size, structure, and temperature in a beam being formed, on the other hand. Specifically, it was shown in Ref. [351] that small nitrogen clusters ($N \cong 50$) possess an amorphous structure. Large nitrogen clusters ($N \cong 4000$) are produced at high gas pressures above the nozzle. It was established that they have crystal structure, resembling the structure of solid nitrogen α-N_2 [351].

4.2 Reflection of van der Waals clusters from a metal surface. The binary collision model

A more detailed investigation into the scattering of van der Waals clusters (exemplified by those of argon and nitrogen) was undertaken in Refs [310, 353–355]. One experimental study [310] was concerned with the collision dynamics of large van der Waals nitrogen clusters interacting with the surfaces of iron and silver single crystals. The researchers measured the angular distributions of scattered fragments and assessed the rotational energy distribution over the fragments, depending on the N_2 pressure above the nozzle (including the use of He as a gas-carrier) and the surface structure, composition, and temperature.

The source of the cluster beam was a solenoid-controlled pulsed nozzle with an opening diameter of 0.8 mm [356]. The gas pressure above the nozzle varied over a range from 20 to 60 atm. Such a high pressure made it possible to produce large-sized clusters. Beams of N_2 clusters with different translational temperatures and cluster sizes were obtained utilizing N_2/He gas mixtures in which the nitrogen content was varied (100, 50, 20 or 5%). The authors believed that they would be able to obtain colder clusters at high partial pressures of helium in the initial mixture.

The cluster beam was extracted from the expanding jet by a skimmer with an opening 0.8 mm in diameter positioned 3.5 cm from the nozzle. To improve beam collimation, a diaphragm having a 1-mm opening diameter was placed, in addition to the skimmer, at a distance of 12 cm from the nozzle. The nozzle-to-scattering surface distance measured 24 cm. The samples used included single crystals of iron, Fe(111) and Fe(110), and silver, Ag(111). The vacuum chamber in which the samples were placed was pumped down to a residual pressure of 10^{-10} Torr. The pumping over, the iron and silver single crystals were annealed in a deep vacuum by heating them up to 900 and 600 K, respectively; in this way, the crystal surfaces were cleaned and purified from carbon. The scattered nitrogen beam was detected by the electron beam-induced fluorescence technique [304, 305].

The studies under consideration revealed a number of characteristic features intrinsic in nitrogen cluster scattering from a solid surface:

(1) The cluster size grows as the fraction of helium in the initial mixture increases, while the internal energy of the clusters decreases (i.e., colder clusters are produced).

(2) The maximum-intensity angle of the scattered beam increases and shifts in the tangential direction as the total gas pressure above the nozzle rises from 20 to 60 atm.

(3) A rise in the molar fraction of nitrogen in the gas mixture has a pronounced effect (see Fig. 3a). At a constant

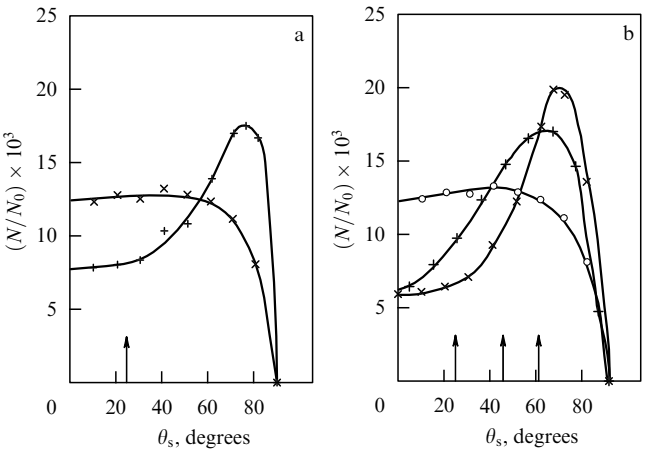

Figure 3. (a, b) Angular distributions of scattered fragments resulting from collisions of nitrogen clusters with the Fe(111) surface. Surface temperature was $T_s = 650$ K. Gas pressure above the nozzle reached $p_0 = 60$ atm. (a) Incidence angle $\theta_i = 25°$. Gas mixtures in the source: 5 %N_2 + 95 %He (+) and 50 %N_2 + 50 %He (×). (b) Gas mixture: 50 %N_2 + 50 %He. Incidence angle: $\theta_i = 25°$ (○), 45° (+), and 60° (×) [310].

total gas pressure (60 atm) and an incidence angle of 25°, the distributions obtained with a $50\,\%N_2 + 50\,\%$He mixture have the form of a wide envelope having an approximately equal intensity between 0° and 60°, whereas the scattering diagram of a beam composed of $5\,\%N_2 + 95\,\%$He exhibits a well-apparent petal concentrated near $\theta_s = 75°$ (see Fig. 3a).

(4) When a mixture with a low nitrogen content ($5\,\%N_2 + 95\,\%$He) was used, the peak position ($\theta_s = 75°$) in the angular distribution of scattered particles was independent of the incidence angle. It is the most prominent characteristic of cluster scattering from a surface.

(5) When a $50\,\%N_2 + 50\,\%$He mixture is used, the maxima in the distributions of scattered particles are displaced towards larger tangential angles, as the normal component $v_\perp$ of the incident beam velocity decreases (Fig. 3b). Conversely, at large $v_\perp$ values, the intensity of the scattered beam is highest in the directions close to the normal to the surface.

The experiments described in the preceding paragraphs also demonstrated that the fraction of particles scattered through angles close to tangential ones grows with a rise in the surface temperature (from 400 to 650 K). Moreover, these experiments showed that the crystal structure of the surface has a marked effect on the angular distributions of the scattered particles, largely because the surface is irregular. In the case of Fe (110), the large surface roughness gives rise to more scattering trajectories of fragmented clusters observed outside the incidence plane. This results in a lower intensity of the scattered beam in the incidence plane. It was found that the rotational temperature T_{rot} of the scattered molecules depends on the scattering angle and the incident beam energy (Table 2). The dependence of T_{rot} on the scattering angle can be accounted for in the framework of the binary collision model [353]. In this model, the cluster dynamics is regarded as a series of collisions between those atoms that are reaching the surface and those scattered from it in the opposite direction. This means that the understanding of binary collisions between monomers in a cluster is crucial for understanding cluster dynamics as a whole. Nitrogen molecules scattered in the direction close to the normal to the surface (0°) are rotationally excited because they are reflected from the outer cluster layers in the absence of contact with the metal surface. Nor do they experience multiple collisions within the cluster. The elevation of T_{rot} (for clusters scattered through an angle of 0°) with the increasing kinetic energy of the incident beam (see Table 2) also agrees with the binary impact model because $N_2 - N_2$ collisions leading to normal scattering also become stronger with a rise in the kinetic energy.

Table 2. Measured rotational temperature of nitrogen molecules scattered through different angles, for two surface temperatures and three collision energies. The angle of incidence of the cluster beam on the surface $\theta_i = 45°$ [310].

Energy of the incident beam, meV/N_2	Scattering angle θ_s, degrees	Rotational temperature (K) at the surface temperature	
		400 K	700 K
90	20	224 ± 30	234 ± 30
	45	148 ± 30	172 ± 30
	70	91 ± 30	88 ± 30
200	20	214 ± 30	240 ± 35
	45	190 ± 25	192 ± 25
	70	91 ± 25	113 ± 25
340	20	280 ± 50	402 ± 50
	45	263 ± 40	269 ± 40
	70	144 ± 50	162 ± 40

To summarize the aforesaid, work [310] demonstrated that the pattern of nitrogen cluster scattering from a surface is essentially dependent on the fraction of helium (hence, the cluster size) in the mixture studied and on the normal component of the cluster incidence velocity. A rise in the normal component $v_\perp$ of the velocity of cluster incidence upon a surface results in a higher intensity of the scattered beam in the perpendicular direction (see Fig. 3b). Wider and wider angular distributions of scattered particles are formed with increasing $v_\perp$, which suggests more complete fragmentation of the clusters. These findings also indicate that the transfer of the normal component of the momentum to the cluster's internal degrees of freedom is an important process at the collision of weakly bound nitrogen clusters and that this energy transfer results in cluster fragmentation.

Based on the measurements of angular distributions of scattered particles, depending on the molar fraction of nitrogen contained in the gas studied, the authors assigned two scattering regimes. Cluster beams produced with the use of a gas with a large helium fraction ($5\,\%N_2 + 95\,\%$He or $20\,\%N_2 + 80\,\%$He) were always scattered through larger angles than the incidence angle. These findings are consistent with the model of layer-by-layer scattering of clusters [353, 354] that implies the transfer of the normal component of the momentum to the cluster internal degrees of freedom, resulting in cluster its fragmentation.

The upper layers of nitrogen clusters are usually scattered from a surface through angles close to the normal to the surface, and the scattered particles become rotationally excited. In contrast, the inner layers of clusters are scattered tangentially. Due to multiple collisions with the remaining part of the cluster, the rotational temperature of these fragments is lower than the rotational temperature of the fragments scattered in the perpendicular direction. The results of measuring angular distributions and rotational energy confirm that the layered cluster model may be used to theoretically describe collisions and recoil effects of compactly bound nitrogen clusters (see Section 4.3).

An alternative scattering regime was documented in experiments with the mixtures of $100\,\%N_2$ and $50\,\%N_2 + 50\,\%$He. In this case, the angular distributions were wide and suggested optimal scattering at angles close to the incidence angles. These distributions were consistent with cluster dissociation resulting from their impact on the surface that led to their diffuse scattering. Under such conditions, clusters in a beam may be hotter than those produced in helium-diluted nitrogen, which results in a higher degree of their fragmentation upon collision with the surface.

Experiments on the scattering of small argon clusters from a Pt (111) surface [353] gave a rather interesting result. They showed that a substantial part of the clusters (around 50%) withstood fragmentation even at a relatively high collision energy (approximately 0.5 eV per atom). Similar results were obtained in Ref. [355] that reports scattering of a model van der Waals molecule $N_2 - Rg$ (Rg is an inert gas atom) from a rigid surface. The high percent of argon cluster survival was explained in Ref. [353] by the fact that the cluster direct impingement on the surface does not lead to immediate dissociation that occurs during subsequent collisions of atoms with one another — that is, as a result of

binary collisions along the van der Waals bond. The impact-induced dissociation of a cluster is feasible if the van der Waals bond has a large component perpendicular to the surface. The results obtained in the aforementioned works were explained in the framework of the binary collision model [353, 354].

4.3 Collisions of large argon clusters with a graphite surface. The thermokinetic model and the model of dynamic zone structure

Research reported in Refs [357–361] made an important contribution to the investigation of the scattering of large van der Waals clusters from a rigid surface. The authors studied the scattering of Ar clusters from a graphite surface. Unlike earlier investigations [310, 353–355], they used a unique experimental setup [362] that allowed for the evaluation of many scattering parameters at a qualitatively new level under well-specified experimental conditions.

In experiments [357, 358], a highly collimated beam of Ar atoms and (or) clusters was separated by a skimmer with an opening diameter 240 μm from an expanding gasdynamically cooled jet generated during gas expansion from a sonic nozzle. The gas pressure above the nozzle was varied over a range up to 26 atm. The cluster velocity in the beam amounted to about 550 m s^{-1}. The beam was scattered from the clean surface of a pyrolytic graphite single crystal measuring 10×10 mm. The sample was mounted on a high-precision manipulator and placed in a fine vacuum ($\leqslant 10^{-10}$ Torr). The crystal could be heated up to about 1000 K. A quadrupole mass spectrometer rotatable in the plane of beam incidence on the surface was used to measure angular distributions of cluster fragments (monomers, dimers, and trimers) and their time-of-flight spectra during scattering of large argon clusters from the surface.

The results of these experiments were in many respects similar to those obtained in earlier studies, barring the fact the authors observed at least two novel scattering features. First, they demonstrated a well-apparent correlation between the sizes and the angular distributions of scattered fragments. Second, they documented the appearance of a new scattering component at large tangential angles when the angles of incidence and (or) gas pressures above the nozzle were large, too. This component arose as a result of the survival of large fragments during cluster impacts on the surface. This phenomenon is readily accountable in terms of energy transfer processes (see this section below).

Paper [358] also reported new experimental data on the scattering of large argon clusters from a graphite surface and developed a thermokinetic model to explain the scattering process. The authors examined the scattering of argon clusters depending on the surface temperature over a wide range of T_s, angle of incidence θ_i, and cluster sizes. They measured angular distributions and time-of-flight (TOF) spectra of the scattered fragments. The experiments demonstrated the existence of three scattering channels (evaporation, tangential component, and survival of large fragments). The results obtained in this study can be interpreted as follows: the fraction of particles scattered through tangential angles grows with increasing surface temperature, cluster size, and angle of incidence.

The thermokinetic model developed for the explanation of the above findings makes it possible to simulate angular distributions of scattered particles using a single adjustable parameter. The introduction of another adjustable parameter permits additionally adjusting the TOF distributions of scattered particles. Let us briefly consider this model. It is based on two assumptions. First, it is suggested that a certain part c_f of the parallel component of the cluster velocity is retained in the incidence plane for the center of masses. This assumption comes from the fact that the graphite surface is a rather smooth one. Second, it is suggested that small fragments are evaporated from the thermalized cluster complex at a certain local temperature T_{loc}. This assumption is based on the fact that the outer atoms in a cluster are the first to come into contact with the surface; thereafter, they are reflected in backward direction and collide with incoming atoms of the same cluster. One such interatomic collision is sufficient to make the subsequent motion of the atom unpredictable. Because all the atoms of a given cluster impinging on the surface are involved in many collisions of this type, they almost instantaneously become locally thermalized. In other words, it may be supposed that the signal observed comes largely from small fragments that are thermally evaporated from the initial cluster sliding over the surface.

In the coordinate system comoving with the cluster, the density of fragments being evaporated, N_{cl}, is found as the product of the Maxwellian velocity distribution and the cosine angular distribution:

$$N_{cl}(w,\varphi)\,\mathrm{d}w\,\mathrm{d}\varphi \propto w^2 \exp\left(-\frac{mw^2}{2kT_{loc}}\right)\cos\varphi\,\mathrm{d}w\,\mathrm{d}\varphi\,, \quad (4.1)$$

where m and w are the mass and the velocity of a scattered fragment, respectively, φ is the scattering angle in the coordinate system attached to the cluster, k is the Boltzmann constant, and T_{loc} is the local temperature in the cluster. In order to compare the results of model computations with experimental findings, it is necessary to pass from the moving frame of reference to the laboratory frame of reference in which the particle number density $N_{lab}(v,\theta)$ has the form [358]

$$N_{lab}(v,\theta)\,\mathrm{d}v\,\mathrm{d}\theta \propto v^2 \exp\left(-\frac{mw^2}{2kT_{loc}}\right)\cos\theta\,\mathrm{d}v\,\mathrm{d}\theta\,, \quad (4.2)$$

where v is the velocity of a fragment scattered in the direction of the scattering angle θ in the fixed coordinate system, w is the velocity for the fixed scattering angle θ, given by the expression

$$w = \sqrt{v^2 + v_\parallel^2 - 2vv_\parallel \sin\theta}\,, \quad (4.3)$$

and the parallel component of the velocity is defined as

$$v_\parallel = c_f v_i \sin\theta_i\,, \quad (4.4)$$

where v_i and θ_i are the velocity and the angle of incidence of the clusters on the surface, respectively. Relationship (4.3) gives the velocity distribution of scattered particles with mass m that leave the surface at an angle θ. By denoting

$$b = \frac{v_\parallel}{v_T}\,, \quad \text{where} \quad v_T = \sqrt{\frac{2kT_{loc}}{m}}\,, \quad (4.5)$$

it is possible to find the most probable velocity v_{mp} of the scattered fragments on the assumption of a zero value of the

first derivative of expression (4.2):

$$v_{\rm mp} = \begin{cases} v_{\parallel}\left[\dfrac{\sin\theta}{2} + \sqrt{\left(\dfrac{\sin\theta}{2}\right)^2 + b^{-2}}\right] & \text{for} \quad b \neq 0\,, \\ \sqrt{\dfrac{2kT_{\rm loc}}{m}} & \text{for} \quad b = 0\,. \end{cases} \tag{4.6}$$

In order to compare the experimentally determined angular distribution of scattered particles with the results of model computation, it is necessary to integrate equation (4.2) over all velocities v. By previously substituting $z = v/v_{\parallel}$, it is possible to obtain

$$A(\theta)\,{\rm d}\theta \propto v_{\parallel}^3 \cos\theta\,{\rm d}\theta \int_0^{\infty} z^2 \exp\left(-b^2u^2\right){\rm d}z\,, \tag{4.7}$$

where

$$u^2 = z^2 - 2z\sin\theta + 1\,. \tag{4.8}$$

Thus, the form of the computed angular distribution depends on a single adjustable parameter b. The integral in expression (4.7) is easy to find by the numerical method. The model considered permits fairly well describing the experimentally revealed features of the scattering of van der Waals clusters from a solid surface [358, 363, 364].

Let us now consider in brief the dynamic zone structure model proposed in Ref. [359] to explain the behavior of the sliding component of the scattering. Such a component was uncovered earlier in both experimental [357, 358] and model [365, 366] studies on the scattering of large van der Waals clusters from a surface. The model of interest is based on the simple energy balance and the Leidenfrost effect. It not only reproduces qualitatively the measured sliding component as a function of the incident cluster size, incidence velocity, angle of incidence, and surface temperature but also gives an estimate (by order of magnitude) of the size of large fragments scattered into this component. The results obtained both experimentally and by calculations along classical trajectories indicate excellent agreement between the observations and the predictions of the model under consideration.

Based on theoretical evaluations and on the experimentally found existence of three scattering channels, the authors proposed the dynamic zone structure (DZS) model in which a cluster is regarded as a structure containing three zones. So that the atoms of each zone are responsible for one scattering channel or another. Let us consider, without going into detail, the qualitative picture of cluster scattering from a surface in the framework of this model [359]. According to the propositions of the model, the atoms of a cluster closest to the surface (atoms of the first zone or n_1-atoms) are the first to hit it. They break their bonds with the cluster and become involved in the adsorption – desorption process. The atoms of the second zone (n_2-atoms) shrink as they collide with the surface-bound n_1-atoms and more outward atoms that continue to travel toward the surface and catch up with the n_2-atoms. In other words, collisions undergone by the n_2-atoms result in their heating to a temperature roughly equal to the boiling point. At a later time, these atoms are evaporated as constituents of small fragments.

Thus, it is henceforth assumed [359] that the main source of heating and evaporation of clusters is the kinetic energy associated with the normal velocity component of the cluster incident on the surface. This assumption is based on the fact that the probability of cluster survival decreases as the normal component of the cluster velocity increases. The mean size of fragments also decreases significantly as the normal component of the incidence velocity increases. The evaporation process lasts till the entire kinetic energy of the incident cluster is used up. By this instant of time, an essential part of the incident cluster may be preserved, having avoided fragmentation. This part consists of n_3-atoms and makes up the third zone of the interacting cluster. Therefore, the atoms from the third zone are decelerated to a zero velocity of the normal incidence before they reach the surface; in other words, they are not subjected to fragmentation. They can acquire a small normal momentum from n_2-atoms and, therefore, repulse from the surface. Because they retain the tangential component $v_{\parallel}$ of the velocity, they will travel in the tangential direction at a sliding angle, with n_2-atoms serving as a 'cushion' for these intact fragments as they slide over the surface.

It should be noted that this model does not imply that all n_3-atoms must be bound into one large fragment. They can be distributed between several rather big fragments. At the same time, theoretical calculations [365, 366] indicate that the formation of a single large fragment is most likely to occur. This part of the cluster does not touch the surface at all, hence it derives no energy from the hot surface atoms. For this reason, this part of the cluster does not undergo fragmentation, which accounts for the survival of large fragments in the sliding component. The results obtained in the framework of the model being considered are in excellent agreement with experimental findings [359, 365, 366].

4.4 Diffuse scattering of atoms (molecules) upon cluster collision with a surface

The data presented in Sections 4.2 and 4.3 demonstrate the existence of two 'direct' scattering channels at the collisions of large-sized van der Waals clusters with a solid surface: one includes scattering of monomers evaporated from the clusters, and the other involves scattering of survived fragments. Both channels are responsible for the formation of a narrow scattering indicatrix of particles near the tangential angle to the scattering surface. In the present section, we shall consider quite a different scattering channel for clusters hitting a surface — that is, diffuse scattering of monomers. This type of scattering is characterized by the thermalization of scattered monomers; in other words, the distribution of their velocities is well described in terms of the Maxwell – Boltzmann distribution function. The diffuse scattering effect was first observed in Ref. [361].

The experiments were carried out using a continuous argon cluster beam. The average cluster size in the beam could be varied from that of monomers to $N \cong 8100$ atoms per cluster by varying a gas pressure above the nozzle. The kinetic energy of clusters in the beam was 65 meV per atom. A sample of pyrolytic graphite material served as the scattering surface. The angle of incidence of the cluster beam onto the surface varied over a range from 45° to 70°, and the surface temperature from 440 to 600 K. Before each experiment, the sample was heated to 800 K to have its surface clean.

The parameters measured in the experiments included the angular distribution of scattered particle number density and TOF spectra of these particles in the incidence plane. These

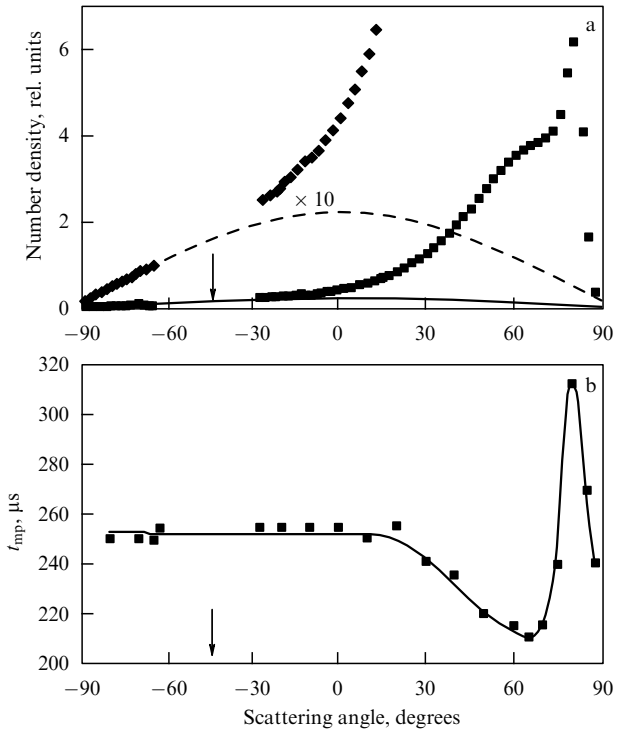

Figure 4. Dependences of the number density (a) and the most probable time of flight (b) for scattered Ar atoms on the scattering angle in the case of collisions of Ar_{4100} clusters with a graphite surface at $T_s = 520$ K. Angle of cluster incidence upon the surface $\theta_i = 45°$ [361].

measurements were made with a quadrupole mass spectrometer which can be rotated about the sample axis. Mass spectra were recorded at a distance of 240 mm from the sample. This allowed obtaining TOF spectra of the particles running at different angles with an angular resolution of around 2°. Also, the most probable time t_{mp} of the particle arrival at the mass spectrometer was determined, namely, the time that the particles spend on traveling from the surface to the detector.

Figure 4 presents a typical result obtained in the experiment with an Ar_{4100} cluster beam incident upon the graphite sample at angle $\theta_i = 45°$ and surface temperature $T_s = 520$ K. The angular distribution of particle number density and most probable times of their arrival at the detector are plotted in Figs 4a and 4b, respectively. For positive scattering angles θ_s, Figs 4a and 4b provide a good illustration of the contributions from the two aforementioned scattering channels (both the atoms evaporated from the clusters and the survived fragments undergo scattering). The contributions from these 'direct' inelastic scattering processes give a negligibly small signal at negative scattering angles where the presence of the third component is definitely confirmed by the absence of the angular dependence of quantity t_{mp} (as distinct from the situation that takes place at positive scattering angles θ_s). A signal multiplied by 10 in Fig. 4a clearly indicates that this contribution is well described by the cosine distribution.

In an in-depth study of this process, the authors displaced the mass spectrometer 20 mm below the incidence plane. In this case, the signal was largely due to the scattering component. It was established [361] that in the case of negative θ_s values, where the contribution of diffuse scattering was most frequently observed, the velocities of the scattered particles did not depend on their escape directions. Moreover, the measured t_{mp} value was related neither to the incident cluster size nor to the angle of incidence. At the same time, the value of t_{mp} was highly sensitive to surface temperature: the higher the temperature of graphite surface, the shorter the time t_{mp}. This temperature dependence was most apparent in the region of negative θ_s values, where the contribution from 'direct' inelastic scattering channels predominated. The measured TOF spectra are fairly well approximated by the Maxwell–Boltzmann distribution over velocities with temperatures listed in Table 3.

Table 3. Translational temperature T_{trans} of scattered argon atoms as a function of surface temperature T_s [361].

T_s, K	660	580	520	440
T_{trans}, K	370 ± 10	340 ± 10	290 ± 10	270 ± 10

The evidences provided by this study demonstrated that the intensity of the diffusive component rapidly grows with increasing cluster size up to a constant value 2–3 times the scattering intensity measured with a monomer beam at the same surface temperature. The authors proposed a very simple phenomenological model to explain this effect, according to which the scattering of an ultrasonic beam from a hot flat surface is associated with quasicapture and desorption [367]. This model fairly well describes the experimental findings [361]. It is worth noting that the scattering of monomers via the capture–desorption process was later observed in experiments on the scattering of large water clusters from the graphite surface [197, 364, 368] (see Section 4.5).

To sum up, the work described in Ref. [361] revealed that collisions of argon clusters with a graphite surface was accompanied by rather intense diffuse scattering of essentially velocity-thermalized atoms, in addition to other known scattering processes. The authors considered two effects that might account for the observed enhancement of scattering intensity. First, the atoms remaining on the surface impacted by clusters may have significantly smaller tangential velocity components than the incoming monomers. Second, the fraction of the total number of incident atoms that remain at the surface may be larger in the case of a cluster beam than for an atomic beam. Both effects contribute to the enhanced capture probability of incoming atoms with a low kinetic energy in the attractive surface potential.

4.5 Ionization of water clusters upon collision with a solid surface

This section is designed to consider experimental data on the formation of positive and negative ions resulting from the collisions of water clusters with a solid surface [188–197], along with model calculations of energy transfer in the course of collisions of $(H_2O)_N$ clusters with a solid surface [369, 370]. Also, we shall briefly discuss the results on ionization of clusters of other polar molecules at collisions with the surface [195]. It should be noted that water clusters are of special interest in that the molecules in a cluster are coupled by hydrogen bonds that are stronger than weak van der Waals bonds. The nature of these clusters is more complicated than that of inert gas clusters. The processes associated with water condensation and the formation of charges play a key role in atmospheric phenomena, and also have important technical implications.

4.5.1 Experimental results. The generation of positive and negative ions in the course of water cluster scattering from solid surfaces was first observed in Refs [188, 189] and studied in Refs [190 – 194]. It was shown in papers [188 – 191] that water clusters hitting a solid surface undergo decomposition into positively and negatively charged fragments (polar fragmentation). This phenomenon was examined in experiments with water clusters having the size $N \geqslant 200$, when the kinetic energy of the cluster collision with the surface reached 35 eV. The authors hypothesized that a collision with the surface might induce the reaction

$$(H_2O)_{N+1} \rightarrow H^+(H_2O)_{N-K} + OH^-(H_2O)_K \,.$$

A more detailed investigation into the interaction of water clusters with solid surfaces was undertaken in Ref. [190] (see also Ref. [194]). These experiments leaned upon the molecular beam method. A source of a supersonic jet contained an overheated vapor [189]. The water temperature in the beam source was maintained at a constant level (450 K), and the mean cluster size in the beam was changed by varying vapor pressure inside the source. The cluster beam was produced using a sonic nozzle with an opening diameter of 1 mm. A rise in vapor pressure in the source to more than 480 Torr triggered the formation of water clusters in the beam with an average size $N \geqslant 100$. Under these experimental conditions, the average velocity of water clusters was roughly equal to the maximum velocity $v \cong 1300$ m s^{-1} achieved in gasdynamic outflow [371]. The pressure in the working chamber was maintained at 1.5×10^{-6} Torr.

The surface electrization effect was discovered in experiments [189] where a cluster beam was normally incident upon the flat surface of a stainless steel plate. Other targets included polished surfaces of metals (gold, steel, duralumin), gallium-doped germanium single crystals [facets (100) and (110)], and fiber glass laminate. The targets were heated to 420 – 450 K.

The experiments were designed to ascertain the dependence of the intensity of current induced by cluster collisions with the studied surfaces on the angle of incidence and the average cluster size. For clusters with an average size $N = 1200$, a sharp maximum was observed in the angular dependences of current intensity at tangential angles of incidence ($\theta_{\max} \cong 70^\circ$). The authors interpreted this finding as a manifestation of the most characteristic feature of neutral cluster scattering from a solid surface, namely, the high reflection probability for the clusters having large tangential components of the velocity [372, 373] (see Section 4.3).

The absolute values of the currents induced by cluster – surface collisions were compared with those of ion currents induced by electron impact ionization of clusters to evaluate the absolute probability of ion pair formation and decomposition during collisions of clusters with a solid surface. The maximum probability of ion pair formation under experimental conditions was found to reach 10^{-4}.

The authors of Ref. [190] conjectured that the kinetic energy of a cluster impinged on a solid surface is converted into the internal cluster energy and is also spent on surface deformation and excitation of the intramolecular as well as intermolecular degrees of freedom in the cluster. The current generation is related to the formation and decomposition of ion pairs. The ion formation resulting from the surface scattering of clusters of a relatively small size and low kinetic energy is a specific feature of water clusters. It is corroborated by the absence of this effect in similar experiments with $(CO_2)_N$ and $(N_2O)_N$ clusters. In experiments with water clusters, the ion signal was observed regardless of the target surface used.

The authors attributed the formation of ion pairs to autoprotolysis of water molecules, which occurred at cluster collisions with the surface:

$$H_2O \rightarrow H^+(aq) + OH^-(aq) \,.$$

It is known that the process of dissociative ionization is characterized by low activation energy ($E_a = 0.58$ eV in the condensed phase) due to the high hydration energy of both the proton and the hydroxyl group [374]. The degree of hydration in water clusters appears to depend on N; hence, E_a for an individual molecule ($N = 1$) will increase from 0.58 to 16.9 eV with a decrease in N. This means that the process of molecular dissociative ionization in a cluster can be observed only at a certain collision energy and threshold cluster size N_*. The authors concluded that the current they observed could not be attributed to the equilibrium fraction of ion pairs. Rather, it was due to the formation of such pairs from water molecules excited by cluster collisions with the surface.

Thus, the results obtained in Refs [188 – 194] reveal that collisions of neutral water clusters with a solid surface are accompanied by efficient dissociative ionization, i.e., the formation of oppositely charged ion pairs. However, it should be emphasized that these experiments did not include mass-analysis of the ions being formed. Therefore, it cannot be excluded that the data obtained might be influenced by other factors, too. For example, Ref. [195] offers quite a different explanation for the observed formation of positive and negative cluster ions during the interaction of H_2O [188 – 194, 197] and SO_2 [375] clusters with a solid surface.

Reference [195] describes a microscopic model of the formation mechanism for charged fragments. This model is based on the results of mass-analysis of charged fragments produced at collisions of SO_2 clusters with a solid surface. The target surfaces used in these experiments were a commercial silicon (SiO_x) plate and a gold coating (produced by electrolytic deposition of this metal onto a steel substrate) at surface temperatures ranging between 400 and 600 K — that is, under conditions where weakly bound molecular adsorbates already evaporated from the surface. SO_2 clusters were formed during gas outflow from a pulsed nozzle (with the opening diameter of 0.5 mm, and the pulse duration about 400 μs). The gas pressure above the nozzle amounted to 20 atm. The SO_2 molecules were diluted in a gas-carrier (He, H_2, Ne). The size and the velocity of clusters in the beam varied in the intervals $\overline{N} \cong 1-750$ and $v \cong 750-1750$ m s^{-1}, respectively, depending on the gas pressure above the nozzle and gas composition. Collisions of SO_2 monomers with the surface at the velocity of $v \cong 1200$ m s^{-1} induced no charges.

Analysis of the mass spectra of positively and negatively charged fragments formed during collisions of $(SO_2)_N$ clusters with the surfaces demonstrated (see Fig. 5) that the negatively charged fragments possess a simple structure, namely, $(SO_2)_N^-$, whereas the positively charged fragments $(SO_2)_N^+$ were virtually absent. Also, it was revealed that all positively charged fragments contained an ion of an alkali metal Na, K, or Cs. Moreover, preliminary etching of the surface (for example, by a beam of caesium atoms) caused a substantial increase of the corresponding peaks of $Cs^+(SO_2)_N$ ions and, as a result, a marked rise in the intensity of all $(SO_2)_N^-$ mass-peaks. Under these conditions, the total number

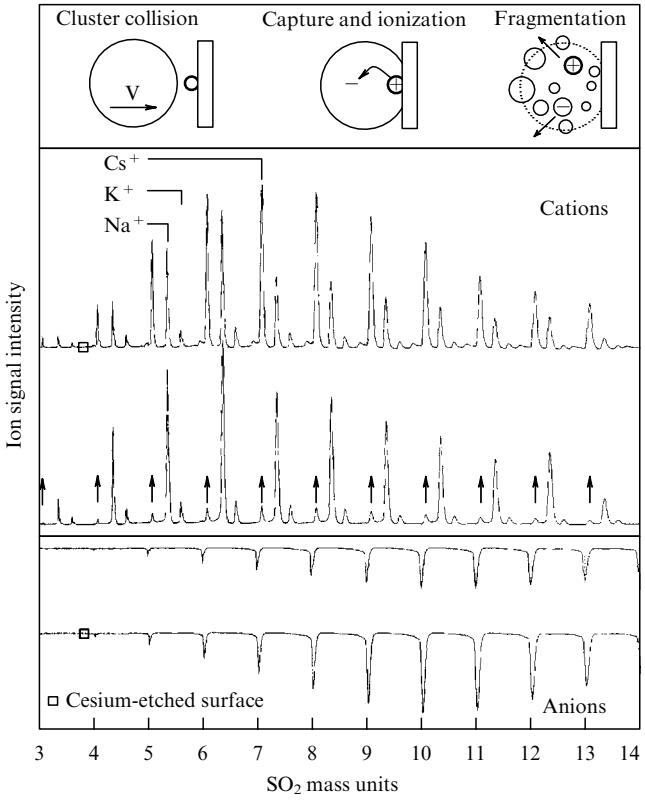

Figure 5. Mass spectra of positively and negatively charged cluster fragments produced upon $(SO_2)_N$ cluster impact on the target surface (gold deposited on steel substrate). Cluster incident velocity equals 1.2×10^3 m s^{-1}. Mean cluster size is $\overline{N} = 500$. Mass scale is given in SO_2 mass units [195].

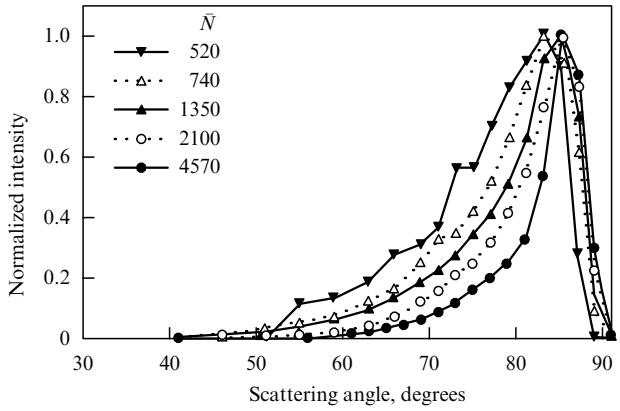

Figure 6. Influence of the incident cluster size on the angular distribution of negative cluster ions emitted during scattering of $(H_2O)_N$ clusters from a graphite surface. Mean cluster size $\overline{N}$ in the incident beam is indicated in the figure frame. Angle of incidence is 71°. Surface temperature amounts to 1450 K [197].

of negative and positive charges was conserved. The authors arrived at the conclusion that the separation of charges was due to the capture of a neutral (but readily ionizable) alkali metal atom from the surface by a cluster during its collision, delocalization of a valence electron of this atom inside the cluster, and impact-induced disintegration of the cluster into charged fragments (see Fig. 5).

The experiments were also carried out with many other molecular clusters and gas-carriers (Ne, Xe, Kr) [195]. The clusters collided with the surfaces of metals and insulators. Collisions of clusters involving nonpolar molecules (O_2, N_2, CO_2, SF_6) failed to produce charge separation. In contrast, all clusters of polar molecules (H_2O, SO_2, NO, NH_3, NO_2, SF_4, CH_3CN, $CHClF_2$, and isobutane) underwent decomposition into positively and negatively charged fragments as they impacted on the surface. This suggested the primary importance of the constant dipole moment of the molecules that constituted the clusters. The authors chose to experiment with the SO_2 molecules as chemically stable ones, permitting them to avoid the difficulties associated with the presence of hydrogen bonds and autodissociation [374]. Moreover, SO_2 clusters are easy to obtain during the gas outflow from a nozzle at room temperature. Unlike small NH_3 or H_2O clusters characterized by low electron affinity [376], the electron affinity of the SO_2 molecule approximates 1 eV [377]. This markedly facilitates the formation of stable anions of a cluster. The results obtained in Ref. [195] were used by the authors to offer quite a different explanation for the production of positively and negatively charged fragments upon the collision of SO_2 and H_2O clusters with a surface. The mechanism of formation of charged fragments, proposed by the authors, appears to be of a general character and to apply to all clusters of polar molecules.

Concluding this section, we shall briefly consider the results of experiments reported in Refs [197, 363, 368, 378]. These studies examined collisions of large water clusters ($N \leqslant 4600$ [197, 363], $\overline{N} = 3800$ [368], and $N \cong 1.4 \times 10^4$ [378]) with a hot graphite surface ($T_s \leqslant 1400$ K) at a collision velocity of 1380 m s^{-1}. It was shown in Ref. [363] that the scattering process at high surface temperatures is well described by a thermokinetic model [358] (see Section 4.3) which postulates the evaporation of fragments from parent clusters sliding over the surface. At a low surface temperature, the clusters are slowed down by friction forces till they are completely evaporated. In this case, the clusters are mainly destroyed via evaporation of monomers whose angular distributions are close to cosine ones. It was shown in Ref. [197] that collisions of water clusters with a surface induce the emission of large negative cluster ions concentrated within angles close to tangential. When clusters are normally incident, the reflected ions concentrate near the normal to the surface. Time-of-flight measurements and analysis of the energy of negative ions allowed the velocities and the sizes of cluster ions to be determined. It turned out that clusters interacting with the surface retain 65–80% of the velocity component parallel to the surface, whereas the normal component ranges 75–100 m s^{-1} and does not depend on the angle of cluster incidence upon the surface. The surface temperature in the range of interest does not practically affect the angular distributions of cluster ions, but they are markedly displaced toward tangential angles as the cluster size increases (see Fig. 6). The clusters experience strong fragmentation as they collide with the surface; in the case of clusters containing thousands of molecules, approximately 0.15–0.25 part of a cluster survive in the form of a small single fragment scattered in the tangential direction.

Results of experiments and model calculations conducted in Ref. [368] indicated that two processes predominate in cluster scattering — one being direct inelastic cluster scattering from the surface, the other desorption of clusters trapped at the surface. The trapped clusters were rapidly heated by the

surface and evaporated. The authors concluded that the formation of charged fragments observed in earlier experiments where water clusters interacted with the surface occurred via the adsorption – desorption channel. The possibility of cluster trapping by the surface at $T_s \geqslant 700$ K was also reported in Ref. [378]. The trapping was followed by desorption in the course of strong fragmentation due to surface heating. In addition, the clusters were inelastically scattered from the surface, their kinetic energy being converted into the internal degrees of freedom. As a result, only insignificant fragmentation of the clusters took place. The authors of the cited publication arrived at a conclusion similar to that made earlier in Ref. [368], namely, the formation of charged fragments during water cluster scattering from a solid surface occurs via the adsorption – desorption channel.

4.5.2 Results of model calculations. Theoretical computations help to better understand experimental findings, as well as the processes of energy transfer to the internal degrees of freedom during collisions of clusters with a surface. The process of water cluster scattering from a solid surface was simulated in Ref. [369] based on the computations along classical trajectories. It was assumed that the clusters had an internal temperature of 180 K. The collision velocities ranged from 400 to 2000 m s^{-1}. The objective of the research was to examine the energy transfer process for $(H_2O)_N$ clusters ($N = 20$, 40, 80, and 123). In the majority of cases, the calculations were made for clusters with $N = 123$. It is worth mentioning that this was the first study on the process of energy transfer in clusters containing hydrogen bonds. The main attention was given to the evaluation of the efficiency of energy transfer from the translational motion of the clusters into their internal degrees of freedom. The study assessed the role of the internal water potential and of cluster size and velocity in the efficiency of energy transfer, as well as the process of cluster fragmentation resulting from the collisions between the clusters and the surface. The calculations were made over a wide range of cluster energies — from low ones at which the fragmentation was negligibly small to energies at which very strong fragmentation occurred. The computations were performed using three different intramolecular potentials (one harmonic and two anharmonic) that were functions of the distance between oxygen and hydrogen atoms and of the bond angle attached to the oxygen atom. The surface – water molecule interaction potential consisted of two parts, each taking into account the interaction between an oxygen atom and hydrogen atoms. The initial conditions were such that the clusters were 15 or 30 Å distant from the surface where the potential energy of cluster – surface interaction almost vanished. Classical particle trajectories were computed on a time scale up to 5 or 10 ps. This time was sufficient for the clusters to completely leave the surface and for the process of their relaxation to the final state to occur.

Setting aside the analysis of the form and parameters of the potentials used in the computation, we shall consider the main results obtained in the work of interest. They give a fairly good idea of the process of cluster scattering from a solid surface. Specifically, the outcome of the scattering largely depends on the cluster energy and coupling strength between different degrees of freedom. The general tendency resides in the following. The translational motion of molecules inside the cluster is strongly coupled to the surface, which results in the compression of the cluster and elevation of its temperature to 500 – 600 K at a collision velocity of around 1300 m s^{-1}. An impact of the cluster on the surface triggers the partial transfer of the translational energy to the rotational degrees of freedom of its molecules and thereafter to intramolecular vibration of the bending mode. The rotation of a molecule is also coupled to the surface potential. The behavior of stretch modes is critically dependent on what intramolecular potential is used in the computation. The cluster having left the surface, the energy becomes distributed over all the degrees of freedom in an equilibrium manner, which leads to the thermal evaporation of molecules from the cluster.

A change in the cluster size, initial temperature, intramolecular potential, and cluster – surface interaction potential has no influence on the qualitative characteristics of surface collisions. The sole parameter being altered is the efficiency of the total energy transfer from the kinetic energy of the cluster's center of mass to other degrees of freedom. As the cluster is decelerated upon impact on the surface, the translational energy converts to the surface potential energy and the internal excitation of the cluster. After the return point is reached, almost all surface potential energy transforms to the center-of-mass translational energy, when the cluster leaves the surface. In this case, the fraction of the total energy that exists as the surface potential energy at the return point will limit the transfer of the total energy from the translational degrees of freedom to the internal degrees of freedom. This outgrowth explains all the effects associated with a change in the cluster size and the interaction potential. For the typical parameters of the model, the efficiency of energy transfer from the translational motion of the cluster's center of mass amounts to approximately 80 – 90% (see also Section 5.2). Dynamic effects also appear to be important. Specifically, clusters contract in the direction of the normal to the surface as they hit the surface and simultaneously undergo ordered expansion – compression motions in the surface plane. The incidence velocity determines the total cluster energy. When it is lower than 1300 m s^{-1}, the probability of cluster fragmentation is very small. The degree of fragmentation rapidly increases at incidence velocities above 1300 m s^{-1}.

The scattering of water clusters from a surface is in many respects analogous to that of clusters with van der Waals bonds [143, 236, 354, 365, 366]. The main difference is due to the different strengths of the respective bonds. Thus, for cluster fragmentation to occur, the higher stability of water clusters (owing to their hydrogen bonds) compared with van der Waals clusters displaces the corresponding energy scale to the higher energy region. Additional minor differences are introduced by the different dependence of the interaction potential in water molecules inside the cluster on the bond angle attached to the oxygen atom.

A water cluster is not so readily compressed upon collision with a surface as an atomic van der Waals cluster is [365]; in the latter, the motion of atoms does not require large potential barriers to be overcome. Strong hydrogen bonds act so as to conserve the initial cluster structure that determines specific features of fragmentation dynamics. The intramolecular degrees of freedom have no appreciable effect on collision dynamics, which makes the two systems more similar to each other. The efficiency of energy transfer in water clusters is also comparable to that in van der Waals clusters [365], while the differences appear to be mostly due to peculiarities of the gas – surface interaction potential.

The calculations conducted qualitatively describe the behavior of neutral particles in scattering experiments with water clusters [191 – 194]. The separation of charges in the liquid phase effectively occurs in the case of laser-induced vibrational excitation of water molecules [379]. The first excited vibrational state of water possesses an energy close to the activation energy (0.6 eV) of protolysis [379]. The authors attributed the production of positive and negative charges [190 – 193] to the vibrational excitation of molecules during collisions of water clusters with the surface.

Reference [370] reports on a dynamic study of collisions of large water clusters ($N = 1032$, 4094) with a graphite surface at velocities from 200 to 1000 m s^{-1} and a cluster temperature of 180 K. The results obtained are in excellent agreement with those presented in Refs [197, 363, 368]. It turned out that an impact on the surface triggers adsorption – desorption processes, together with direct scattering channels. In particular, clusters with $N = 1032$ molecules are trapped by the surface and undergo complete fragmentation due to evaporation. Clusters with $N = 4094$ are partly conserved after collisions if the surface temperature is high enough ($T_s \geqslant 600$ K). They are trapped by the surface and remain on it for up to 50 ps. Thereafter, the clusters leave the surface. These events are accompanied by intense evaporation of small fragments from the cluster surface. The sizes of the clusters emitted from the surface are 15 – 25% of those incident upon it. The time spent by the clusters at the surface depends on their size and incidence velocity. The larger the cluster and the lower the velocity of its incidence upon the surface, the longer it stays on it.

4.6 Summary

The results of the studies reviewed in this section indicate that collision dynamics of van der Waals clusters impacted on a surface in the case of moderate (thermal) energies can be interpreted in the following way. The clusters are involved in inelastic collisions, when they are sliding over the surface as if being suspended above a gas cushion. Small particles evaporated from them are in thermal equilibrium with the parent clusters. There are two more scattering channels in addition to this main evaporation channel. One is diffusion of atoms involved in the adsorption – desorption processes off the surface, and the other is the sliding component of large and slow fragments survived after collisions.

The evaporation channel is well described by a thermokinetic model [358] that postulates thermal evaporation of small particles from the surface of a cluster having temperature T_{loc} and travelling over the target surface with velocity $c_f v_{\|}$, where c_f is the coefficient of conservation of the velocity component parallel to the surface. Parameters T_{loc} and c_f can be derived from the angular distributions and time-of-flight spectra of the particles being evaporated. This model fairly well describes the results obtained in studies on the scattering of uncontaminated and mixed clusters from the surface over a broad range of experimental conditions [366, 380] (see also Refs [381 – 383]). The sliding component of the scattering of large van der Waals clusters from the surface is equally well described by the dynamic zone structure model [359].

A peculiar feature of the scattering of molecular water (and also SO_2) clusters by a solid surface is the possibility of vibrational and rotational excitation of scattered particles. Specifically, the scattering of water clusters from solid surfaces at collision velocities $\geqslant 1000$ m s^{-1} is probably accompanied by the formation of positively and negatively charged ions due to vibrational excitation of the molecules and initiation of the autoprotolysis reaction. At the same time, there is found quite a different channel for the formation of positive and negative ions at the collisions of clusters involving polar molecules with a surface. Hence the necessity of further experimental studies to obtain a deeper insight into the mechanisms of production and separation of charges during collisions of water clusters with a solid surface.

5. Impact of high-energy clusters on a surface

5.1 Emission of electrons

One of the processes accompanying collisions of high-energy clusters and cluster ions with a solid surface is exemplified by the emission of electrons [198 – 215] and other charged and neutral particles (atoms, molecules, clusters) [215, 384, 385]. The particles are emitted from either side of the surface (input and output with respect to the incident beam) if it is represented by a thin foil (5 – 300 nm in thickness) [211, 215]. The mechanisms of particle emission resulting from the bombardment of solids by clusters are in many respects analogous to the mechanisms acting when atomic [386, 387] and molecular [384, 388] ions impinge on a solid surface. It is worth noting that the emission of particles at the collisions of fast ions with a solid has long been the focus of extensive research (see, for example, review articles [388 – 394]). A wealth of similar studies was devoted to the electron emission [198 – 215, 384, 386, 387] which is the subject matter of the present section.

Studies on the emission of electrons and ions from a solid body provide information about the mechanisms of interaction between high-energy particles and atoms or electrons of target materials, mechanisms of deceleration of incident particles inside a solid body, mechanisms of channel formation and destruction of target materials, and ionization mechanisms of the target's atoms and colliding particles. Also, the emission of electrons may be used to study electronic properties of solids. Moreover, particle emission studies have important practical implications. The process of electron emission from solid surfaces underlies the work of particle detectors. Hence the special importance of electron emission studies in connection with the development of methods for the detection of large biological molecules, as well as low-energy particles of cosmic dust (fogs) [215, 384]. Emission of electrons is routinely employed in mass spectrometry for the detection of ions. It plays an important role in maintaining gas discharges and in such effects as electrization of spacecraft and other bodies in space.

It needs to be emphasized that, unlike collisions of fast atomic ions with a surface, the impact of high-energy clusters results in a situation where a large number of atoms fall practically at one time on a small surface area. This accounts for the concentration of substantial energy in the impact zone. A collision of a high-energy cluster with a surface provides in essence a unique possibility to reach a very high concentration of energy at a small portion of the surface ($\leqslant 5 – 10$ nm^2 in area) in conjunction with an extremely high power density ($\geqslant 10^{16}$ W cm^{-2}). Such a collision, similar to that of a polyatomic ion, results in the superposition of processes accompanying the impact of a single atomic ion on the surface. These processes may give rise to cooperative as well as temporal and spatial coherent effects. Due to these effects, the rates and the yields of the processes associated with cluster

impingement on the surface may be considerably different from those observed during collisions of single atomic ions. The nature and the mechanisms of electron emission, the methods of its investigation, and selected results obtained in the studies of interactions between clusters and surfaces are considered in Sections 5.1.1 – 5.1.3.

5.1.1 Character and mechanisms of electron emission. Emission of electrons from solid surfaces, resulting from their interaction with impacted atomic and molecular ions, has been fairly well studied in both theory and experiment (see, for instance, review articles [384, 393 – 396]). The results of these studies indicate that electron emission is a very complicated process due to the existence of multiple mechanisms and specific features of electron emission from a solid surface and from the surfaces of colliding clusters. These mechanisms depend on the cluster type (elemental composition), velocity, charge, and size, as well as on the type, structure, and cleanness of the surface [215, 386]. Surface-bombarding atomic, molecular, and cluster ions may knock electrons out of a solid body via two processes — one requiring kinetic energy that is transferred to the surface atoms and electrons in the course of binary collisions (kinetic emission), and the other using potential energy released during Auger neutralization or deexcitation (potential emission) [384, 386, 387]. The total yield of electrons is the sum of these two contributions: $\gamma_{\rm tot} = \gamma_{\rm PE} + \gamma_{\rm KE}$.

5.1.1.1 Potential emission. The potential emission of electrons occurs by virtue of radiationless processes of Auger neutralization and ion deexcitation near a solid surface [384, 386, 387]. As an atomic particle approaches the solid body, it interacts with it, giving rise to a variety of electron transitions. When the colliding particle has a large internal energy and moves with a velocity higher than the thermal velocity ($E_{\rm col} \geqslant 5-10$ eV), the predominant processes are resonant and Auger transitions [384, 386, 387]. In such a case, the probability of radiative transitions proceeding in a time of around 10^{-8} s is rather small because the interaction time between the particle and the surface is several orders of magnitude shorter. If an incident particle has a vacant energy level lying below the Fermi level in a metal, the particle – metal system may be regarded as excited, and this excitation can be removed [215, 384, 386, 387] with the aid of the Auger effect. The removal is accompanied by the transition of one of the electrons to the vacant level, while the energy thus released is transferred to another electron. It may be either the second electron of the metal or the electron previously resided in the particle's excited level. The latter case is realized when the excited atom impinges on the surface or when the bombarding particle is represented by an ion that first experienced resonant neutralization (resonant transitions are more likely to occur provided the corresponding levels are available). Thus, the potential emission of electrons may occur from both the solid surface and the surface of the colliding particle.

The maximum energy that is released in the above process and can be transferred to the second electron equals $E_{\rm i} - U$, where $E_{\rm i}$ is the energy of ion ionization or excitation, and U is the minimal electron binding energy in a solid. In metals, $U = \Phi_{\rm w}$, where $\Phi_{\rm w}$ is the work function, and in insulators, $U = \chi$, where χ is the electron affinity. Electrons are ejected from a solid into a vacuum when the condition $E_{\rm i} - U > U$ is fulfilled. Consequently, there is a threshold excitation energy ($E_{\rm i} \geqslant 2U$) in the case of the potential emission of electrons, but such a threshold is absent for an ion velocity even though the velocity dependence can be manifested when different deexcitation mechanisms compete between themselves, especially when the size of the molecular ions is small [384]. Paper [390] suggests an empirical relation for the electron escape from metals in the case of potential emission induced by the collision of an atomic ion:

$$\gamma_{\rm PE} \approx 3 \times 10^{-2}(0.8E_{\rm i} - 2\Phi_{\rm w})\,. \tag{5.1}$$

It follows from this relation that the quantity $\gamma_{\rm PE}$ is small (smaller than unity) for the majority of singly charged ions. The higher the ionization energy of the colliding particle and the smaller the work function of the target material, the larger the potential emission yield.

Gross potential emission yields may be achieved during collisions of multiply charged atomic or cluster ions with a surface. In the case of quasiresonant capture of electrons from the target, the atomic ions undergo recombination and become multiply excited 'hollow' atoms (atoms with unoccupied or partly occupied inner electron shells) [397] which subsequently emit electrons owing to autoionization. Because the said autoionization and neutralization processes proceed very rapidly (for times $\leqslant 10^{-14}$ s), one and the same multiply charged ion possessing a high internal energy may undergo several recombination and autoionization cycles while it interacts with the surface. Autoionization of 'hollow' atoms usually makes a major contribution to potential emission [398].

Similarly to atomic ions, multiply charged molecular and cluster ions impinging upon a solid surface also give rise to 'hollow molecules' or 'hollow clusters' [212, 213]. However, their subsequent deexcitation does not necessarily occur in the same manner as that of atomic ions. The acquired potential energy may undergo rapid redistribution due to internal conversion [399] between numerous vibrational modes, which leads to the strong heating of colliding particles. This results in delayed emission of electrons (see Section 5.1.1.3). For example, a C_{60}^{5+} cluster that hits a gold-coated surface ($\Phi_{\rm w} = 5.1$ eV) delivers enough energy (around 50 eV) to ensure a high yield of potential emission. A 'hollow atom' with such an internal energy makes an important contribution to the potential emission yield [398]. At the same time, a number of experiments [208, 209, 212, 213] failed to document potential emission from slow 'hollow fullerenes', including the C_{60}^{5+} cluster (see also Section 5.1.3).

5.1.1.2 Kinetic emission. When the velocity of an incident particle is high ($v \geqslant 10^7$ cm s^{-1}, $E_{\rm col} \geqslant 50$ eV per atomic mass unit), kinetic emission of electrons from a solid surface prevails [213, 215, 384]. At such velocities, polyatomic particles (molecular and cluster ions) undergo fragmentation when they hit a target and penetrate into its material [215] (see also Section 5.7). Electron emission from a solid body is induced by each individual fragment formed as a result of collisions. The electron emission yield depends on the mechanisms of particle interaction (atom – atom or atom – electron collisions) and deceleration (atomic or electronic stopping). Excited electrons arise along the entire particle's path in a solid body; however, they are emitted to a vacuum only from a small zone of depth $\lambda_{\rm e}$ that is only several times (2 – 5) larger than the mean free path of electrons in a solid. The electron mean free path in metals and semiconductors varies approximately from 0.5 to 2 nm. It is significantly

longer on the average in insulators where free electrons are absent. Therefore, the depth of the region from which the electrons are ejected amounts to 100 nm [215].

Kinetic emission is usually described as a process proceeding via the following three stages [215]: (1) production of excited electrons; (2) transport of free electrons within a solid, including their multiplication, and (3) passage of electrons through the surface potential barrier. The excitation of electrons can result from a variety of processes that can be divided into direct collisions of incident particles with atoms and electrons of a solid body, and secondary processes. The former include excitation of 'free' valence electrons of the solid during binary collisions of the incident particle with electrons, ionization of inner electron shells of atoms in the target, and ionization of the incident particle itself. They can also include the loss of electrons from the bombarding particle if it does contain electrons. The secondary processes comprise cascade multiplication of primary electrons inside the target material, excitation of the target electrons by reflected atoms or a backscattered projectile following its collision with target atoms, one-electron decay of plasmons, and Auger decay of electronic excitation from the inner electron shells in the projectile and in the target atoms [215]. Unlike potential emission, kinetic emission of electrons is characterized by a collision velocity (kinetic energy) threshold. Kinetic emission takes place when the energy released in a particle collision with the surface is at least higher than the work function of an electron leaving the target material. In the framework of the free electron model, the threshold velocity can be found from the relation [215]

$$v_{\rm th} = v_{\rm F}\,\frac{1}{2}\left[\left(1+\frac{\Phi_{\rm w}}{E_{\rm F}}\right)^{1/2}-1\right], \qquad (5.2)$$

where $v_{\rm F}$ and $E_{\rm F}$ are the Fermi velocity and energy of the electrons, respectively. For the majority of metals, where $\Phi_{\rm w} = E_{\rm F}$ and $v_{\rm F} \approx 10^8$ cm s^{-1}, the threshold velocity $v_{\rm th} \approx 0.2 v_{\rm F} \approx 2 \times 10^7$ cm s^{-1}, while the energy threshold is about 200 – 250 eV per atomic mass unit. However, kinetic emission of electrons may occur below this threshold, too [213, 215]. It is probably due to quasimolecular autoionization in close collisions between a neutral incident particle and the target ion nucleus that becomes the predominant source of kinetic emission at velocities below the threshold ones [215]. The electron yield in the case of kinetic emission may be very high compared with that in potential emission, namely, from one to several dozen electrons per colliding ion [213 – 215].

5.1.1.3 Thermal electron emission. When large clusters or polyatomic molecules (and also their ions) impinge upon a solid surface, one more type of electron emission is possible, namely, thermal electron emission [198 – 206]. Tightly bound clusters that hit the surface at moderate velocities ($v \leqslant 10^6$ cm s^{-1}, $E_{\rm col} \leqslant 0.5$ eV per atomic mass unit) are strongly heated during collisions (up to 3000 – 5000 K); nevertheless, they are scattered by the surface as indestructible. It was shown in Section 4 that van der Waals clusters hitting a surface undergo fragmentation at as low an energy as $E_{\rm col} \leqslant 0.5$ eV per atom. Unlike them, clusters of metals, semiconducting materials, or carbon, having strong bonds, withstand collisions with solid surfaces without fragmentation at energies of up to $E_{\rm col} \approx 10$ eV per atom (see also Section 5.7). This energy is comparable with the damage threshold of a solid (2 – 10 eV). Such clusters bounce off the bombarded surface in a strongly excited state. The subsequent process of their dissociation is described by the theory of unimolecular decay [400], according to which large excited clusters live rather long prior to dissociation. This accounts for a possible delay of fragmentation (dissociation) and ionization of the clusters. Such an ionization is a cause of delayed emission of electrons (thermal electron emission) [399]. The ionization and fragmentation processes may compete between themselves and influence each other.

Finally, it is worthwhile emphasizing that the collision of high-energy particles with a solid surface can also induce excitation of their constituent atoms or molecules into autoionizaton states. The subsequent decay of these states may likewise cause electron emission both from the collision zone at the instant of impact and from the scattered particles.

5.1.2 Methods for studying electron emission. The processes of potential emission do not last longer than the typical time $\sim 10^{-13}$ s [401], and subsequent (later) processes of kinetic emission of electrons are completed within $10^{-12} - 10^{-11}$ s [402, 403]. In other words, both potential and kinetic emissions of electrons induced by collisions of bombarding particles with a surface constitute rather fast processes. Electrons produced as a result of potential and kinetic emissions reach the detector in a time shorter than the detector's time resolution, i.e., usually $\geqslant 10^{-9}$ s. Thermal electron emission from a scattered cluster may last as long as several microseconds [198 – 200, 399]. Moreover, it is worth noting that the dimension of the region where the potential and kinetic emissions of electrons occur is rather small ($\leqslant 2-5$ nm for kinetic emission). The thermal electron emission is possible even at a long path of an excited cluster scattered from a solid surface. This means that different methods are needed to measure electron emissions of these two types.

Thermal electron emission is most often measured by the time-of-flight method using time-of-flight mass spectrometers [198 – 207]. Such measurements allow one to obtain the distribution of emitted electrons over energies [198, 199], the rate of emission [200], and the emission's quantum yield [207].

Potential and kinetic emissions are investigated by different methods [208, 209, 404 – 406]. The problem of distinguishing between potential and kinetic emissions needs to be resolved if their mechanisms are to be understood. The available experimental techniques for the measurement of the electron emission yield during collisions of atomic or ionic clusters with a solid surface make it possible to distinguish between the contributions from potential and kinetic emissions [407]. To this effect, the total emission yield is measured in experiments taking into consideration statistics of emitted electrons [208, 209, 404 – 407]. The experimental methods also permit us to determine the upper threshold energy for kinetic emission. As shown in Section 5.1.1.2, it is not necessarily coincident with the energy threshold for kinetic emission, found based on the direct energy transfer from a colliding particle to valence electrons of the surface material [407].

Figure 7a depicts the layout of the experimental setup for the measurement of potential and kinetic emissions of electrons. In experiments measuring the emitted electron statistics, the intensity of a flux incident upon the target surface must not be higher than a few thousand particles per second. This constraint permits increasing the time between collisions of individual ions with a surface and separately

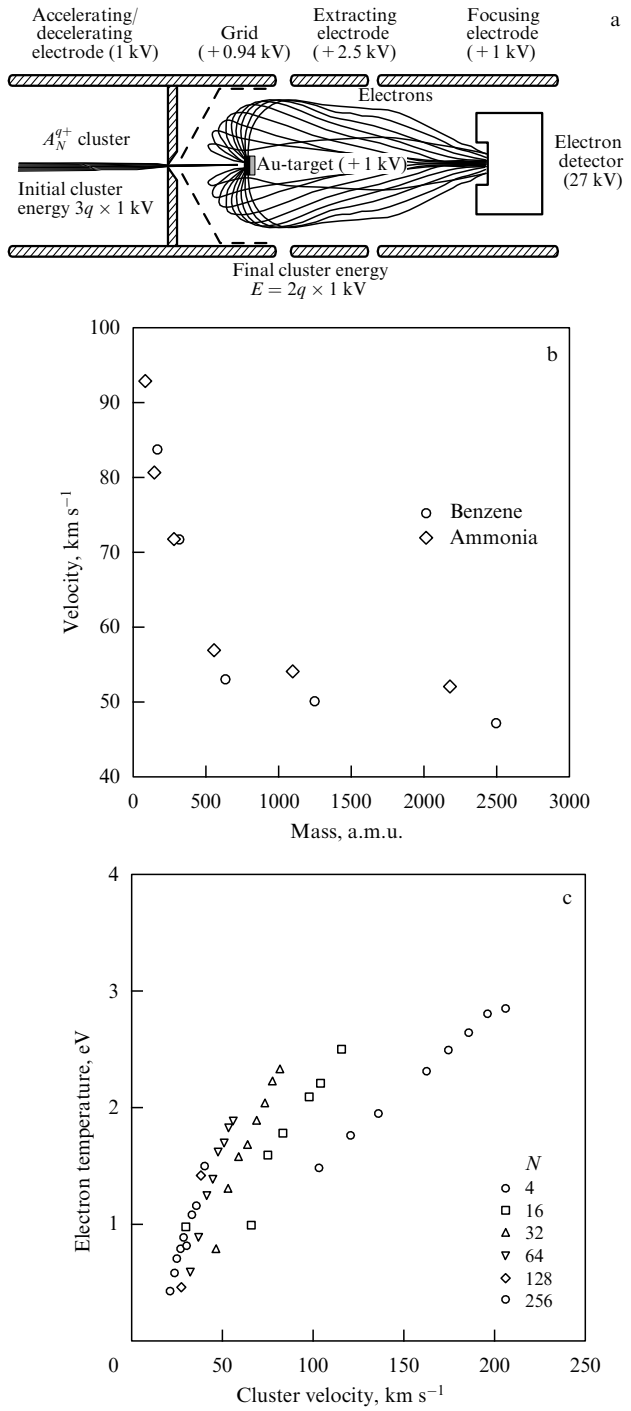

Figure 7. (a) Schematic of the experiment for measuring electron yield statistics [209]. (b) Cluster velocities necessary for inducing emission of electrons with a temperature of 2 eV depending on the cluster mass. Collision energy is 12.8 keV. Protonated ammonia $(NH_3)_N H^+$ clusters and benzene $(C_6H_6)_N^+$ ion clusters impinged upon a gold-coated surface. (c) Plots of electron temperature versus cluster size and velocity. Protonated ammonia $(NH_3)_N H^+$ clusters collided with the gold-coated surface. The number of molecules in a cluster is shown in the inset. The collision energy range is 2 – 13 keV [207].

measuring signals induced by each colliding ion. Practically all electrons with an energy smaller than 60 eV, emitted by the target and also by an ion located near the target surface into the front hemisphere, are turned back by an electric field, accelerated, and delivered to the detector with a surface potential barrier. The electron-turning field is an electric field applied between the 96%-transparent conical grid and the target. The electron detector is kept under the potential of 26 kV with respect to the target. The time resolution of the recording system amounts to $\geqslant 10^{-6}$ s [209, 404, 405]. As a result, n electrons emitted as a consequence of the collision of an individual ion with the surface are registered as a separate electron with energy $n \times 26$ keV. Hence, c_n areas under each nth peak of the thus measured signals (proportional to the total number of countings) are directly related to the probability W_n of emission of n electrons. The relationship between W_n and the total number of electrons emitted upon the collision of a single ion with the solid surface is established by the expression [209, 404, 405, 407]

$$\gamma = \sum_{n=1}^{\infty} n W_n \,, \qquad \sum_{n=0}^{\infty} W_n = 1 \,. \tag{5.3}$$

The probability W_0 of emission of no electrons in the experiments under consideration is usually low and may be neglected given that electron yields are relatively high ($\gamma \geqslant 3$) [406].

Potential emission can be distinguished from kinetic emission by two methods. First, potential emission occurs at relatively small velocities $v \leqslant 10^6 - 10^7$ cm s^{-1}, too low for kinetic emission to begin. Second, kinetic emission grows rather rapidly with increasing collision velocity, provided it is sufficiently high ($v \geqslant 10^7$ cm s^{-1}), whereas potential emission of electrons is less sensitive to the collision velocity. Its contribution to the total signal constitutes a 'constant background' that can be easily separated from the total signal measured by the electron number statistics method [407].

5.1.3 Experimental results. The main objectives of experimental studies include not only elucidation of mechanisms of electron emission but also direct measurements of its yield and rate, as well as the evaluation of the dependences of these parameters on the type, composition, charge, and size of clusters along with the properties and composition of the surface material. One more important characteristic is the dependence of the electron yield γ_N on the number of atoms in a given cluster. The measure of this characteristic is usually specified by the ratio R_N (normalized to a single particle) of the yield of electrons from the cluster to their yield from a unit constituent particle of the cluster [210, 211]:

$$R_N = \frac{\gamma_N}{N\gamma_1} \,. \tag{5.4}$$

Cooperative effects may differently influence the electron yield depending on the velocity, structure, and bonding type (atomic, molecular, van der Waals, or metal-specific) of a colliding cluster and on the structure, purity, and composition of the surface material. This accounts for the observation of both nonlinear ($R_N > 1$ or $R_N < 1$) and linear ($R_N = 1$) dependences of electron yields. Of special interest is the determination of the fraction of cluster kinetic energy transformed into the energy of the internal atomic (molecular) motion upon collision of the cluster with the surface; this parameter has a marked effect on the electron yield.

Electron emission induced by collisions of high-energy clusters with a surface was first reported in the paper [198] (see also Ref. [199] by the same authors). These publications offer a qualitative explanation of the effect observed. High-energy molecular clusters were produced during the outflow of

molecules from a pulsed nozzle in a mixture with a light gas-carrier (helium). The velocity of helium atoms outflowing from the nozzle at room temperature approached 1600 m s^{-1}. At such a velocity, the energy of a cluster with a mass of 600 a.m.u. was roughly 10 eV. The experiments were carried out with C_6H_6, CCl_4, and CH_3CN molecular clusters. Electron emission was induced when polycrystalline surfaces of Cu, Ni, and Al and an Si single crystal were bombarded by clusters. The crystals rested on a manipulator housed in a high-vacuum chamber where the pressure was maintained at about 10^{-8} Torr. The chamber was equipped with an X-ray spectrometer, electron and argon ion guns, and an electron energy analyzer. The energy of emitted electrons was measured with a spectrometer having a resolution power of about 0.3 eV. The electrons themselves were detected with the help of a multichannel counter.

Emission of electrons was observed from all studied surfaces. Their energy distributions were roughly similar within the limits of experimental accuracy. The relative electron yields decreased in the following order: Ni > Cu, Al > Si. The absolute electron yields were impossible to measure because the distribution of neutral clusters over masses in the initial beam was unknown. Also, the electron emission strongly depended on the type of molecules constituting the cluster. For example, benzene clusters induced less intense signals than CCl_4 or CH_3CN clusters. Moreover, it was found that bombardment of uncleaned surfaces resulted in a 20% higher yield of electron emission than for clean surfaces.

The distribution of electron energies measured by the authors was fairly well described by the dependence

$$Y = Y_0 \exp\left(-\frac{E - \Phi_w}{kT_s}\right) \quad (E \geqslant \Phi_w),$$

where Y is the electron yield, Y_0 is the yield at $E = \Phi_w$, E is the electron energy, Φ_w is the work function, and T_s is just the surface 'temperature' determined in the experiment. Measurements taken with the use of a CCl_4 cluster beam gave the surface temperature $T_s \cong 5000$ K; it was also found to be weakly dependent on the gas pressure above the nozzle and the surface material.

The authors accounted for the observed effect by the fact that the energy of colliding clusters was partially transferred to the atoms of the surface, which resulted in its heating. As distinct from the collisions of single molecules with the surface when it derives only a small fraction of the arriving energy (about 1% [408]), a substantially larger fraction is acquired by the surface as clusters impinge upon it. This phenomenon is related to stronger resonant coupling between low-frequency cluster vibrations and the vibrational frequencies of surface atoms as compared to that of free molecules, especially if they are high-frequency ones. The authors believe that at an interaction distance between the cluster and the surface of approximately 1 Å, the force acting on a cluster flying with a velocity of roughly 1600 m s^{-1} contains frequency components of up to 1.6×10^{13} s^{-1}, which are significantly higher than typical van der Waals frequencies but hardly reach lattice vibration frequencies [409]. For this reason, 'phonons' of the van der Waals cluster may be strongly excited, the collision energy may be absorbed, and the colliding clusters may undergo deformation. However, the surface deformation is limited because the frequency of the surface phonons is higher.

It is pertinent to note that the study considered was the first to establish electron emission during collisions of molecular clusters with a surface at the kinetic energy of the clusters in excess of the work function of metals or semiconductors. The authors emphasize that although emission of electrons during certain processes was reported in an earlier publication [410], the induction of electrons by collisions of high-energy clusters with a solid surface had never been observed before; they can be named exoelectrons.

Thus, on the one hand, the emission of electrons by excited atoms or molecules develops almost instantaneously (in a time $\leqslant 10^{-16}$ s) [200]. On the other hand, thermal emission of electrons from the surface of condensed matter (e.g., tungsten filament) is characterized by activation rates that gradually increase with increasing excitation energy and temperature. The statistical theory of thermal electron emission usually suits well the microscopic description of this process [411]. Investigations with the use of clusters demonstrated slow electron emission from tightly bound atomic clusters, including those of tungsten [201, 202], carbon [203, 204], and silicon [205, 206]. The results of these studies reveal that delayed electron emission is a simple activated process that depends on the cluster internal energy and size and has a common mechanism. However, the Arrhenius formula derived for the rate of electron emission in clusters is inconsistent with the formula for the rate of emission from the surface of bulky media. These results have implications for the correct quantitative microscopic description of the observed electron emission process in clusters.

One study [200] was designed to examine the dependence of the emission rate on cluster energy and temperature in order to elucidate the nature of electron emission rate and thus to develop a correct microscopic theory. The experiments were carried out with carbon clusters. It was found in the course of the study [200] that the emission of electrons at a collision velocity of less than 14 km s^{-1} occurred from scattered undestroyed negatively charged clusters. The rate of electron emission was examined as a function of the collision energy for clusters of different sizes ($N = 58$, 60, 70, 80, and 96). It was shown to strongly depend on both the energy and the size of the clusters. The emission was also observed for rather a high duration following a cluster impact on the surface. It was found in addition that the emission rate was not fully exponential. These findings reflect the fact that the internal energy of the clusters after their collisions with the surface was spread within a certain range.

It was established in the paper [200] that the rate of electron emission as a function of the collision energy is fairly well described by the Arrhenius formula

$$k(E_i) = A \exp\left(-\frac{E_a}{\lambda E_i}\right), \tag{5.5}$$

in which the collision energy E_i plays the role of the temperature parameter, while preexponent A and activation energy E_a have the usual meanings. The linear dependence of $\log k$ on $1/E_i$, obtained in Ref. [200], confirms that the process of interest is actually an activated one and that it is the collision energy that determines the cluster temperature. The activation energy for electron emission is evidently equal to the electron affinity for C_{60} or C_{70} molecules (2.65 eV [412]). The dimensionless parameter λ in relationship (5.5) characterizes the conversion of the collision energy to the effective temperature ($k_B T$) of a molecule: $\lambda = s/\alpha$, where $\alpha = U/E_i$ is the fraction of the collision energy transferred to the cluster's

internal energy, and $s = 3n - 6$ is the number of vibrational modes in the molecule. The value of $\alpha \cong 0.5$ was found from the experimentally obtained slope and the known electron affinity. This is the limiting value for large clusters. Quantity α ranges from 0.1 to 0.15 for medium-sized molecules, and from 0.15 to 0.3 for bigger colliding particles composed of essentially larger number of atoms.

It was established in the work [200] that the electron emission rate at a fixed collision energy substantially tapers off with decreasing cluster size. This observation is equally easy to explain with the help of the Arrhenius formula. In this case, the process-controlling parameter is the collision energy per atom. All the dependences obtained in this experiment intersect the abscissas axis at approximately one and the same level close to 10^8 s^{-1}. This suggests a similar (common) mechanism underlying the process under consideration. However, this value is at variance with the predictions of the statistical theory of thermal electron emission from metallic surfaces [200]. The authors demonstrated that the statistical theory of electron emission rate is unfit for the description of electron emission from negatively charged fullerenes. The authors hypothesized that the energy released as a result of cluster impact on the surface is transferred to the cluster's vibrational degrees of freedom. Therefore, the process limiting the electron emission is probably the energy transfer from vibrations to electronic excitation. In this case, the preexponent must include an electronic – vibrational coupling constant of approximately 10^{-8} s, which is in agreement with the experimentally obtained result.

Detailed studies of electron emission induced by collisions of high-energy molecular clusters with a surface were reported in Ref. [207]. Charged clusters selected by mass were accelerated in a linear accelerator to speeds of 3 – 100 km s^{-1}. The measured parameters included the electron emission quantum yield and the distribution of kinetic energies. The results permitted assessing the degree of conversion of the ion kinetic energy to the internal energy.

The clusters were produced by means of supersonic expansion of a light gas-carrier containing so much molecular gas and charged by electron impact. The experiments were carried out using positively charged benzene clusters comprising up to 100 molecules each and protonated ammonia clusters containing up to 250 molecules, obtained from a gas mixture with 10% NH_3. Negatively charged clusters in which for every iodine atom there is up to 120 water molecules were produced by electron bombardment of iodine – benzene vapor containing a small amount of water. The targets were placed at the focus of a magnetic time-of-flight electron spectrometer used to measure the energy of electrons emitted from the target surface.

The following parameters were thoroughly evaluated: the efficiency of electron emission with positively and negatively charged cluster ions, the electron distribution over energies (electron bundle temperatures), and the dependence of electron yield on cluster type and mass. A series of regularities was established. Figure 7b shows collision velocities necessary to induce electrons with a temperature of 2 eV as a function of the cluster ion mass. Also presented are the results for two types of cluster ions (benzene and protonated ammonia) that hit the gold-coated surface. These data are indicative of a cooperative effect. The difference in the behavior of an isolated molecule and clustered molecules is quite apparent. Also, the experimental results demonstrate the importance of the mass of colliding clusters for electron emission. Figure 7c depicts the width of the kinetic energy (temperature) distribution of electrons emitted at collisions between protonated ammonia clusters of different sizes and a gold surface as a function of the cluster ion velocity (energy). The dependences shown in the figure indicate that the velocity necessary to achieve a given electron temperature decreases as the cluster size increases.

Thus, the results of the work [207] demonstrate that detailed information about a cluster or surface finish quality plays a subordinate role in the yield of secondary electrons. This fact is probably due to a rather high energy concentration during collisions. Emission of electrons was observed in all cases when the threshold velocity was exceeded. Negatively charged clusters induced approximately thrice as many electrons as positively charged cluster ions. This effect may be attributable to the lower electron binding energy in negative clusters. The number of emitted electrons is not proportional to the number of monomers in the cluster. This suggests the cooperative nature of the electron emission process. Electron temperatures are extremely high (tens of thousands of degrees) but lower than the temperatures computed with reference to a single potential surface. It should be noted that the results of measurements performed by the authors [207] quantitatively confirm a well-known fact in mass spectrometry, namely, that large molecules are difficult to detect (due to emission of secondary electrons) unless they are accelerated to high velocities.

Studies [208, 209] reported electron emission during collisions between ionized clusters of various elements, having different types of bonds [van der Waals atomic Ne_N^+ ($N \leqslant 100$) clusters, van der Waals molecular $(N_2)_N^+$ ($N \leqslant 120$) clusters, and fullerene-like valence $C_{60,70}^{q+}$ ($q = 1-4$) clusters], and the atomically clean crystal surface of gold at a kinetic energy up to 6 keV per cluster charge unit (qe). The principal objective of these studies was to evaluate the total electron yields near their corresponding emission thresholds. The choice of these clusters was dictated by the fact that they had totally different binding energies ($\approx 7.1 \pm 0.4$ eV for the break of the $C_{58} - C_2$ bond in carbon clusters [413], and ≈ 0.24 eV for $(N_2)_{N=50}^+$ clusters [414]). Moreover, in the case of $(N_2)_N$ and $C_{60,70}$ clusters, a considerable amount of collision energy may be stored in vibrational modes. This was expected to lead to different energy redistribution patterns and various electron emission kinetics. The studies being considered demonstrated distinct electron yields for the three types of above-mentioned clusters despite their approximately equal masses and velocities. The authors hypothesized that this difference might be due first to the different character of kinetic energy distributions of the clusters after collisions between their constituent particles and surface atoms, and second to the different character of intramolecular vibrational excitation of the clusters. It was shown that the electron yield per particle for $(N_2)_N^+$ clusters increased with the growth of the cluster size, whereas this dependence was practically linear for the $(Ne)_N^+$ clusters.

An interesting effect was observed in work [210] in which electron emission from a solid insulating (CsI) surface was assessed following the impact of gold clusters Au_N ($N = 1-5$) with a very high energy ($E_{col} = 33-11000$ keV per atom). It was established that the number of emitted electrons per atom decreased with increasing size and energy of the cluster. The authors explained this effect by the 'sweeping out' of electrons from the outer shells of the surface atoms lying on the path of a rapidly flying

($\sim 10^7$ cm s^{-1}) cluster. This process was largely induced by frontal atoms of the cluster. It led to a decrease in the number of electrons along the cluster's path, which might have contributed to the emission during subsequent ionization of surface atoms by rarefied cluster atoms. It should be noted that a similar effect of decreased electron emission yield per cluster atom was also observed in Ref. [211] where a carbon film was bombarded by hydrogen H_N^+ ($N = 1-13$) clusters with an energy ranging between 40 and 120 keV per proton.

Studies [212, 213] were concerned with the electron emission yield during the bombardment of a gold crystal surface by C_N^{q+} ($N \leqslant 60$, $q = 1-5$) clusters with a kinetic energy of 165 keV. These experiments ascertained that the electron yield was linearly dependent on the cluster size ($R_N = 1$) over a range $15 \leqslant N \leqslant 60$. At the same time, the electron yield was practically independent of the cluster charge. This finding is in drastic conflict with the results of experiments on the collision of multiply charged atomic ions with a surface. The authors attributed the absence of the dependence of the electron yield on the cluster charge to the rapid transfer of the excitation energy acquired by a cluster in the course of collision to the cluster's vibrational degrees of freedom, leading to its strong heating and fragmentation. According to the molecular dynamics calculations presented by the authors of works [212, 213], the energy relaxation largely occurred via more rapid fragmentation of the clusters rather than through electron emission.

Thus, the available results of research indicate that the electron emission is critically dependent on a variety of factors. It is different in the case of clusters containing van der Waals and covalent bonds. For example, in the event of cluster ions $(N_2)_N^+$ and $(Ne)_N^+$, the electron yield is proportional to the cluster velocity, while a similar dependence for fullerene cluster ions exhibits a nonlinear character [208, 209]. The initial kinetic energy of cluster ions $(N_2)_N^+$ and $C_{60,70}^{q+}$ may be imparted, at least partially, to the internal cluster bonds. Each vibrational bond may store up to 1 eV of energy. The release of this energy by means of fast electron emission is delayed. However, it is able to cause thermal electron emission from a heated cluster after a short span of time. On the other hand, the rapid heating of a cluster may cause its 'instantaneous' fragmentation and, therefore, result in the declined electron emission yield.

To conclude this section, it is worthwhile to note that the results of the above investigations provided a deeper insight into the mechanisms of electron emission resulting from the collisions of clusters with a solid surface. Nevertheless, a number of problems remain to be elucidated [385]. For example, an ensemble of jointly moving fast atoms that may be strongly ionized in the first layers of a solid target behaves differently than an individual atom. For this reason, the processes induced at the surface and in the bulk are unpredictable at high velocities. The rate of emission increases considerably with increasing the number of particles in a colliding cluster, but the emission yield is not directly related to the amount of energy deposited to the material. The strong dependence of electron emission on gas particles adsorbed at the surface has long been known but the cause of it remains to be clarified [390].

5.2 Fragmentation of clusters upon collision with a surface

The fragmentation of clusters and cluster ions impinging upon a surface was investigated in much experimental and theoretical research [46, 119, 120, 216–235]. The most detailed study of the fragmentation processes was reported in Ref. [46]. This work was focused on the size distribution of charged cluster fragments forming at the collisions of cluster ions having a kinetic energy ranging between 1 and 100 eV with the surface of a p-type diamond film. Clusters were effectively produced during supersonic expansion of a molecular gas mixed with a gas-carrier; their subsequent ionization at the nozzle outlet has been done by electrons emitted from a pulsed source. The molecular beam was separated from expanding jet and then passed to the primary time-of-flight mass spectrometer where ions were extracted in the direction perpendicularly to the axis of the molecular beam and accelerated to a kinetic energy of about 2000 eV. Mass selection of the ions was achieved by pulsing the high-voltage field applied to a planar ion mirror at the stated instants of time; this made it possible to deflect cluster ions of a chosen size by 90° into the scattering chamber (approximately 10^6 ions per pulse). Cluster ions extracted from the beam were directed perpendicularly to the target surface heated to approximately 400 K. The collision energy of incident cluster ions could be varied by their decelerating in a strong retarding field between the grounded grid (positioned in front of the surface) and the target surface to which a high voltage was applied (Fig. 8). The same high-voltage field that decelerated the incoming ions was also used to effectively collect and accelerate scattered ions for a mass-analysis of ionic fragments by registering their time of flight from the target to the detector. For this purpose, the secondary time-of-flight mass spectrometer equipped with a retarding potential-based energy analyzer was placed in front of the ion detector to determine the kinetic energy distribution of ionic fragments. The spread in energies of cluster ions incident on the target did not exceed 1% of their mean kinetic energy.

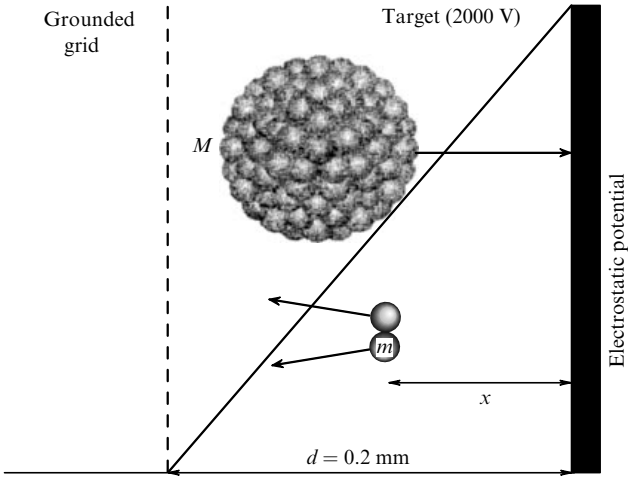

Figure 8. Schematic diagram illustrating experimental setup for recording the time of cluster fragmentation induced by surface collisions. The measuring method is based on the kinetic energy analysis of ionic fragments (see the text) [46].

Applying such a potential U_{tar} to the target that is higher than the kinetic energy of the incident ions caused them to reflect elastically, i.e., without impacting the target surface. In order to initiate collisions of cluster ions with the scattering surface, the voltage applied to the target had to be lower than the kinetic energy of the ions. Thus, the collision energy E_{col} was determined by the difference between the average kinetic

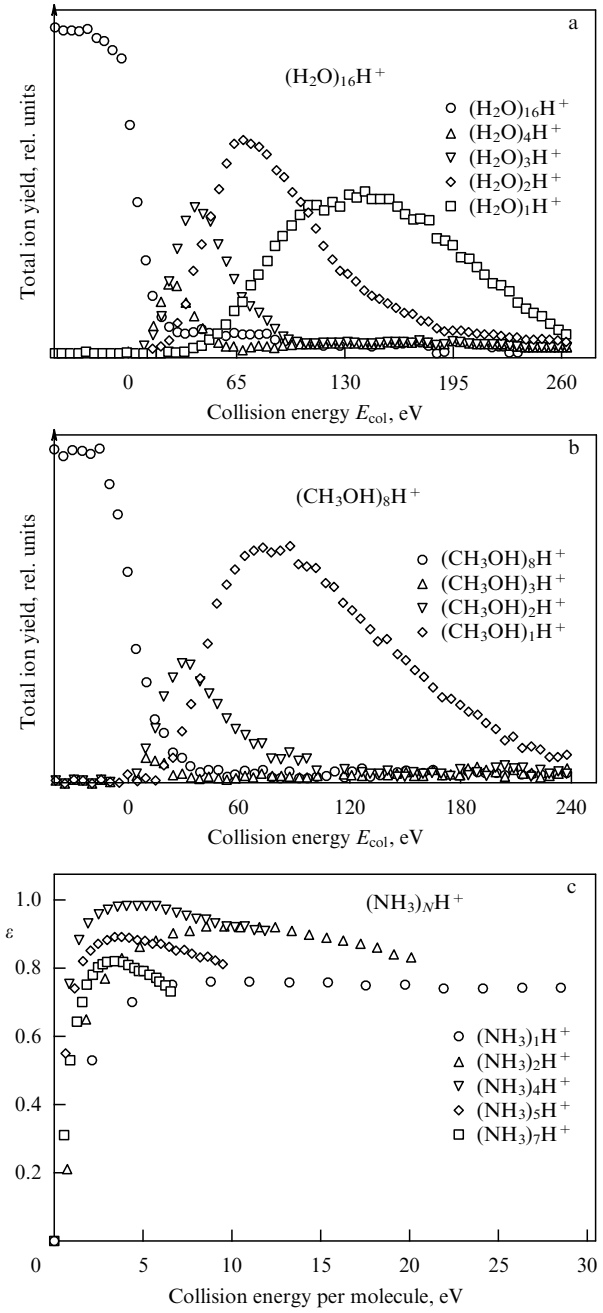

Figure 9. (a) The yield of charged cluster fragments resulting from the collision of protonated water cluster ions $(H_2O)_{16}H^+$ with a diamond surface and plotted as a function of the collision energy E_{col}. The measured signal of scattered cluster ions was integrated for each mass. Data points to the left of $E_{col} = 0$ eV represent reflected cluster ions. (b) The yield of charged cluster fragments resulting from the collision of protonated cluster ions $(CH_3OH)_8H^+$ with a diamond surface as a function of the collision energy E_{col} [46]. (c) Coefficient of collisional elasticity $\varepsilon = E_{rec}/E_{col}$ for protonated ammonia cluster ions $(NH_3)_NH^+$ as a function of the collision energy E_{col} [46].

energy E_i of the impinging ions and the target potential U_{tar}: $E_{col} = E_i - eU_{tar}$, with e being the elementary charge. Negative collision energies meant ion reflection.

Figure 9a portrays the fragmentation patterns of protonated clusters comprising 16 water molecules as a function of the collision energy. The studies showed that at very low collision energies ($E_{col} \cong 0$) most of the impinging cluster ions $(H_2O)_{16}H^+$ experienced no fragmentation upon their collisions with the target surface. However, even at slightly higher collision energies, only few undestroyed incident cluster ions were left, with the simultaneous production of small ionic fragments $(H_2O)_NH^+$, where $N = 1-4$. No larger cluster fragments were detected. As the collision energy was increased, the size of cluster ionic fragments decreased. The large 'dip' in the fragment yield at collision energies in the range from 1 to 10 eV could be attributed to the efficient neutralization of slow cluster ions (see Fig. 9a) [46].

As a general outcome, for all the cluster compositions and sizes, the ionic fragments produced were rather small (typically monomers). Neither ionic fragments that lost one or two monomers from the incident cluster ions nor intermediate-sized ones were detected. Obviously, there occurred an abrupt change from the fragmentation-free collision regime to a regime where the clusters were completely disintegrated. It should be borne in mind that in the work under consideration only positively charged cluster ions were detected.

A similar fragmentation pattern is observed in the case of other hydrogen-bonded cluster ions, such as ammonia [216, 217], water [218], and methanol [46] ionic clusters (Fig. 9b). For example, when small $(CH_3OH)_8H^+$ clusters impinge upon a surface, ionic fragments comprised of up to three monomers can be detected. This observation reflects a general picture that the larger the incident cluster, the bigger the fragments observed. But even for clusters of up to 64 molecules, the largest detected ionic fragments consisted of a maximum of 6 molecules only [46].

Thus, the results of experimental studies indicate that the distribution of cluster fragments produced at the collisions between high-energy clusters (or cluster ions) and a surface is substantially different from that of the fragments formed at low collision energies. In the latter case, the process of interaction between the clusters and the surface is described in terms of the cluster evaporation model in which the gradual loss of individual monomers from a cluster occurs via evaporation [415] (see Section 4.3).

The size distribution of ionic fragments explored in the above experiments [46] covers a broad range of conditions, from the multiple fragmentation regime [219–224] up to complete cluster disintegration [225]. With a rise in collision energy there occurs an abrupt change from the regime where fragmentation is absent to that where complete fragmentation takes place; this behavior has been predicted theoretically in Refs [226, 227] and can be explained as due to the competition between two system's entropy-dependent effects. This theoretical approach is based on one underlying assumption, namely, that there is a rather rapid thermalization of the translational degrees of freedom [228]. Consideration of the system in the thermodynamic context makes it possible to account for the abrupt passage to the regime in which the clusters are completely destroyed. Moreover, the theory also predicts that cluster fragmentation upon collision with a solid surface is practically instantaneous (it takes less than 1 ps).

5.2.1 Measuring cluster fragmentation time. In Ref. [46], the fragmentation time was determined experimentally using protonated ammonia clusters $(NH_3)_NH^+$. The authors measured the kinetic energy (velocity) of the fragments being formed. They have accounted for the fact that because the kinetic energy realized during unimolecular decay of $(NH_3)_NH^+$ cluster ions did not exceed 10 meV [229, 230], their recoil energy could be neglected. Assuming a homogeneous electric field between the grounded grid and the

target surface, the kinetic energy E_{kin} of a cluster ionic fragment with mass m as a function of the distance to the site where fragmentation took place will be defined by the relationship

$$E_{kin} = eU_{tar}\left(\frac{xm}{dM} - \frac{x}{d} + 1\right). \quad (5.6)$$

Here, x is the distance from the target to the point where fragmentation occurred, and M is the mass of the intact cluster ion. The authors measured the kinetic energy of an NH_4^+ fragment ion arising from the fragmentation of an $(NH_3)_2H^+$ cluster ion at three different collision energies (30, 40, and 48 eV). In all these cases, the mean kinetic energy of NH_4^+ ions was roughly identical with the potential applied to the target surface. Bearing in mind the final time resolution of the experimental setup (about 120 ps), the authors found that the process of cluster fragmentation took less than 120 ps to be completed. They also measured the mean kinetic energy of dimeric and monomeric ions as the last fragments to form in the course of disintegration of an $(NH_3)_{10}H^+$ ion cluster; it was found that the time needed for fragmentation is less than 80 ps.

It follows that the process of fragmentation of cluster ions at their collisions with a surface proceeds much faster than the evaporation process during which they gradually lose single monomers (see Section 4.3) [415], as was demonstrated by molecular dynamics computations [217]. It should be noted [46] that the time of metastable dissociation of protonated ammonia cluster ions, which can be expressed as

$$(NH_3)_N H^+ \rightarrow (NH_3)_{N-x}H^+ + xNH_3\,, \qquad x \geqslant 1\,, \quad (5.7)$$

is reduced to several microseconds [230–232]. This means that high-energy clusters impinging upon the surface undergo ultrafast heating accompanied by the redistribution of energy within the cluster and its dissipation following cluster disintegration. This phenomenon has implications for collision-induced chemical reactions (see Section 5.3). Specifically, the products of chemical reactions that occur during collisions of clusters with surfaces are kinetically stable because the clusters rapidly disintegrate after the impact and the conditions are thus lacking for the confinement of the reaction products in the cluster and their relaxation.

5.2.2 Energy loss due to its transfer to the surface. An important aspect of research on the interaction of energetically rich clusters or cluster ions with a solid surface is the knowledge of the collision energy loss due to energy transfer from impinging clusters to the target. This problem may be addressed, for example, by measuring the recoil energy of intact cluster ions that bounce off the surface [46]. The recoil energy E_{rec} is determined by the difference between the mean kinetic energy of scattered ions, E_s, and the target potential U_{tar}: $E_{rec} = E_s - eU_{tar}$.

Figure 9c presents the results obtained in Ref. [46] for the coefficient of collisional elasticity, ε, given as the ratio of the recoil energy E_{rec} to the collision energy E_{col}: $\varepsilon = E_{rec}/E_{col}$, for protonated ammonia clusters $(NH_3)_N H^+$ ($N = 1, 2, 4, 5, 7$) as a function of the collision energy. It can be seen that at low collision energies (< 2.5 eV per molecule) cluster ions scattered from the target surface lose a substantial part ($\geqslant 60-70\%$) of their initial kinetic energy, whereas at high collision energies only a small fraction ($< 20-30\%$) of the kinetic cluster energy is lost. Hence, at high E_{col}, elasticity of cluster–surface collisions is surprisingly high. As a rule, about 75% of the kinetic collision energy is retained by the intact scattered cluster ions. Due to the hardness of a diamond surface, the small energy transfer to the target is not completely unexpected. It is consistent with the results of molecular dynamics calculations [119, 120, 143].

To close the present section, it seems appropriate to consider some interesting data reported in Refs [233–235]. Collisions of $Na_{14}F_{12}^+$ cluster ions with a graphite surface at rather low collision energies (0–20 eV) were studied in Ref. [233]. The authors observed the formation of $Na_{13}F_{12}^+$ fragments, which suggested cluster demetallization in the course of collisions. The authors interpreted this fragmentation channel in terms of desorption of $Na^{(0)}$ atoms from the cluster surface. The existence of such a (low-energy) fragmentation channel had been predicted in paper [416]. The energy of cluster fragmentation via this channel was found to be around 1.1 eV, i.e., much lower than the evaporation energy of NaF (2.5–3.5 eV) or the electron binding energy (3.5–4 eV) [233].

Experiments with carbon ($C_{60}^{\pm}$, C_{70}^+, C_{84}^+) cluster ions reported in Ref. [234] demonstrated that the clusters were scattered from silicon (100) and graphite (001) surfaces without fragmentation even at rather high collision energies (over 200 eV). When the collision energy of C_{60}^- clusters exceeded 120 eV, the scattering of parent ions was accompanied by the electron emission. Analogous results were obtained in the fragmentation study [235] that was concerned with the collision dynamics between C_{60} clusters and a diamond (111) surface. It was shown that clusters sustained collisions without fragmentation, although a large part (25–30%) of the collision energy ($E_{col} = 150-200$ eV) was transformed into the internal energy of the clusters which underwent heating up to 3000–4000 K. A similar result (high cluster strength) was also obtained when C_{60}^+ clusters were excited in quite a different way, namely, through multiphoton absorption of laser UV radiation [417]. These experiments reveal that carbon clusters (molecules) with a closed hollow structure are characterized by very high stability against fragmentation (see also Refs [418–420]).

5.3 Chemical reactions induced by cluster–surface collisions

5.3.1 Dissociation of molecules. The data presented in the previous sections indicate that collisions of cluster ions with a surface lead to their rapid and efficient fragmentation, as well as energy redistribution within cluster ions and small kinetic energy loss due to its transfer to the target surface. Another sign suggesting the presence of large amounts of energy inside the cluster ion is the breaking of its molecular bonds during surface collisions (see, for instance, Refs [110–120]). Let us consider, by way of example, dissociation of toluene cluster ions impinging upon a surface [46]. Figure 10 presents the time-of-flight spectra of ions scattered from a diamond surface bombarded by toluene pentamer $(C_6H_6CH_2)_5^+$ ions. At low collision energies $E_{col} \leqslant 30$ eV, a small number of intact scattered parent cluster ions are detected along with a certain amount of $(C_6H_6CH_2)_2^+$ dimers and toluene monomer ions. At collision energies ranging from approximately 16 to 160 eV, the ion peak is dominated by toluene monomers. The cluster ions begin to dissociate when the collision energy exceeds 60 eV. Then, $C_6H_i^+$ ionic fragments predominate in the mass spectrum. When the collision energy is higher than 120 eV, the

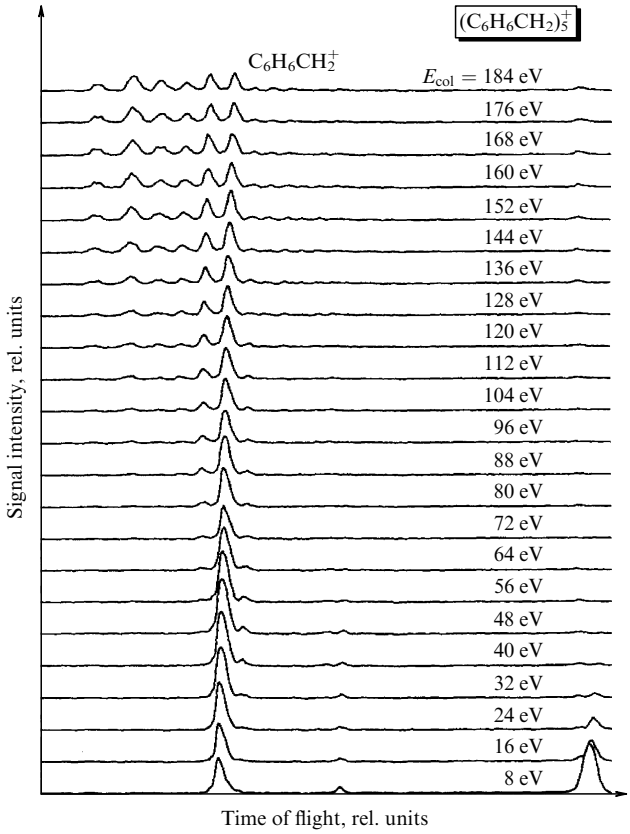

Figure 10. Time-of-flight spectra of ions scattered from a diamond surface upon the impact of cluster cations $(C_6H_6CH_2)_5^+$ on the surface with different collision energies E_{col} [46].

molecules are completely destroyed, and the entire set of $C_nH_i^+$ fragments with $n = 2-6$ is produced.

5.3.2 Dimensional effects. Molecular wedge. Molecular dissociation accompanying the impact of high-energy clusters on a surface was described for other types of cluster constituent molecules, too [115–117]. A powerful impulse of force generated in a cluster hitting the surface is able to initiate specific chemical reactions inside the cluster that do not proceed under thermal excitation conditions. The simplest example of chemical reactions induced by collisions of clusters with surfaces is the dissociation of diatomic molecules or ions inserted into clusters comprising chemically inert solvate molecules and atoms (solvent-assisted dissociation) [110, 111]. Indeed, molecular dynamic calculations [118–120] reveal that the dissociation of I_2 molecules inside an $I_2(Rg)_N$ cluster colliding with a solid surface is substantially accelerated by solvate atoms of inert gases; in other words, chemically inert atoms promote the dissociation of I_2 molecules. Such a dissociation process must strongly depend on the spatial arrangement of solvate atoms (i.e., on their geometric structure) and, hence, on the number of atoms surrounding a reactive molecule.

It may be supposed [116] that the dimensional effect is better manifested during the dissociation of charged clusters than during that of neutral ones because solvate molecules in the formers are closer to one another. Moreover, cluster ions are easier to select by size with the help of a mass spectrometer. The mechanisms of such reactions were investigated in experimental studies and by computer simulation of the dissociation of an I_2^- diatomic reactant inserted into an

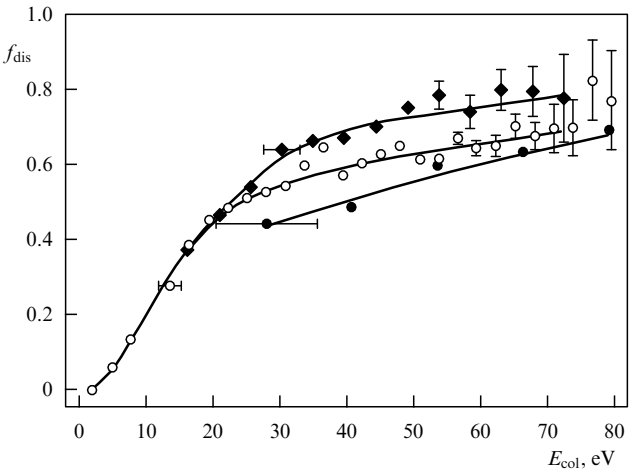

Figure 11. Fraction f_{dis} of dissociated I_2^- molecular ions plotted as a function of the collision energy per one I_2 molecule during impact of $I_2^-(CO_2)_N$ on a silicon surface: ● — $N = 0$, ○ — $N = 10$, and ◆ — $N = 20$ [116].

$I_2^-(CO_2)_N$ cluster anion impinging upon a silicon surface [115–117]. This cluster anion is very convenient to use for the purpose because CO_2 molecules are oriented near I_2^- molecular ion in a quite definite way [421, 422]. This greatly facilitates elucidation of the role of solvate molecules in the dissociation of diatomic reactants as clusters hit the surface.

In experiments [115–117], $I_2^-(CO_2)_N$ cluster anions $(N = 0-30)$ interacted with a silicon surface at a collision energy from 1 to 80 eV per I_2^- molecular anion in a high-vacuum chamber equipped with a time-of-flight mass spectrometer using retarding potential. The mass spectrometer was used to detect anionic products scattered from the surface. These studies demonstrated that a collision of an $I_2^-(CO_2)_N$ cluster with the surface resulted in the dissociation of the central I_2^- ion. The authors analyzed the fraction f_{dis} of the dissociated I_2^- anions as a function of the collision energy and the number N of the CO_2 molecules in the cluster. They established a rather strong dependence of f_{dis} on both the collision energy and the number N (for $E_{col} \geqslant 30$ eV) (see Fig. 11). It should be emphasized that the authors attributed the strong dependence of f_{dis} on N to the wedge effect. This effect resides in that a certain number of CO_2 molecules $(N = 5-10)$ arranged near an I_2^- bond form something like a molecular wedge breaking this bond mechanically when the cluster impacts on the surface, exactly as the strike of a mallet on a wedge splits wood. Also, it was shown in works [115–117] that the I_2^- dissociation was suppressed when the solvation shell was totally occupied. There is the so-called cage effect when the I_2^- dissociation is hampered by the recombination of the dissociation products (I atoms and I^-) in the fully filled solvation shell. The results of experiments and the observed effects were confirmed by molecular dynamics calculations [115–117]. Specifically, it was shown [116] that, given the proper geometry of a cluster anion colliding with a surface, even one CO_2 molecule localized near the 'waist' of a molecular I_2^- bond is sufficient to break this bond.

It was also ascertained that the dissociation of the I_2^- anion is due to the conversion of the collision energy to the vibrational energy of the molecular anion. The solvate atoms or molecules surrounding the reactant assist in concentrating the internal energy of the cluster on the molecular bond and

thereby increasing the vibrational energy of the reactant. Thus, the results of the above investigations indicate that environment effects and dimensional effects (cluster geometry) strongly influence the efficacy of chemical reactions induced by collisions of clusters with a surface.

5.3.3 Formation of chemical bonds. Collision-induced dissociation reactions are also well known from studies on the interaction of individual molecules with surfaces (see, for instance, Refs [423–425]). On the other hand, collisions of high-energy clusters with a solid surface are accompanied by specific collective phenomena characteristic of clusters alone, such as, for example, the formation of chemical bonds [121–128, 426]. It was shown in Refs [122, 123, 125] that such collisions may be utilized to induce chemical reactions with high activation barriers. In this approach, a cold cluster with van der Waals bonds containing solvated reactants hits a hard wall at supersonic velocities [143, 198, 236, 426–428]. During collision, the kinetic energy is redistributed inside the cluster, which is therefore subject to ultrafast (for dozens of femtoseconds) heating. Assuming the equivalence of temperature to the kinetic energy of random motion, it is possible to roughly evaluate the temperature inside the impinging cluster. If the total kinetic energy of the directed motion of such a cluster is converted in the course of collision to the energy of random motion of its constituent particles, then the cluster may be heated to a temperature in excess of 10^4 K at a collision energy of 4 km s^{-1} or so. Even if some portion of the kinetic collision energy is transferred to the surface [46, 179], the temperature reached inside the cluster may be very high. Shortly after heating, the cluster undergoes disintegration into fragments [216, 217, 227, 429].

Both computer simulation and experimental findings [46, 115–117, 120] (see also Section 5.3.1) reveal the possibility of dissociation of chemical bonds within a cluster. Much less likely is the formation of new bonds in the cluster during its very short lifetime after onset of heating and prior to fragmentation. This time interval is really too short because the cluster rapidly (for $\cong$ 100 fs) disintegrates [217, 227]. Nevertheless, as computer simulations indicate, such reactions are possible because this time is enough for 3–5 particle collisions between themselves to occur. This inference is equally true even of four-center reactions [123] that occur only under conditions of vibrational excitation of reactants [121]. The vibrational excitation necessary for such reactions to proceed takes place when the reactants are solvated in a chemically inert cluster. The computation reported in Ref. [123] clearly indicate that the reactants are activated by the surrounding particles prior to the onset of the reaction.

One such reaction is exemplified by that of $(CH_3I)_N^-$ iodomethane cluster ions giving rise to an I_2^- molecular ion [46] (see also Refs [114, 128]). Figure 12a presents the secondary time-of-flight spectra of $(CH_3I)_5^-$ cluster anions scattered from the surface of a diamond target at different collision energies. At low collision energies ($E_{col} < 20$ eV), the reaction products include hydrogen and atomic iodine anions, and a small number of $(CH_3I)_2^-$ dimeric ions in addition to the parent cluster ions. As the collision energy increases, the yield of dimeric ions is blocked, and a new peak corresponding to the molecular iodine ion I_2^- appears for collision energies $E_{col} > 45$ eV. This peak has a maximum at $E_{col} \cong 200$ eV; a further rise in the collision energy results in the saturation of the I_2^- yield. Figure 12b depicts the dependence of the normalized reaction product yield on the

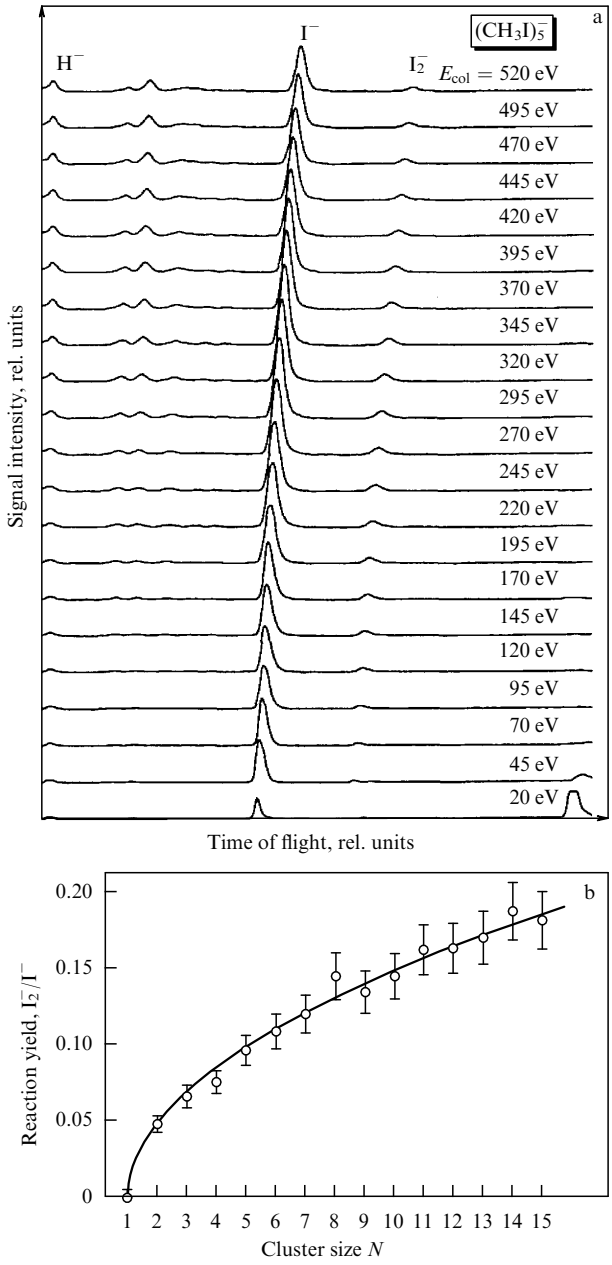

Figure 12. (a) Secondary time-of-flight spectra of iodomethane cluster ions $(CH_3I)_5^-$ impinging upon the diamond surface at different collision energies E_{col}. (b) Reaction product yield of molecular I_2^- ions normalized to atomic iodine ion I^- as a function of the size N of the impinging iodomethane cluster anions $(CH_3I)_N^-$. Collision energy $E_{col} \cong 200$ eV corresponds to the maximum product yield. The solid line fits the experimental data points [46].

size of the colliding cluster [46]. It is fairly well described by the functional dependence in the form $I_2^-/I^- \propto \sqrt{N-1}$ [46].

Certain important peculiarities of the above findings [46] are noteworthy. First, there is an energy threshold approaching 3 eV for the formation of molecular iodine upon collisions of iodomethane pentamer anions with the surface (see Fig. 12a). Second, there is rather a strong dependence of the product yield on the cluster size. It is worth noting that molecular iodine fails to form in the collisions of iodomethane molecular ions with the surface, whereas the collisions of cluster ions composed of 15 iodomethane molecules result in a 15% rise in the reaction yield. Also

noteworthy is that the flux of cluster ions at the surface was relatively weak in the above experiments. Hence, the probability of forming a molecular bond by the recombinative desorption mechanism may be neglected even if the adhesion coefficient is assumed to be unity [46].

In order to study the effect of a solvent (molecular composition of the cluster) on the reactive capacity, the authors of Ref. [46] also considered collisions of trifluoromethane anions $(CHF_3)_N^-$ with the surface of a diamond film. At collision energies in excess of 25 eV, they detected $C_2H_2^-$ anions, the number of which was highest at an intermediate collision energy of roughly 150 eV. Such a behavior was considerably different from the behavior of the ion peaks corresponding to F^- fragments and F_2^- products. The intensity of the latter peak increased with increasing collision energy.

The results of the experimental work under consideration can be compared with the results of computer simulation of molecular iodine synthesis resulting from the impact of neutral $(CH_3I)_N$ clusters on a solid surface [128]. Strictly speaking, these results are incommensurable because the former approach makes use of charged ions, and the latter of neutral ones. However, it follows from calculations that cluster dynamics is in the first place determined by high-energy heavy atomic nuclei and that the yield of molecular iodine amounts to almost 10% per CH_3I molecule. It fails to grow further for $N \geqslant 15$ despite the growing cluster size. In both simulation and experiment, the molecular iodine yield decreases at high collision energies. The ratio of molecular to atomic iodine yields shows similar if not identical dependence on the cluster size. The high activation barrier for a four-center reaction or dissociation suggests the existence of a high reaction threshold for the formation of products; nevertheless, a certain excess energy causes dissociation of the newly formed molecular iodine. It is also shown that the mechanisms of cluster excitation and molecular iodine synthesis are well described by a model taking into account hard binary collisions between cluster constituent particles (see Section 4.2).

5.3.4 Air burning. Let us now consider in brief the results of the study [125] in which the computer simulation technique was applied to ascertain the possibility of the induction of the air burning reaction ($N_2 + O_2 \rightarrow 2NO$) as clusters impinged upon a solid surface (see also Refs [122, 124] by the same researchers). It should be emphasized that the energy barrier for this reaction was around 13 eV [125]. It was shown in paper [125] that the air burning reaction was possible to induce under a certain combination of conditions realized in a cluster heated due to the collision with the surface at a supersonic velocities. The calculations were made for both uncontaminated O_2/N_2 clusters and clusters of an inert gas that contained a few N_2 and O_2 molecules. In either case, a rather large amount of NO was found to form (up to 30% of the initial number of the molecules) along with a small amount of N_2O, resulting from cluster heating upon collision with the surface (Fig. 13). N_2O is a product of the four-center reaction $N_2 + O_2 \rightarrow N_2O + O$. The results of computations suggest that the newly formed N_2O molecules are rather hot and disintegrate in the course of cluster fragmentation. The efficient formation of the reaction products begins at collision velocities approaching 3 km s^{-1}, consistent with the Mach number M of about 11. This result is in agreement with the one reported in Ref. [430] where it was demonstrated that

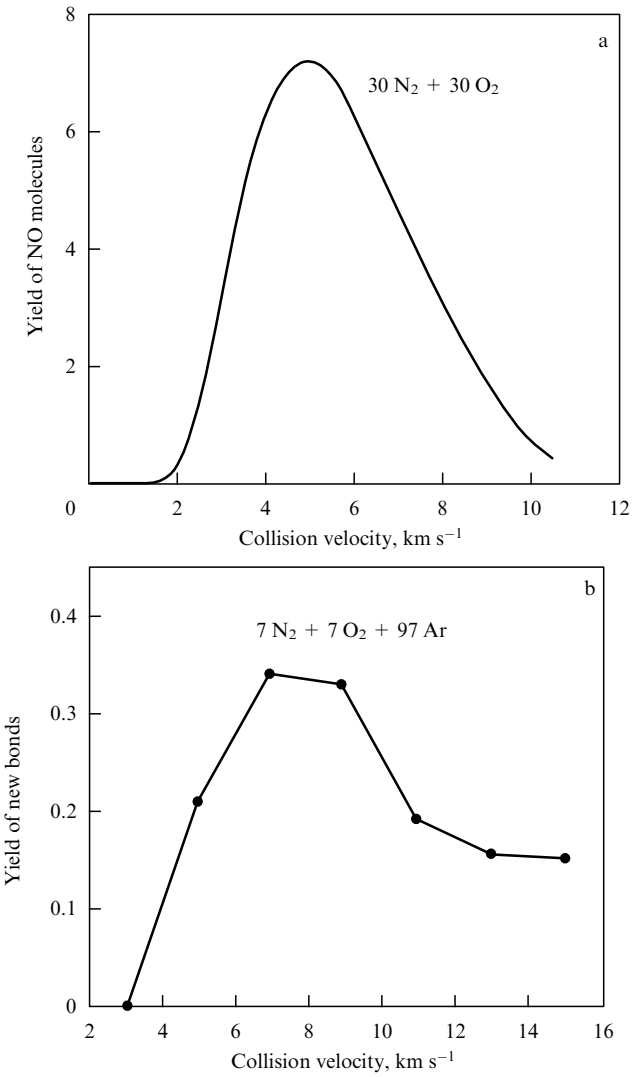

Figure 13. Formation of new bonds in an overheated cluster O_2/N_2 system as a function of the collision velocity: (a) the yield of NO molecules plotted versus collision velocity for a cluster comprising 30 N_2 molecules and 30 O_2 molecules. The dependence was obtained using maximum entropy formalism; (b) the yield of new bonds (normalized to the initial bond number) obtained by the molecular dynamics method in the conditions when a cluster of 7 N_2 molecules and 7 O_2 molecules was embedded into a cluster of 97 argon atoms and impacted on a cold (30 K) surface [125].

intense air burning takes place in the forepart of a spacecraft reentering the Earth's atmosphere at a speed of about 15 M. Because such a spacecraft undergoes very strong heating, it can probably induce the reaction of air burning even at lower velocities. It follows from Ref. [125] that the threshold for the product yield is virtually independent of surface temperature up to its rather high values, provided the surface is flat, clean, and chemically inert. This is not surprising if bearing in mind that the kinetic energy of molecules under these conditions is very high. It may be said that Ref. [125] theoretically substantiated the possibility of effective ignition of clusters composed of O_2 and N_2 molecules or of O_2 and N_2 molecules mixed up with an inert gas as they impact on a surface at accessible collision velocities. To our knowledge (see also Refs [125, 129]), the 'air burning' reaction during collisions of clusters with surfaces has not thus far been observed in experiment. Calculations made for $30\,N_2 + 30\,O_2$ clusters also suggest the formation of electronically excited particles

and O^+, N^+, and NO^+ ions at collision velocities higher than $7-8$ km s^{-1}.

To conclude, it is worthwhile mentioning the recently published article [129] where the vibrational excitation of N_2 and O_2 molecules during collisions of $(N_2)_N$ and $(O_2)_N$ clusters with a solid surface was investigated by the molecular dynamics method. It was found that the vibrational excitation and dissociation of monomers in a cluster were well apparent only at collision velocities higher than 5000 m s^{-1}. Simultaneously, it was shown that the cluster enlargement did not increase the probability of vibrational excitation of monomers and their dissociation; rather, it promoted relaxation of such excitation. The results obtained by the authors point to the existence of an optimal cluster size which is most preferable for experimental investigating cluster-catalyzed chemical reactions.

5.4 Formation and propagation of microshock waves in clusters

The generation and propagation of microshock waves in clusters impinging upon a solid surface was investigated in great detail in Refs [236, 237] (see also Ref. [118]). Computer simulation of molecular dynamics in Ref. [236] was employed to examine the formation of a microshock wave at collisions of high-energy krypton Kr_N clusters ($N = 8-512$) with a solid platinum surface at an initial velocity and kinetic energy $v = 5 \times 10^4 - 10^7$ cm s^{-1} and $E^0_{\rm kin} = 10-10^6$ eV, respectively. The study reported in Ref. [237] covered the formation of a microshock wave in argon Ar_N ($N = 55-555$) clusters impinging upon a platinum surface at collision velocities $v = 10^5 - 10^6$ cm s^{-1}. In the work [236], the interaction was described by the Lennard-Jones potential

$$U(r_{ij}) = 4\varepsilon\left[\left(\frac{\sigma}{r_{ij}}\right)^{12} - \left(\frac{\sigma}{r_{ij}}\right)^{6}\right] \qquad (5.8)$$

with parameters $\sigma_{\rm Kr,Kr} = 3.60$ Å, $\varepsilon_{\rm Kr,Kr} = 0.0147$ eV, $\sigma_{\rm Kr,Pt} = 2.00$ Å, and $\varepsilon_{\rm Kr,Pt} = 0.272$ eV. The initial distance between the cluster's center of mass and the surface was taken equal to 20 Å to ensure that the cluster–surface interaction was negligibly small.

In the work [237], the computation was performed with two types of the interaction potential, viz., the Lennard-Jones potential and the exp-6 potential

$$U(r) = \varepsilon\left\{\frac{6}{\alpha-6}\exp\left[\alpha\left(1-\frac{r}{r_{\rm m}}\right)\right] - \frac{\alpha}{\alpha-6}\left(\frac{r_{\rm m}}{r}\right)^6\right\}. \qquad (5.9)$$

In the former case (Lennard-Jones potential), the parameters were as follows: $\sigma_{\rm Ar,Ar} = 3.40$ Å, $\varepsilon_{\rm Ar,Ar} = 1.044 \times 10^{-2}$ eV, $\sigma_{\rm Ar,Pt} = 4.01$ Å, and $\varepsilon_{\rm Ar,Pt} = 5.18 \times 10^{-3}$ eV. In the latter case (exp-6 potential), the parameters of the Ar–Ar interaction potential were $\varepsilon_{\rm Ar,Ar} = 1.19 \times 10^{-2}$ eV, $r_{\rm m} = 3.77$ Å, and $\alpha = 14.8$, and those of the Ar–Pt interaction potential $\varepsilon_{\rm Ar,Pt} = 1.50 \times 10^{-2}$ eV, $r_{\rm m} = 4.13$ Å, and $\alpha = 14.8$. Such parameters of the exp-6 potential ensured a semiempirical potential that sensibly met the requirements for the repulsive potential. The collision velocity was bounded from above by the value of $v < 10$ km s^{-1}, in order to exclude the necessity of taking into account effects associated with electronic excitation of the clusters and to be confined to the processes in the ground electronic state. At the above collision velocity, the kinetic energy per particle amounted to $E_{\rm kin}/N < 26$ eV.

5.4.1 Energy acquisition process. The studies being considered included an examination of the evolution of the cluster potential energy (CPE), temperature ($T_{\rm cl}$), and cluster–surface interaction energy (CSIE) (Fig. 14). The calculations were made using both the Lennard-Jones and exp-6 potentials. The authors of Refs [236, 237] emphasized the following most salient features of the evolution of these parameters. It was ascertained that the time dependences of the above quantities for the potentials used differed by less than 20%. At the instant of collision τ_0, all these parameters (CPE, $T_{\rm cl}$, and CSIE) started to grow. The CPE and CSIE maxima practically coincided, and the $T_{\rm cl}$ maximum tended to be saturated. The dwell time τ during which a cluster remained near the surface was given by the width of the CPE curve contour that was rather similar to the width of the CSIE curve contour. Time $\tau_{\rm max}$ corresponding to the maximum CPE value determined the cluster energy acquisition time $\tau_{\rm CEA} = \tau_{\rm max} - \tau_0$.

5.4.2 Microshock wave inside the cluster. A cluster excited upon collision with a surface is a small-sized system existing under extreme temperature and pressure conditions. The cluster temperatures may be strikingly high. Suffice it to say that Ar_N ($N = 555$) clusters impacting on the surface at a velocity $v \cong 10$ km s^{-1} ($E_{\rm kin}/N = 21$ eV) at the instants of time corresponding to the CPE maximum have temperature $T_{\rm cl} = 1.2 \times 10^5$ K (Fig. 15). $T_{\rm cl}$ grows linearly with $E_{\rm kin}$ satisfying the relationship $T_{\rm cl} = \alpha(E_{\rm kin}/N)$, where $\alpha = (5 \pm 0.5) \times 10^3$ eV^{-1} K, and does not depend on the cluster size for $E_{\rm kin}/N = 0.2-22$ eV.

In order to study the propagation of a shock wave inside a cluster, the authors of Refs [236, 237] considered the cluster to be composed of many spatial layers, analogous to the approach adopted in investigating continuous media [431]. Because, in the present case, the problem is characterized by cylindrical symmetry (the axis of symmetry is perpendicular to the surface and coincides with the vector of collision velocity), the cluster is divided into layers parallel to the surface. Each layer consists of roughly $1-3$ atomic layers (Fig. 16), so that the total number of atoms in each of them amounts to $10-40$. After that the total energy of each layer can be computed. Figure 16 demonstrates the typical correlation between the internal energy (kinetic plus potential energies) of the layers and their distance from the metal surface at different instants of time. The time scale origin is chosen at $\tau_0 = 0$.

At instants of time preceding the cluster–surface collision ($t < 0$), the energy is uniformly distributed inside the cluster (see Fig. 16). Immediately after the collision, the bulk of the energy is accumulated in a spatial cluster region closest to the surface. Prior to the collision (Fig. 16, upper left part, $t = -10$ fs), the cluster energy profile reflects the fact that the spherical cluster is subdivided into thin layers parallel to the surface, the central layer containing the greatest number of atoms ($30-40$) and having minimal energy. After the collision, the high-energy region extends to the outer layers of the cluster (see Fig. 16), thus demonstrating the propagation of a microshock wave within the cluster at the instant of its impact-induced compression. Until a maximum of CPE is reached, i.e., at instants of time $t < \tau_{\rm CEA}$ and $t < \tau$ (e.g., up to $t \sim 200$ fs for Ar_{555} at the collision velocity $v = 10$ km s^{-1}), the compression shock wave propagates towards the cluster as a single wave (Fig. 16, left column). At longer times, namely, $t > \tau_{\rm CEA}$ and $t > \tau$, the primary wave is overlapped

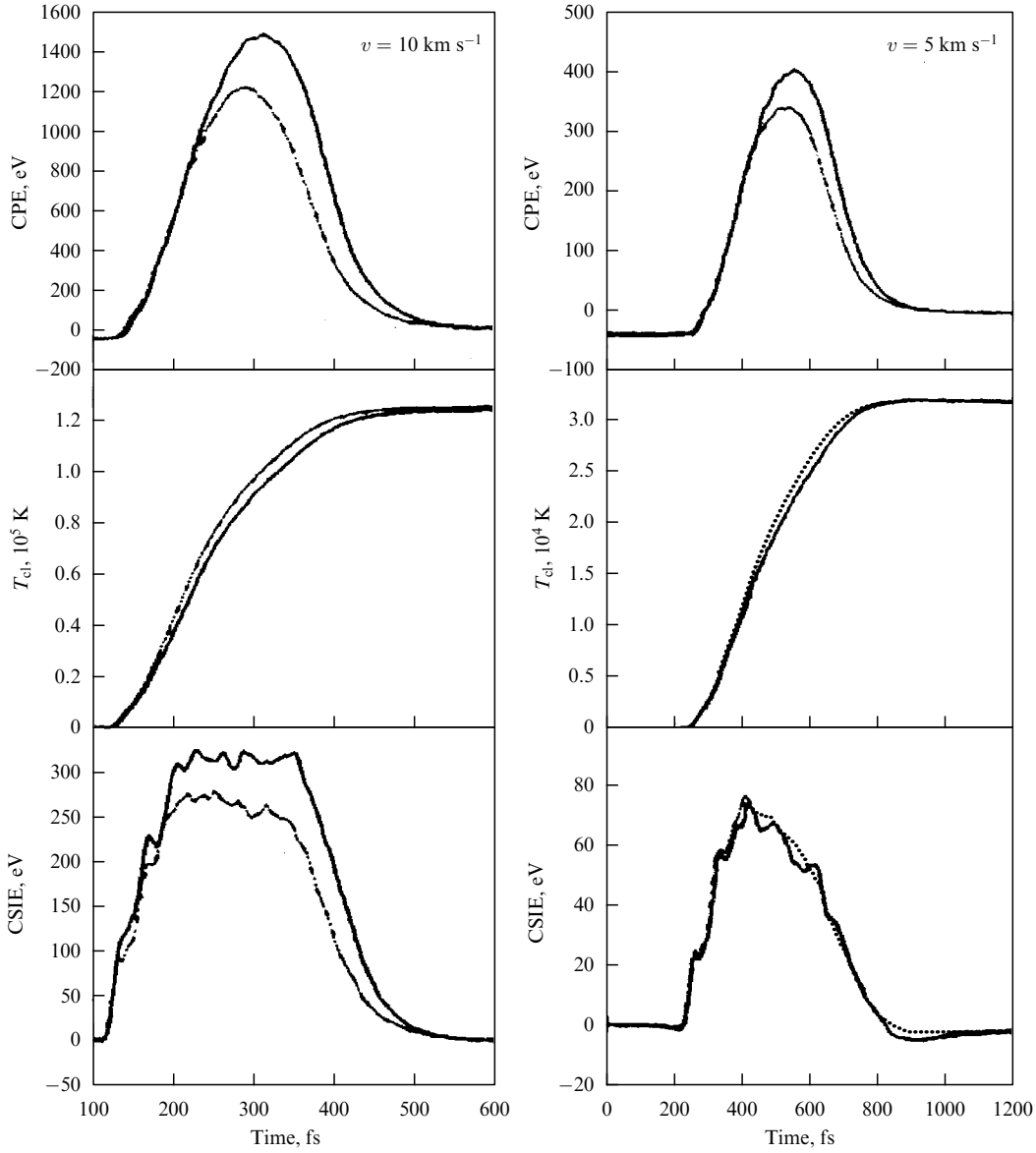

Figure 14. Comparison of the temporal evolution of the cluster potential energy (CPE), temperature T_{cl}, and cluster – surface interaction energy (CSIE) at two collision velocities of an Ar_{555} cluster hitting the surface [10 km s^{-1} (left), and 5 km s^{-1} (right)] for two model potentials: exp-6 potential (solid line), and Lennard-Jones potential (dotted line) [237].

by the secondary one originating near the platinum surface and propagating ahead of it. Thereafter, the primary and secondary waves run apart locally (see Fig. 16). Even later, a tertiary wave and higher-order waves are generated as a result of collisions of the appropriate low-order waves with the surface. The propagation and reflection of high-order shock waves lead to cluster destruction.

The authors of Ref. [237] determined the velocity u_s of a shock wave in clusters and found that it depends linearly on the velocity v of cluster impact on the surface, viz., $u_s = \eta v$. Parameter η is a function of the cluster size. Analysis of the data obtained brought the authors to the conclusion that, when the cluster size is relatively large ($N \geqslant 321$), $u_s/v = 1 \pm 0.15$; in other words, the velocity of a microshock wave propagation within a cluster is approximately equal to the velocity of the cluster – surface collision. At first sight, this estimate of the velocity of a microshock wave propagation in a cluster is at variance with theoretical predictions of the velocity of a compression wave propagation in macroscopic objects [431, 432]. For a one-dimensional shock wave propagating with the velocity U_s after it is induced by a plunger moving with the velocity U_p inside a macroscopic body, the law of conservation of mass under thermodynamic equilibrium leads [432, 433] to the following relation between the shock wave velocity and the plunger speed:

$$\frac{U_p}{U_s} = 1 - \frac{\rho_0}{\rho_1},$$

where ρ_0 and ρ_1 are the initial medium density and the density in the shock wave, respectively. In an heuristic attempt to draw an analogy between the propagation of a shock wave within a cluster and in a bulky medium, the authors of Ref. [237] assumed that the cluster collision velocity may be related to the plunger velocity (i.e., $v = U_p$) and the velocity of a shock wave propagation inside the cluster to the velocity of its propagation in the bulk (i.e., $U_s = u_s$). Because $\rho_0/\rho_1 \ll 1$ in the case of cluster collisions, it is possible to arrive at

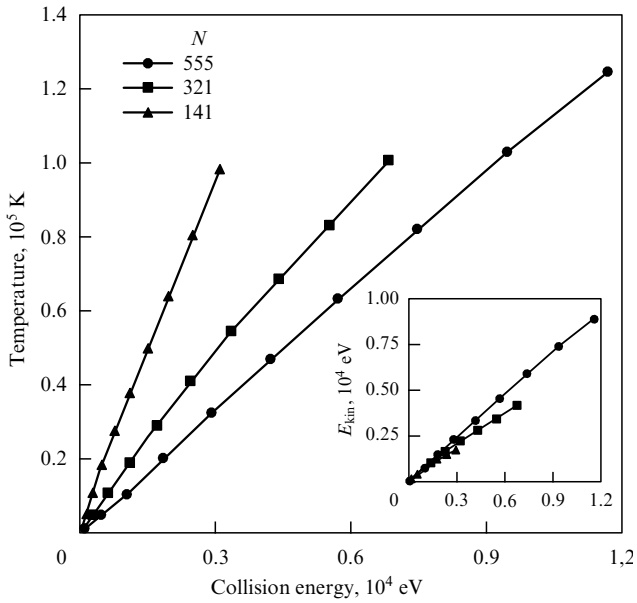

Figure 15. Maximum temperature of Ar_N clusters ($N = 141$, 321, 555) impinging upon a platinum surface versus the collision energy. The inset shows maximum kinetic energies of the clusters [237].

$U_p/U_s \cong v/u_s \cong 1$. This inference is in fairly good agreement with the results of investigation into the propagation of microshock waves inside clusters. Also, it was revealed in Ref. [237] that the dependences of temperature on the pressure [$p(T_{cl})$ relationships] inside clusters of a sufficiently large size ($N > 300$) are analogous to the corresponding dependences for a macroscopic substance.

Let us briefly discuss why the above conclusions ensuing from Ref. [237] may be regarded as reflecting the real situation. A large cluster of a limited size or a bounded system may be regarded as an infinite medium if the mean free path of particles prior to the formation of a shock wave is smaller than other physical dimensions [433]. The cross section of interatomic collisions in an Ar_N cluster or in bulky argon is $\sigma = \pi r_0^2 \cong 45$ Å^2, where $r_0 \cong 3.77$ Å is the interatomic distance estimated from the parameters of the exp-6 potential. Hence, the mean free path $\lambda = (\sigma\rho_0)^{-1} \cong 0.74$ Å, where $\rho_0 = 3 \times 10^{22}$ cm^{-3}. It follows from the results presented in Fig. 16 that the front width l_s of a microshock wave equals approximately 5–8 Å, which constitutes $\sim 2r_0$. Accordingly, $\lambda \ll l_s$; therefore, the internal structure of the shock wave may be neglected, which justifies the consideration of the above cluster as a continuous medium.

At the end of this section, it is worth mentioning [237] the attractiveness of the use of microshock waves in systems of limited dimensions and short lifetime, for example, for the compression of nuclear matter during collisions of high-energy nuclei among themselves [434], which are close analogs of cluster–surface collisions. Selected aspects of this problem are briefly discussed in the following section.

5.5 Nuclear fusion induced by cluster–surface collisions

In the late 1980s and early 1990s, i.e., very soon after the previous cold D–D nuclear fusion boom [435–438] (see also the critical article [439] in *Physics–Uspekhi*), a new boom was triggered by the growing interest in warm D–D nuclear fusion. In 1989, researchers at the Brookhaven National Laboratory, USA published a paper [100] that contained very important and intriguing information. In their experiments with a beam of $(D_2O)_N^+$ clusters (with size N ranging from 25 to 1300) accelerated to a final energy of ~ 300 keV (i.e., to a velocity of $\sim 10^7$ cm s^{-1}) and impacted on the surface of a TiD target (a titanium target doped with deuterium atoms), the authors detected protons with an energy of 3 MeV. They believed that these protons were products of a deuterium nuclear fusion reaction [D(d, p)T] induced by collisions of heavy water clusters with the target. In essence, this was the realization of a rather old idea about the initiation of nuclear fusion by collisions of highly accelerated particles containing nuclear matter [440]. As is known, the strong compression and heating of matter in shock waves generated by collisions of microparticles with a barrier (or with similar microparticles) are likely to create conditions for nuclear fusion. This problem was extensively discussed in Ref. [441]. The authors of Ref. [100] estimated the proton yield at a level of 10^{-11} per each colliding cluster, i.e., ten orders of magnitude higher than the yield expected from evaluations taking into account the cross section for the D–D nuclear fusion at a deuteron energy below 1 keV under the conditions of the given experiment. In addition, the study [100] also demonstrated that the proton yield for D_2O clusters comprised of 150 molecules increased by more than one order of magnitude with a rise in the cluster energy from 220 to 300 keV. The maximum proton yield was observed using clusters containing from 150 to 500 molecules.

This work had great repercussions in the scientific community (see, for instance, Refs [101, 102, 442–445]) and initiated a large series of publications on this topical problem. The idea was especially attractive because the fusion reaction described in Ref. [100] was easy to perform compared with experiments on controlled thermonuclear fusion requiring huge laser systems and massive magnets. Some researchers were skeptical about this observation, others showed restraint, and still others welcomed the publication (see, for instance, Refs [101, 102, 443–445]). Soon after the paper [100] came out, interested researchers made calculations (or estimates) of the D–D fusion rate under conditions described by the authors and performed a detailed analysis of their results [102, 442, 446]. In both calculations and estimates, the well-known expression for the cross section of the fusion reaction was used [447]:

$$\sigma(E) = \frac{S(E)}{E} \exp\left(-\frac{A}{E^{1/2}}\right) = \frac{S(E)}{E} \times 10^{-B/E^{1/2}}, \quad (5.10)$$

where E is the relative collision energy, $S(E) = 0.55 \times 10^{-22}$ cm^2 keV, $A = 31.28$ keV$^{1/2}$, and $B = 13.58$ keV$^{1/2}$. Similar studies were carried out with deuterium ($D_{200}^+ - D_{300}^+$) [448], $(CD_4)_N^+$ [449], and $(N_2)_N^+$ clusters [450]. The results of practically all these studies and estimates (except Ref. [451]) indicated that such a high yield of fusion reaction products could not be achieved under the laboratory conditions described in Ref. [100]. Some researchers emphasized the possibility of artefacts disregarded in Ref. [100]. Specifically, the authors of Refs [102, 442, 444, 446] pointed to the possibility of proton generation in the work [100] due to the impact of lighter ionic fragments (e.g., D_2^+, OD^+, and D_2O^+) on the surface. These light fragments could be present either in the initial beam or produced upon the collision of clusters with the target from which they subsequently reflected, entered the cluster beam (including its acceleration zone), and were accelerated up to very high energies.

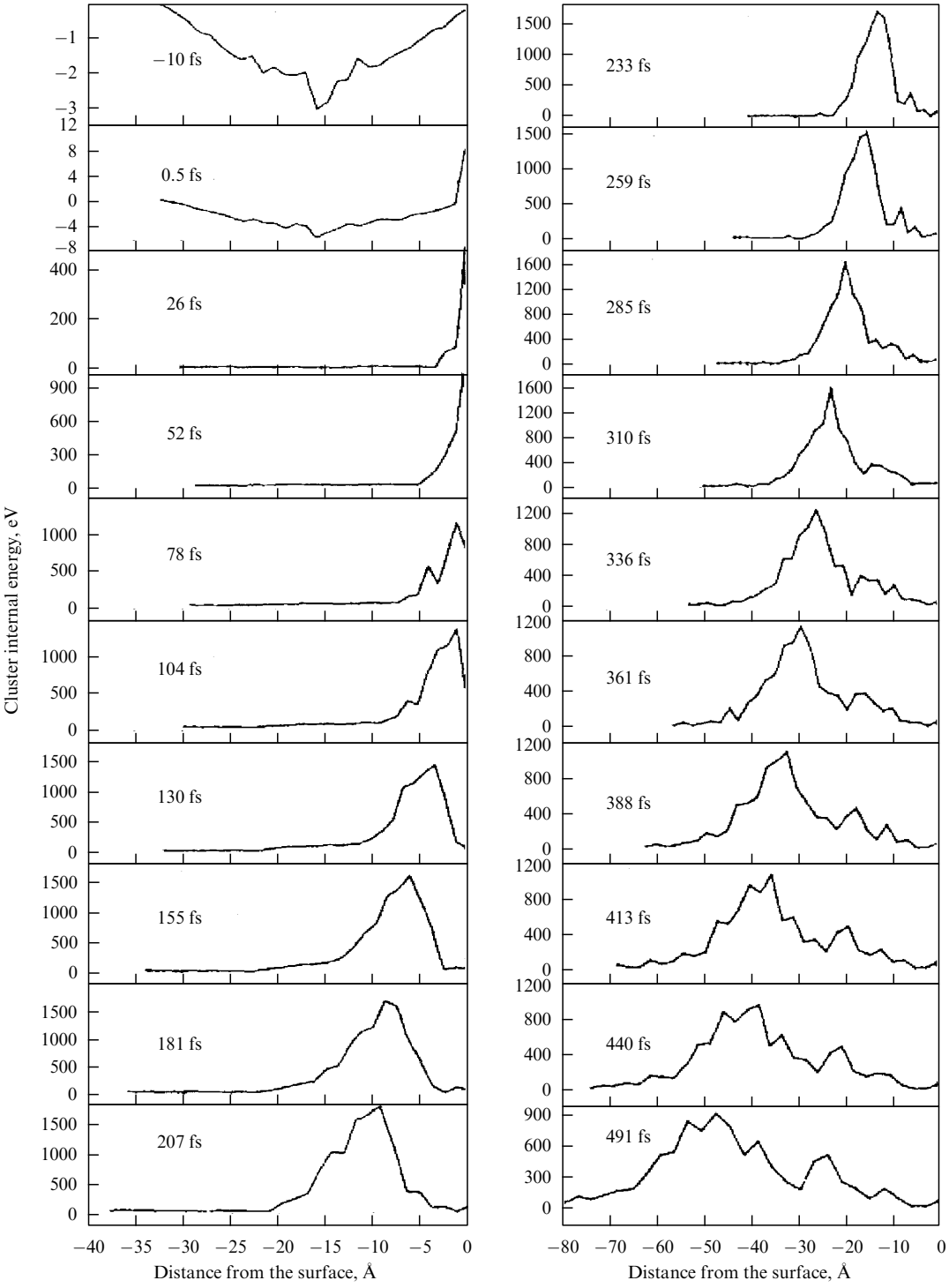

Figure 16. Internal energy profiles of an Ar_{555} cluster impacting on a platinum surface with a velocity of 10 km s^{-1} [prior to collision, during collision, and after staying on the surface (-10 fs $< t \lesssim 500$ fs)]. Zero time $t = 0$ corresponds to the threshold increase in the cluster potential energy [237].

However, the authors of Ref. [100] argued (see Refs [103, 104]) that the probability of forming small ionic fragments under conditions of their experiments was very low and fragments, if any, could not influence the results obtained. They also presented additional evidences [103, 104] on nuclear fusion, including the results of bombardment of other targets [$(C_2D_4)_N$, $ZrD_{1.65}$] by D_2O clusters as well as $(C_2D_4)_N$ targets by H_2O clusters [103]. Based on the analysis of experimental results [103, 104] and the first critical articles [102, 442–444, 448], the authors of the much-talked-of publication [100] arrived at the conclusion [452] that they had overestimated the rate of the D–D fusion reaction by approximately two orders of magnitude.

It is worthwhile mentioning that the observation of a deuterium nuclear fusion reaction and data similar to those presented in Refs [100, 103, 104] were also reported by one more group of researchers [105] who bombarded targets of deuterated polyethylene ($(C_2D_4)_N$) with $(D_2O)_N$ and $(H_2O)_N$ clusters ($N = 1-150$) at their collision energies ranging from 135 to 225 keV. In other words, experimental conditions in

this study were not significantly different from those in Refs [100, 103, 104]. The authors of Ref. [105] also observed an enhanced rate of deuterium nuclear fusion even when they used small clusters $(D_2O)_N$ $(N < 10)$. However, the results reported in Ref. [105] were not confirmed in subsequent experiments [106, 107, 449].

In order to clarify the situation created by the experimental data of Ref. [100], the authors of Ref. [453] employed the molecular dynamics method for the calculation of collisions of Al_{63} clusters with the surfaces of aluminium and gold targets, as well as Al_{32} clusters with a gold-coated surface. The collision energy per atom in both cases reached 1 keV. It was shown that the maximally achievable retention coefficient $n\tau$ (the product of nucleus density by confinement time) was roughly 3×10^8 cm^{-3} s, i.e., seven or eight orders of magnitudes smaller than the Lawson criterion. As shown by computation, the increased nuclear fusion rate might be due to nonlinear effects in a sequence of atomic collisions. At the same time, the authors stated that the high fusion rates reported in Ref. [100] could not be explained by purely collisional mechanisms even with the allowance for nonlinear effects. Hence, only a collective effect or a certain unknown exotic mechanism could be responsible for the results observed. It was shown in Ref. [107] by the example of carbon clusters and atoms that the fusion reaction yield (at collision energies of 20–320 keV per atom) was not influenced by collective effects because the yield per atom was the same for both the clusters and atoms. The author of Ref. [102] ascertained the possibility of increasing tunnel transition probability when deuterium atoms were drawn together due to the energy transfer from oxygen to the deuterium atom as a result of the realization of 'correlated' collisions in the chain (Ti–D–D–O). At such collisions, light deuterium atoms find themselves among Ti (target) and O (cluster) heavy atoms, i.e., as if they were between the hammer and the anvil, with a consequent approaching deuterium atoms more closely. The authors of Ref. [451] managed to explain the high reaction rates of Ref. [100] in terms of the shock sample heating mechanism. They postulated an abnormally high (500 eV) temperature of matter during collisions, produced by the contribution from the high-energy 'tail' of the Maxwell–Boltzmann distribution of cluster energies, and actually adjusted the computed reaction rates and energy dependence of the proton yields to the observed values.

In later studies, other mechanisms leading to an increased rate of D–D-fusion were elucidated. For example, the possibility of achieving conditions for the initiation of the D–D-fusion reaction in the course of deuterium cluster impact on a solid surface was evaluated in Ref. [108] by a numerical method. The authors assumed that cluster–surface collisions at the velocities of $(0.6–6) \times 10^7$ cm s^{-1}, leading to the very rapid (in a time of about 10^{-14} s) generation of strong shock waves, slow down the appearance of free electrons and their heating (because the ion–electron relaxation time approaches 10^{-12} s). Under these conditions, the heating of ions predominates. In such a case (i.e., when electron temperature $T_e = 0$), the neutron yield in the D–D-fusion reaction for clusters of size $N = 100–200$ may be 10–12 orders of magnitude greater than under conditions of equal electron and ion temperatures. It has recently been shown [109] that an 'abnormally high' yield of the D + D reaction products with large clusters may be realized due to nonequilibrium effects produced by collective interactions of D atoms with heavy O, Ti atoms through the Fermi mechanism, i.e., by multiple reflection and acceleration of deuterium atoms when interacting with oxygen atoms. Based on the analysis of experimental data and simulation results, the authors proposed a method for the realization of the nuclear fusion process at relatively low energies per cluster nucleon (0.005–0.8 keV). It should be emphasized, however, that the reaction of deuterium nuclear fusion during collisions of clusters with a solid surface has not thus far been realized in practice despite extensive investigations of the problem of interest.

It seems appropriate to mention at the end of this section that very many current studies (both experimental and theoretical) are devoted to the synthesis of clusters (largely fullerenes) during their collisions among themselves and with solid surfaces (see, for instance, Ref. [99] and references cited therein). The study reported in Ref. [99] pointed to the synthesis of C_{120}, C_{130}, and C_{140} clusters during mutual collisions of fullerenes: $C_{60}^+ + C_{60}$, $C_{60}^+ + C_{70}$ (or $C_{70}^+ + C_{60}$), and $C_{70}^+ + C_{70}$. One of the principal objectives of these works is to measure cross sections of the reactions and investigate the process of fragmentation of hot products being synthesized.

5.6 IR radiation emission in clusters upon their collisions with a surface

High-energy cluster collisions with a solid surface result in the excitation of the impinging particles. Due to the high density of the excited states, the primary electronic and vibrational excitations (if any) undergo rapid dissipation, which results in strong cluster heating. A very hot cluster emits light as any hot 'black body' does. The radiation spectrum depends on cluster temperature; the emitted radiation serves to cool the cluster. Such equilibrium radiation also appears when clusters are excited, say, by electron impact [454–456] or laser light [457] or as a result of a chemical reaction [458]. Light emission by metal clusters is observed when they reside in a hot or ionized gas at temperatures $T \cong 3000–3600$ K [44]. At high temperatures ($T \cong 3200–3500$ K), the cluster radiation spectrum is concentrated in the visible region [454–457]. The radiation power emitted by a cluster (small macroscopic particle) varies as $\sim T^5$ [44]. This situation is different from the temperature dependence for large systems ($\sim T^4$) with an absolutely black surface.

The absorption cross section for a cluster or a small macroscopic particle is proportional to the number of particles in the respective system [44]. This means that the specific absorption cross section (cross section per atom) is independent of the cluster size. Therefore, the particle radiation power per unit volume is proportional to the total number of bound atoms in the unit volume. This number is unrelated to the size distribution function of clusters or particles. Thus, the overall radiation power for a given volume of a gas or plasma is determined by the total number of bound atoms residing in it and does not depend on the size of clusters or particles formed by them. This general conclusion [459–461] is based on the proportionality between the absorption cross section and the number of bound atoms and holds for both clusters and macroscopic particles.

Clusters and small particles introduced in a hot or ionized gas may be responsible for the radiation from these systems. In particular, such is the case with a flame where radiation is produced by small soot particles [459–462]. Radiation is

induced in a similar way in the combustion products of a solid fuel. Clusters of refractory materials, such as tungsten or rhenium are also used as radiators in cluster light sources (see, for instance, Refs [44, 463 – 466]).

In this section, we shall consider light emission by clusters through quite a different mechanism. The radiation is produced by virtue of short-term induction of dipole moments during collisions of unlike inert gas atoms inside clusters when they are strongly compressed at the instant of impact on the target surface. The radiation spectrum is largely concentrated in the IR region. However, radiation may extend over the visible region, too, if the cluster collision velocity is sufficiently high ($\geqslant 15$ km s^{-1}). The emission of IR radiation induced by collisions of high-energy Ar–Xe clusters with a solid surface has recently been studied in Ref. [238] by means of computer simulation. The collision velocities were 5, 10, and 15 km s^{-1}. Let us briefly consider the results of this work.

To begin with, it should be noted that inert gas mixtures at room temperature absorb radiation in the far-IR region [467, 468]. The dependences of absorption intensity on the gas density, temperature, and chemical composition give reason to think that the absorption is due to the induction of the dipole moment as a result of the collision of two unlike atoms. The width of the absorption band (and the most probable frequency) is proportional to the square root of the temperature [468], because the induced dipole exists only for the duration of the collision. The collision time is $\tau_{\rm col} \sim a/v$, where a is the distance at which intermolecular interaction forces act, and v is the atomic velocity as it hits the surface. Therefore, the spectral width is given by the frequency range corresponding, in accordance with the Fourier transform, to the dipole motion. Hence, it can be expected that the spectral width is determined by the quantity $1/\tau_{\rm col} \sim v/a$ or, in the case of an atomic ensemble, by the quantity $\sqrt{T}$, where T is the translational temperature. This line of reasoning is confirmed by the results of experimental studies (see, for instance, Ref. [467]).

The velocity of the chaotic thermal motion of atoms inside a cluster after its impact on the surface is comparable to the collision velocity if the energy transferred to the target surface is sufficiently small. For this reason, a cluster heated during impingement constitutes for a short time a medium in which very hot collisions take place. Such collisions result in vibrational excitation of molecules inside the cluster (see Section 5.3). At high collision velocities, electron excitation of atoms or molecules in the cluster is equally possible. However, all attempts to detect radiation from excited cluster electronic states in experiment have thus far failed, one of the causes being effective electronic excitation quenching by the surface.

Another possible mechanism responsible for radiation is related to dipoles induced for a short time in a cluster by collisions between unlike atoms at the instant of time the cluster hits a surface. It was shown in Ref. [238] that radiation from a hot cluster may have a maximum in the near-IR region or even in the visible region of the spectrum. It was assumed for the purpose of computation that the system on the whole remains in the ground electronic state throughout the collision process. Such an assumption is unjustified at collision velocities in excess of 10 km s^{-1}. However, the authors of Ref. [238] considered only collision-induced radiation.

Table 4. Parameters of the 12,6 Lennard-Jones potential [238].

Atom	ε, kJ mol^{-1}	σ, Å
Ar	0.996	3.41
Xe	1.377	3.735
	1.904	4.04

It was further assumed in the molecular dynamics simulation that clusters were in equilibrium at a temperature of 30 K. The interatomic interactions within a cluster were described by the 12,6 Lennard-Jones potential. The authors made calculations for clusters of different sizes and compositions. The results presented in Ref. [238] refer to clusters composed of 256 Ar and Xe atoms taken in equal amounts. The parameters of an Ar–Xe cluster are presented in Table 4. The interactions between the atoms and the surface were also described by the 12,6 Lennard-Jones potential with a well depth of $\varepsilon = 0.966$ kJ mol^{-1} and interaction parameter $\sigma = 5$ Å. Friction between the atoms and the surface was disregarded, which accounted for the absence of energy transfer from the cluster to the target surface. The cluster–surface collision under consideration resulted in complete cluster fragmentation after a short (subpicosecond) time interval following the collision event. Calculations included integration of the equations of atomic motion up to the instant of time when the velocities of all atoms were equilibrated and no further collisions occurred.

As a result of the collision, the kinetic energy of the translational motion of the cluster was converted to the chaotic thermal motion of atoms inside it. Figure 17a illustrates a rise in temperature (or the energy of random motion of atoms inside the cluster) as a function of the time elapsed since the onset of the motion. All trajectories of the motion originate at the same distance from the surface. Due to this, slow atoms reach it later than faster ones. By the energy of random motion is meant the kinetic energy of atomic motion with respect to the cluster's center of mass:

$$T_{\rm rand} = \sum_{\rm all\,atoms} \frac{1}{2}\, m(v - v_{\rm c.m.})^2 , \tag{5.11}$$

which is defined as a fraction of the cluster kinetic energy equivalent to the temperature

$$T_{\rm rand} = \frac{3}{2}\, k_{\rm B} T \sum_{\rm all\,atoms} 1 . \tag{5.12}$$

Because the cluster is relatively cold ($T \cong 30$ K, see above) before it hits the surface, its kinetic energy is roughly equal to the energy of motion of the cluster's center of mass:

$$T_{\rm init} = \frac{1}{2}\, v_{\rm imp}^2 \sum_{\rm all\,atoms} m . \tag{5.13}$$

Figure 17b portrays translational temperature dependences of the most probable frequency in the absorption spectrum induced by the collision of the cluster with the surface. The results refer to three collision velocities: 5, 10, and 15 km s^{-1}. Figure 17c shows frequency dependences of radiation intensity from a hot cluster at two collision velocities: 5 and 10 km s^{-1}. It follows from these results that the cluster radiation spectrum extends over the visible region at high velocities of cluster collisions with the surface.

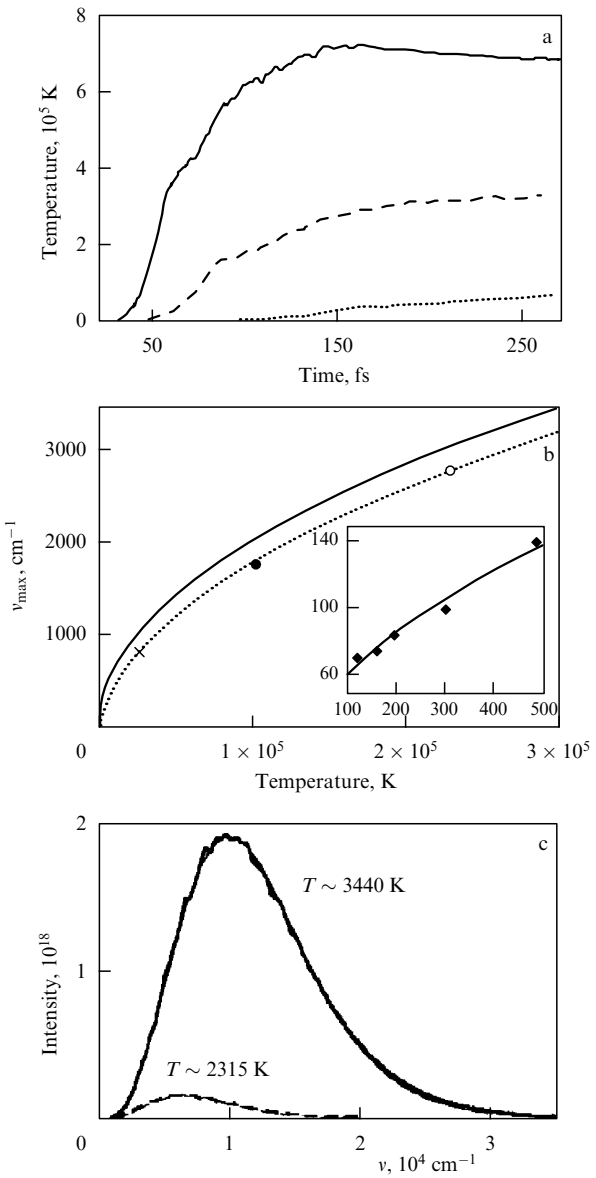

Figure 17. (a) Time dependences of cluster translational temperature at three collision velocities: 5 km s^{-1} ($\cdots$), 10 km s^{-1} ($- - -$), and 15 km s^{-1} (—). (b) The most probable frequency in the cluster absorption spectrum as a function of translational temperature at three collision velocities: 5 km s^{-1} ($\times$), 10 km s^{-1} ($\bullet$), and 15 km s^{-1} ($\circ$). The spectrum was induced by cluster impact on the surface. The dotted line is a fit to dependence $\sqrt{T}$. The inset shows experimental results from Ref. [467], obtained at ordinary temperatures. The solid line is a fit of experimental data points to dependence $\sqrt{T}$. This line extrapolated to a region three orders of magnitude higher is shown in the main figure. (c) Calculated cluster radiation spectra at 5 km s^{-1} ($- - -$) and 10 km s^{-1} (—) collision velocities [238].

According to the data presented in Ref. [238], a hot cluster may be characterized by two temperatures. One is translational temperature associated with the kinetic energy of random atomic motion within the cluster after its collision with a surface. The collision results in an effective transformation of the major part of the kinetic energy of the cluster's directed motion into the kinetic energy of random atomic motions inside the cluster. Therefore, the translational temperature of atoms in the cluster *is proportional to the collision energy*. The other temperature characterizes deformation of electron shells of colliding atoms at the instants of time after strong compression of the cluster. The measure of this temperature is the width of the cluster radiation spectrum. The spectral width of the radiation *is proportional to the velocity* of the cluster collision with the surface (Fig. 17c). Therefore, the electron temperature which is calculated by modelling collision processes is proportional to the cluster velocity. In the case of supersonic collision velocities, the electron temperature is many times higher than room temperature (see Fig. 17c) but much lower than the translational temperature of the atoms inside the cluster (cf. Figs 17a and 17c).

Emission may also be stimulated by the dipole moment induced as a result of collisions between cluster and surface atoms. However, this radiation is effectively damped by the surface [238]. Thus, it was shown in Ref. [238] that emission in the near-IR and visible spectral regions, induced by the rapid motion of atoms relative to one another inside a hot cluster, is possible to observe even in the absence of electronic excitation of the clusters. The collision-induced emission lasts only a short time during which the clusters remain compact so as to ensure interatomic collisions. Because the hot cluster rapidly disintegrates following the collision, photons are emitted only for a very short time interval. This explains why this emission can probably be observed in experiment only with the help of synchronous detectors and the stroboscopic technique [238].

5.7 Production of microfilms and new materials, and treatment of the surface

Interactions of low- and high-energy cluster beams of metals, semiconductors, and alloys with a solid surface have been extensively investigated lately in connection with their technological applications. A major area of their practical implementation is the modification of surface properties by means of film deposition and various methods of treatment, as well as the production of new materials. The interest in these studies is dictated by the necessity of having surfaces with well-defined properties for a variety of modern technologies, including microelectronics, optoelectronic devices, electrochemistry, large memory systems, and plasma displays (see, for instance, Refs [469–472]). The most promising use of cluster beams is the production of materials assembled of clusters that are characterized by specific properties and represent one of the twelve currently known types of nanostructures [473].

The cluster–surface collision process is of primary practical importance for three areas of application, viz., preparation of microfilms, production of new materials, and treatment (cleaning) of surfaces. The advent of cluster-based technology for manufacturing microfilms to be used in microelectronic devices dates to the 1980s (see, for instance, Refs [10, 130–138]). Film deposition on a solid surface with the aid of cluster beams has aroused great interest because this method permits preparation of films with specific properties that cannot be produced by routine epitaxy techniques with atomic and molecular beams. It is worth noting that the aforementioned lines of research have been discussed at greater length in Refs [1, 10, 44, 56, 154, 172].

There are two methods for the deposition of thin films: one is the deposition of neutral clusters at low energies (LECBD or low-energy cluster beam deposition) [152–166], the other is the deposition of cluster ions with broadly varying energies (ICBD or ion cluster beam deposition) [10, 130–151]. The latter technique permits, in addition, working with mass-selected clusters but, at the same time, provides

significantly smaller (by approximately an order of magnitude) film growth rates [44, 56, 154]. Therefore, its application is largely limited to microelectronics. In film deposition using cluster beams, the cluster size is an additional variable parameter, as distinct from film deposition techniques making use of neutral atoms, molecules, and monomer ions. It should be emphasized that homogeneous thin films can be deposited on a surface by any of the above methods. However, thin films with solid clusters imbedded in them ('cluster-assembled materials' [160 – 164]) are possible to prepare only by depositing low-energy cluster beams.

The processes accompanying cluster – surface collisions are rather complicated. They depend on the collision energy, cluster size, and surface type. In the limiting case corresponding to very high impact energies, the surface fracture processes predominate. Therefore, high-energy cluster beams can be employed for surface erosion. The intensity of erosion is diminished with decreasing cluster energy. The release of energy in the collision zone leads to marked cluster fragmentation, the appearance of local surface defects (amenable or not to 'healing' in the subsequent period due to high temperature), and implantation of cluster fragments in the surface material. In Sections 5.7.1 – 5.7.3, we shall consider the influence of cluster size, composition, and kinetic energy on these processes and analyze their effects in concrete situations. One advantage of using cluster beams in the applications discussed above is the possibility of charging clusters and controlling them by an electric field. Simultaneously, their energy can also be varied.

5.7.1 Film deposition. Cluster beams can be utilized to produce homogeneous thin films of various materials, such as metals, insulators, semiconductors, and organic substances (see, for instance, Refs [10, 133 – 160] and Section 5.7.1.2). A detailed description of experimental methods employed for the film deposition can be found in Refs [152 – 154] covering low-energy cluster beams and in Refs [10, 143, 144, 146 – 149] focusing on high-energy ones. In the former group, the energy of the clusters impacted on a solid surface is largely determined by the atomic mass of the substance used to prepare them and also by the nature of the gas-carrier and operating conditions in the cluster beam laser source. The cluster energy in the beam equals $\leqslant 0.1-0.5$ eV per atom. In the latter group, the cluster ion energy depends on the ion-accelerating electrical potential. With these methods, metal clusters (Al, Co, Cu, Fe, Mo, or Ti) containing a single charge and from 10^3 to 10^4 atoms are accelerated in an electric field to energies $\geqslant 10$ eV per atom and deposited on the surface. It was shown in experiment [146 – 148] that the morphology of the film being deposited strongly depends on the kinetic energy of the clusters incident on the surface.

Let us consider in more detail the process of formation of thin films as described in Ref. [144] where computer simulation was applied to investigate the following processes: (1) collision of a single Mo_{1043} cluster with a molybdenum (001) surface at collision energies of 0.1, 1, and 10 eV per atom; (2) successive collisions of 50 Mo_{1043} clusters, and (3) the film growth. The surface temperature in all cases was fixed at $T_s = 300$ K. We shall discuss, without going into detail, the most important results of this study.

5.7.1.1 Impact of a single cluster on a surface. In the study on the collision of a single Mo_{1043} cluster with an Mo (001) surface, the time interval chosen for the purpose of computation was 1 fs. Figure 18 demonstrates the results of cluster deposition. The energy range of collision processes extended from the soft landing of a cluster on a surface at an energy of 0.1 eV per atom, through the stage of cluster flattening at 1 eV per atom to the meteoric collision regime at 10 eV per atom. Atoms were not ejected even at the maximum collision energy. At an energy of 10 eV per atom, the pressure in the collision zone amounted to about 100 GPa (1 Mbar) and a shock wave was generated that propagated into the depths of the target material and was absorbed in it. The cluster temperature reached maximum values of roughly 596 K at a collision energy of 0.1 eV per atom, 1799 K at 1 eV per atom, and 6607 K at 10 eV per atom within the few first picoseconds after the cluster was in touch with the surface. At energies 1 and 10 eV per atom, cluster recrystallization occurred after a lapse of 20 ps. Assuming that this process proceeds under temperature equilibrium, the cluster must have melted at the collision energy of 10 eV per atom. However, the concept of temperature equilibrium is inapplicable within the few first picoseconds. It holds only for longer time intervals. At the collision energy of 10 eV per atom, the cluster completely decomposes and the final distribution of atoms is highly nonequilibrium.

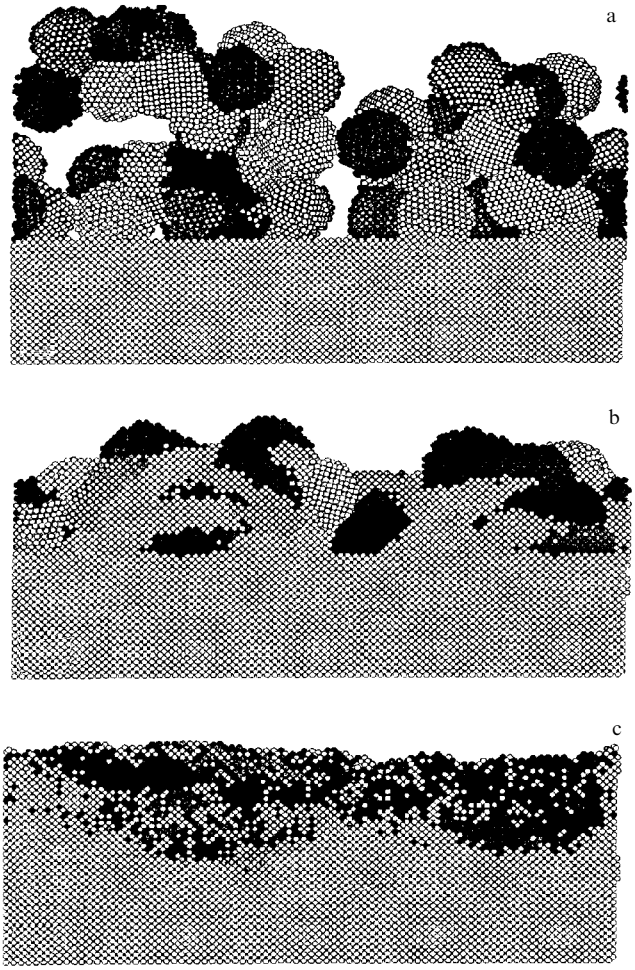

Figure 18. Films formed by Mo_{1043} clusters with a kinetic energy of 0.1 eV per atom (a), 1 eV per atom (b), and 10 eV per atom (c) interacting with an Mo (001) surface [144].

Here are the results of simulation of successive collisions of 50 Mo_{1043} clusters with an Mo (001) surface at a surface

temperature $T_s = 300$ K for the above three collision energies. Cluster deposition at low kinetic energy results in formation of porous films, whereas at the highest kinetic energy it gives rise to dense mirror-smooth surfaces. This result is consistent with experimental data [146–148].

5.7.1.2 Simulation of film formation process. In a model study of collisions between a single cluster and an Mo (001) surface, the authors of Ref. [144] found that the result of computations did not appreciably change when the time interval was extended to 5 fs. This made it possible to simulate the process of film growth. The results of the simulation for three different collision energies suggest three different pictures for film morphology (see Fig. 18). Slow clusters (0.1 eV per atom) remain intact upon collision and smoothly land on one another, giving rise to a black dendrite-like film having a very large surface. The cluster and surface atoms fail to mix very extensively, and the film is easy to mechanically remove from the surface. Moreover, the film density is approximately twice as low as the bulk one.

Clusters with an intermediate collision energy (1 eV per atom) are deposited to form a denser epitaxial film containing only a few cavities [144]. The largest cavities are the size of an incident cluster. The clusters and surface atoms are mixed at distances comparable to the lattice constant. This accounts for their better adhesion compared with that achieved in the case of low-energy collisions. The film density reaches 80% of the bulk density.

Clusters with a collision energy of 10 eV per atom form a dense epitaxial film with a density approaching that of the bulk substance. The film has but few hollows. Initial shapes of individual clusters are practically indistinguishable within the film thickness because they decompose in the course of collisions. The cluster and surface materials mix and the film strongly adheres to the surface.

It follows from the above that model calculations provide a microscopic picture of film growth patterns and predict the final result. The computed dependence of the film microstructure on the energy of molybdenum clusters is in good agreement with the one obtained in experiment [146–148]. It may be expected that the formation of thin films of other materials occurs in a similar way. No significant difference was documented after molybdenum was replaced by Al, Cu, Ti, or TiN, at least under experimental conditions [148].

In the experiments [146–148], a substrate was impacted by a flux of 10^{12} clusters $(cm^2\ s)^{-1}$. The resulting film growth rate was approximately 1 layer per second. In other words, each small area of the surface and its immediate surroundings received one impacting cluster for one second. In the case of a sufficiently high surface temperature, the atoms may extensively diffuse over the surface throughout the deposition time and (or) the surface may be flattened by a nondiffusional mechanism. Such long times are impossible to simulate by molecular dynamics methods. The calculations were confined to a time interval of up to 20 ps, i.e., 11 orders of magnitude shorter than the duration of the experiment. For this reason, the final result of experiment may differ from that in computations. However, in the case under consideration [144], both the experiment and the calculations were performed at a surface temperature of 300 K, i.e., about 10% of the melting temperature of bulky molybdenum. At such a low temperature, it is possible to neglect the mobility of molybdenum atoms or clusters over the surface. Therefore, it can be concluded that inferences concerning film growth by means of molecular dynamics simulation at room surface temperature provide the correct explanation of the experimentally established structure of thin films.

An interesting approach to the controlled growth of nanophase (nanostructural) materials was proposed in Ref. [149]. Nanophase materials are said to be solids composed of nanometer-sized structural units that retain their individual characteristics after assembling [149]. The study [149] was designed to investigate the dynamics and energy transfer and redistribution processes during collisions of Cu_{147} clusters with a clean Cu (111) surface and with a surface covered by an adsorbed liquid film by means of computer simulation. The study demonstrated that collisions of Cu_{147} clusters having an ordered icosahedral structure with the clean surface at velocities higher than thermal ones induced a number of processes, including the embedding of cluster atoms in the surface, erosion of the surface, structural disordering, and expansion of the clusters. At the same time, the deposition of clusters on a low-density liquid film (composed of argon atoms) was accompanied by the effective energy transfer to the liquid film. At cluster–surface collision velocities of up to 2–4 km s^{-1}, this process could give rise to controllable soft deposition of crystalline clusters on a solid surface. At an incidence velocity of up to 2 km s^{-1}, the clusters did not melt and retained their structure, whereas at a collision velocity of 4 km s^{-1} they became overheated and melted. Thereafter, the clusters smoothly landed on the Cu (111) surface and underwent recrystallization. When clusters impinged upon a liquid xenon film at velocities of 2–4 km s^{-1}, a larger (than in case of argon film) part of their translational energy was converted to internal energy. Such collisions led to a rapid decrease in the cluster incident velocity due to the liquid film. This was accompanied by ultrafast heating of the clusters to a high temperature, their overheating, and melting. At the same time, clusters incident on a xenon film at some selected velocities, e.g., 2 km s^{-1}, tended to be rapidly cooled as their energy was transferred to the liquid film. As a result, such solid clusters were amenable to vitrification [149].

5.7.2 Production of new materials. By using low-energy cluster beams (in the framework of the LECBD method) it is possible to make films assembled of clusters and possessing previously unknown surface morphology and properties [152–154]. The interaction between a cluster beam and a substrate onto which it is incident depends on the cluster size and energy [44, 172, 173]. If the energy is low (usually smaller than 1 eV per atom), the cluster is deposited on the surface without fragmentation. It adheres to the substrate and its atoms disperse over it. In this case, the cluster impacts the substrate as a liquid drop and forms a flat contact with it. Thereafter, the atoms from the cluster outside surface spread over the entire substrate area by virtue of their diffusive motion. As a result, they make up a thin film on the substrate surface. In this way, it is possible to produce nanostructural films from different types of materials (metals, semiconductors, organic substances, and alloys) with a variety of properties, depending on the conditions of film formation, which include the size, intensity, and composition of the incident clusters, the nature and temperature of the target surface, and the depth of vacuum in the vacuum chamber where the film deposition occurs [152–154]. Films of new materials can also be manufactured by depositing a solid inert gas matrix (e.g., Ar or Kr) on the substrate and subsequently bombarding it with

solid clusters [154, 165, 166]. These materials make up homogeneous films containing closely sized clusters imbedded in them (because the beam is dominated by 'magic' clusters). Such films may serve as optical filters due to the ability of the inserted clusters to absorb radiation in specific spectral regions [159]. The spectral characteristics of such filters depend on the cluster size, type, and density. Given a transparent matrix, these materials may be utilized as optoelectronic elements. The process of cluster (and atom) absorption may come to saturation. Due to this, films produced by the method being considered may serve as optical gates by virtue of their nonlinear transparency [44, 56, 154].

Films with embedded clusters of magnetic materials (Fe, Co, Ni) are magnetic nanostructures [44, 56, 154]. They resemble magnetic materials consisting of domains. However, the size of individual grains in these films, i.e., the size of individual clusters, being several times smaller than the size of domains in ordinary magnetic materials, the magnetic saturation field for these new materials is also weaker. Moreover, the virtually close sizes of the grains (i.e., imbedded clusters) ensures a higher precision and selectivity of devices constructed with the use of these new magnetic materials. Furthermore, the possibility of changing the type and size of embedded clusters permits us to control the parameters of magnetic films. Because of this, cluster-embedded film, as well as the materials built up from clusters, hold promise in manufacturing precision instruments.

It should be noted in connection with the questions considered in the present section that clusters formed by means of atomic agglomeration, including that on solid surfaces, represent a new state of matter. They possess a variety of novel properties that depend on their size, shape, composition, and characteristics of constituent particles [167, 168]. The chemical properties of stable metallic clusters may be similar to those of diverse atoms of the Periodic System. For example, the chemical properties of an Al_{13} cluster are reminiscent of the properties of halogen atoms even though aluminium belongs to metals. The properties of a CAl_{12} cluster resemble those of an inert gas atom, and the properties of an NAl_{12} cluster resemble those of an alkali metal atom. This means that clusters may be assembled as 'superatoms'. Using such clusters as 'building blocks', it is possible to synthesize crystals. A real advantage of utilizing clusters for this purpose lies in the fact that their properties can be modified by varying their size and composition. Complicated calculations (see the paper [168] and references cited therein) indicate that cluster solid bodies made up of such 'superatoms' are actually metastable. Interestingly, the intercluster bonds can be either weak (of the van der Waals type) or strong (of ion type) even though the constituent atoms of the clusters are metals, while crystals produced from them may be nonmetal [168].

5.7.3 Treatment of the surface. High-energy cluster beams are also employed to treat surfaces [169 – 187]. With high-energy clusters, it is possible to drill holes in metal foils to produce sieves [169] or make craters at solid surfaces [186, 187] or clean [174, 175] or smooth [181, 183] them. High-energy cluster beams are also used in lithography [176, 177]. When drilling holes and making craters, each cluster acts as a small projectile. The ultimate hole size depends on the cluster size and energy. The higher the energy, the larger the hole diameter. Thus, it is possible to control the size and the density of holes in a sieve. However, unlike the case of atomic ion beams, where the size of the defects being formed is comparable to the atomic size, cluster beams produce holes the size of which is much bigger than the cluster size. For example, a focused beam of gallium atomic ions allows a spot some 8 nm in diameter to be created on the surface [170], whereas fast metallic clusters impacted on a micrometer-thick foil make a hole with a diameter of around 1 μm [169, 171], even though their own diameter does not exceed 10 nm. At the same time, the mechanism of formation of such big holes remains unclear. Cluster beams in the capacity of energy carriers are also used to clean surfaces. In this case, surface atoms are evaporated under the action of fast clusters [174, 175].

Crater formation on solid surfaces impacted by high-energy clusters will be briefly considered based on the results of recent works reported in Refs [186, 187] (see also Ref. [143]). The authors of Refs [186, 187] studied the process of the collision of high-energy Ar_N and $(CO_2)_N$ clusters ($N \cong 960$) with a diamond (111) surface. At a collision energy of 100 keV per cluster, the craters formed were hemispherical in shape. Simultaneously, two- and three-layer shock waves were generated at an earlier stage of the collision. Thereafter, hot melted carbon very quickly (for roughly 2 ps) filled up the craters again. When CO_2 clusters were used, a peak arising at the site of collision persisted for a longer period. Short-lived craters were observed to form at lower collision energies, too ($30 \leqslant E_{col} \leqslant 70$ keV per cluster), whereas only elastic strain of the surface was apparent at $E_{col} = 10$ keV per cluster. The volume of a short-lived crater was roughly proportional to the collision energy E_{col}, while the volume of the plastically strained area and the fraction of the kinetic energy transferred to the surface by a shock wave were the linear functions of E_{col} (with a threshold energy of about 10 keV subtracted). At a collision energy of 100 keV per cluster, the number of carbon atoms emitted from the surface upon impact of CO_2 clusters was approximately 3.4 times that in the case of argon clusters. However, the crater surface following energy relaxation was more densely packed in experiments with argon clusters (see Fig. 19). One of the aims in the study [187] was to assess the penetration depth of argon clusters and absolutely hard spherical particles of a similar size into the surface material. The lateral dimensions of the clusters and the particles were identical (10 Å). Argon clusters and hard particles were found to go as deep as approximately 30 Å and 40 Å, respectively, into the surface. In either case, the penetration time was about 0.7 – 0.8 ps. The authors attributed the difference in the penetration depth to the formation of a backward shock wave behind a colliding solid particle, which hampers transfer of the pulse momentum to the surface.

In lithography, the employment of high-energy cluster beams permits obtaining very smooth surfaces with sharp boundaries. By way of example, the authors of Ref. [176] made hexahedral blind-holes (pits) with very sharp edges at the surface of boron – silicon glass (pyrex). The bottom of the pits was as smooth as the initial target surface. Detailed studies showed that a cluster impact on the surface caused the surface material to melt [178].

The surface erosion by a cluster beam may be accelerated by the so-called RACE (reactive-accelerated cluster erosion) method [172, 176, 177]. This method makes use of the reaction between a cluster and the surface material. For example,

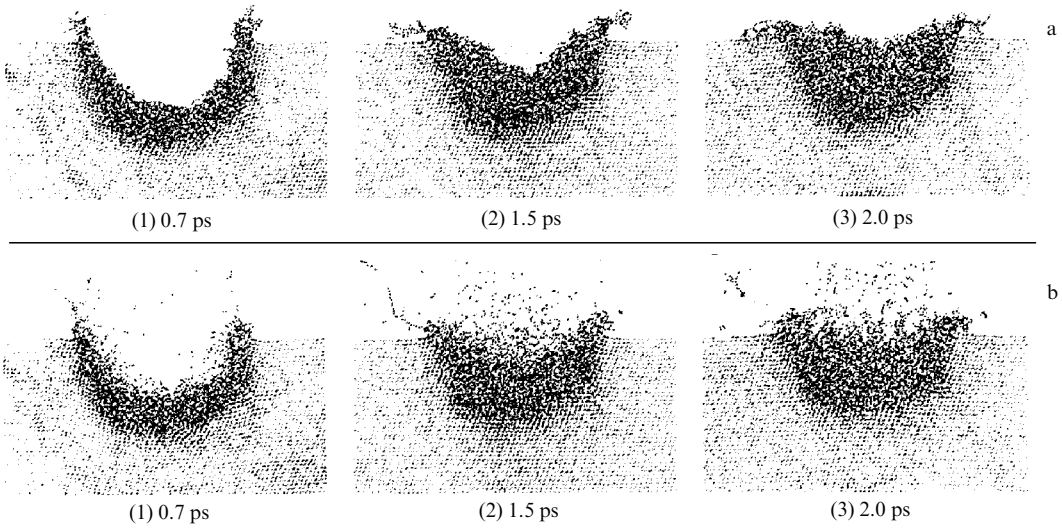

Figure 19. Comparative results of collisions between Ar (a) and CO_2 (b) clusters and a diamond surface (lateral view, magnified) [186].

erosion of a diamond surface impacted by CO_2 clusters occurs at the same rate as that of a silicon surface, despite the much greater strength of the diamond [177]. At a high temperature induced by cluster–surface collisions, CO_2 molecules dissociate and release oxygen atoms that interact with carbon atoms and give rise to CO. Volatile CO molecules ensure efficient removal of carbon from the erosion zone. Surfaces treated by this method contain no residual carbon. Erosion of a silicon surface by SF_6 clusters is also a chemically accelerated process because it is accompanied by the formation of volatile SiF_4 compound.

High-energy cluster beams are also used to smooth roughly structured metallic surfaces [181, 183]. It was shown in Ref. [181] that the treatment of the rough surface of a structured copper film with high-energy metal cluster ions $(Cu)_N^-$ ($\overline{N} = 1400$, $E_{kin} = 18$ eV atom^{-1}) made it smoother tangibly. The efficiency of the planing treatment improved as the cluster size increased from 15 to 72 nm. The authors developed a model according to which smoothing is due to the formation of a film of deposited clusters on the treated surface and the subsequent flow of cluster particles and surface material from the tips to the base of the hillocks at the structured surface. In the course of this process, the upper parts of the hillocks were transported to the valleys.

5.8 Summary

Collisions of high-energy atomic or molecular clusters and cluster ions with the surface of insulators, semiconductors, and metals lead to the formation of a medium with extremely high density, temperature, and energy density. Such a medium is generated within a very short time ($\leqslant 50-500$ fs) during which a microshock wave generated by the cluster impact on a surface propagates inside the cluster. Investigations into extreme processes induced by cluster collisions with the surface (such as electron emission, cluster fragmentation, generation of microshock waves, breaking and making of chemical bonds, nuclear fusion, light emission, bombardment of the surface) provide information about a variety of homogeneous and heterogeneous processes of energy transfer and redistribution that occur within the ultrashort time scale of molecular motion.

The data resulted from the investigations indicate that the scattering of molecular cluster ions from a solid surface may be close to elastic and accompanied by the transfer of only a small part of the kinetic energy to the target. In the specific case of protonated ammonia cluster cations $(NH_3)_N H^+$ impinging upon a diamond-coated silicon target, about 75% of the initial kinetic energy as a rule remains with intact scattered cluster ions. However, as soon as the colliding cluster ions acquire sufficient internal energy, they undergo fragmentation, largely into monomers. Such a sharp passage from a damageless scattering regime to the complete decomposition of the clusters, depending on the collision energy, is especially apparent due to the absence of intermediate-sized fragments or fragments of a size close to that of parent ions. It may be supposed that such a behavior is characteristic of all cluster ions containing hydrogen bonds.

Ultrafast redistribution of energy within cluster ions can be employed for obtaining 'ultrahot' clusters with energies sufficient to break practically all intermolecular bonds. The method of high-energy cluster impact on a solid surface provides a new energy regime under which an energy of 1–50 eV per molecule can be delivered for a time of 10–100 fs. This energy may be used to break the existing molecular bonds or even make new chemical bonds. It was shown that chemical reactions induced by cluster impact on the surface lead to rather a high yield of reaction products. Even in the case of a small $(CH_3I)_N^-$ cluster ion ($N < 15$), the relative yield of I_2^- ions per I^- ion amounts to 15%. Similar yields are obtained in reactions with other cluster ions [122–125]. Therefore, it may be concluded that chemical reactions induced by cluster–surface collisions represent a new and rather general mechanism of femtosecond chemistry.

Studies on the interaction of cluster beams of metals and semiconductors with a solid surface demonstrated that it may be utilized for treating surfaces and producing thin films and totally new materials. Nanostructures, thin films, and cluster materials obtained with the use of cluster beams are characterized by specific properties and a structure relevant to modern technological applications. These materials are highly promising for the creation of new elements to be applied in microelectronics, optics, and optoelectronics, for the development of devices and other instruments with valuable unusual characteristics.

6. Comparison of cluster excitation upon impact on a surface and by superhigh-power ultrashort laser pulses

6.1 Interaction of clusters with a laser pulse

In Sections 4 and 5, we discussed processes induced by collisions of large clusters with a solid surface. In this context, it appears appropriate to compare the excitation of clusters impacting on a surface and their excitation by high-intensity ultrashort laser pulses. Such a comparison may provide a clearer view of the techniques currently available for 'instantaneous' strong excitation of clusters and help in better understanding similar and dissimilar features of the processes inherent in cluster excitation by these two methods. It should be emphasized from the very beginning that the cluster excitation by superhigh-power ultrashort laser pulses has already been the subject of numerous studies. It is therefore impossible to discuss in one short section of this communication even the most important results obtained thus far in the field of interest, nor can the current state of research, recent progress, and the most demanding challenges be considered in full measure. That is not the goal here. A rather detailed analysis of the processes associated with the excitation of clusters by superhigh-power ultrashort laser pulses is presented in review articles by B M Smirnov [53, 56], V P Krainov and M B Smirnov [54, 55], and T Ditmire et al. [57 – 59]. We shall briefly discuss here some of the more interesting and important data with reference to the differences and similarities intrinsic in cluster excitation by the above two methods.

The excitation of clusters by superhigh-power ultrashort laser pulses has become possible to explore due to rapid recent progress in the development of superhigh-power laser systems producing ultrashort pulses [474, 475]. This is a relatively new and rapidly growing research area [53 – 59, 77 – 83, 476 – 478]. The results of the studies [53 – 59, 478] suggest a rather close analogy between the two types of cluster excitation in question.

Typical laser energy flux densities and pulse durations in such experiments (see, for instance, Refs [53 – 59, 478]) are $10^{16} - 10^{20}$ W cm^{-2} and $\tau_p \sim 30 - 300$ fs, respectively. The electric field strength in a laser wave is much stronger than that typical of a hydrogen atom (about 10^9 V cm^{-1}). Therefore, a laser pulse can ionize cluster atoms by inducing an overbarrier electron transition. This is also true for the newly formed ions. As a result of interaction with a laser pulse, clusters give rise to a system of multiply charged ions and free electrons [53 – 59]. When some electrons leave a cluster, it becomes positively charged, whereas the remaining electrons are confined by the self-consistent cluster field. The resulting system of multiply charged ions and electrons is unstable and disintegrates when the ions fly off. However, the system being destroyed at ion velocities, its decay time may be significantly longer than the laser pulse duration. This plasma formation stage affects its properties [53 – 59]. The character of interaction between a cluster beam and a superhigh-power ultrashort laser pulse permits conveying a higher specific energy to the electron subsystem (reaching $\geqslant 1$ keV per electron). Absorption of the laser pulse energy by the cluster beam leads to the formation of specific hot plasma [56].

It should be emphasized that the interaction between a superhigh-power ultrashort laser pulse and cluster beams is substantially different from the pulse's interaction with single atoms [53 – 59, 478] and solid targets (see, for instance, Refs [479 – 481] and references cited therein). The structure of a cluster beam is intermediate between that of gaseous and solid targets. The beam is composed of separate atoms or molecules and clusters measuring less than 10 – 100 nm, each containing from a few hundred to a few million atoms. The mean number density of atoms in the beam ranges $10^{16} - 10^{19}$ cm^{-3}, and the local density, i.e., cluster atomic density, is around 2×10^{22} cm^{-3}. The fraction of atoms assembled into clusters in the beam varies between 10 and 100% of the total number of particles, depending on the cluster beam production conditions [53 – 59].

When a cluster beam is irradiated by a superhigh-power ultrashort laser pulse, it is transformed into plasma with unique properties [478]. On the one hand, there is plasma at the sites harboring clusters with a density substantially higher than the critical one [55, 58, 482, 483]. It consists of multiply charged ions and electrons with energies in the kiloelectronvolt range [476]. On the other hand, an electromagnetic wave freely propagates and interacts with all atoms of the target owing to the subcritical mean electron density of the medium and the small size of individual clusters. In other words, the wave penetrates unobstructed into regions with an electron density higher than the critical one and is not reflected, as in the case of solid targets [484]. Due to this, it is possible to achieve a high level of specific laser energy absorption in the cluster beam and, accordingly, to ensure higher specific excitation of the substance, i.e., a higher energy deposition to each atom compared with that in other types of targets. Hence, the data obtained are considerably different from the results of experiments with both solid and gaseous targets [53 – 59, 478].

6.2 Processes in clusters excited by laser pulses

When clusters are excited by ultrashort laser pulses, atomic ions are not immediately heated. After rapid initial multiple ionization, the substance of a cluster ion during most of the laser pulse time is in the form of an ideal plasma composed of electrons and multiply charged atomic ions. As long as excitation by the laser pulse lasts and for some time after it, the strongly excited cluster is a site where a number of nonequilibrium extreme processes develop [53 – 59]. They include internal and external cluster photoionization, Coulomb and hydrodynamic explosions, nuclear fusion, generation of higher harmonics, X-rays, and neutrons. Some of these processes are discussed at greater length below.

6.2.1 Coulomb and hydrodynamic explosions. Formation of homogeneous cluster plasma and the aforementioned processes follows an explosion (expansion) of clusters. Let us consider explosion mechanisms [57, 83, 485, 486]. There are two forces acting on a cluster and responsible for its expansion during the course of the excitation pulse and after it. One is the pressure exerted by hot electrons. Hot electrons expand outward and extrude cold and heavy ions to the outside of the cluster. The characteristic velocity of expanding electrons is equal to the speed of sound in the plasma:

$$v_{\mathrm{exp}} \sim \left(\frac{ZkT_e}{m_i}\right)^{1/2}, \qquad (6.1)$$

where Z is the charge of the cluster ion, kT_e is the electron temperature of the cluster, and m_i is the ion mass. The other

force acting on the cluster is associated with the formation of the electric charge of the cluster. The laser field causes rapid ionization of cluster atoms. The electrons and ions arising in the cluster create a self-consistent field that interacts with the laser field; this, in turn, leads to the ejection of a portion of the electrons outside the cluster. The cluster charge that forms in the course of this process induces an electric field that causes internal atomic ions of the cluster to fly away, leading to its Coulomb explosion [54 – 56].

Because the electron pressure is given by the expression

$$p_e = n_e k T_e \tag{6.2}$$

(n_e is the electron concentration), the rate of cluster temperature lowering associated with the expansion is determined by the following relation [57, 83]

$$\left.\frac{\partial T_e}{\partial t}\right|_{exp} = -2\,\frac{T_e}{r}\,\frac{\partial r}{\partial t}\,, \tag{6.3}$$

where r is the cluster radius.

The force of the accumulated charge acting on cluster expansion is evaluated by considering the cluster plasma sphere [57] as an ideal conductor and assuming that the accumulated charge Q_e is located at the cluster surface. The stored energy of the spherical 'capacitor' is given by

$$E_{Q_e} = \frac{Q^2 e^2}{2r^2}\,. \tag{6.4}$$

Then, the force acting on unit surface area equals

$$p_{Coul} = \frac{Q^2 e^2}{8\pi r^4}\,. \tag{6.5}$$

Factor $1/r^4$ in relationship (6.5) indicates that in the case of small clusters the Coulomb force predominates. It is worth comparing relative contributions of the forces acting on the cluster from Coulomb and hydrodynamic pressures to understand which of them dominates in clusters of a given size. It follows from relationships (6.2) and (6.5) that for clusters measuring 100 Å with electron number density 10^{23} cm^{-3} and temperature 1000 eV, the Coulomb pressure becomes comparable to the hydrodynamic one, when $Q \cong 10^5$. This situation corresponds to the excitation of only some 20% of the cluster electrons (for $Z = 8$), suggesting the important contribution of the Coulomb force to the cluster expansion rate. However, the hydrodynamic force comes into predominance as the cluster expands because the hydrodynamic pressure is proportional to $1/r^3$ (due to n_e), whereas the Coulomb pressure is proportional to $1/r^4$ [57].

It is worth noting that very hot clusters expand rather quickly regardless of the explosion mechanism [57]. Suffice it to say that the Coulomb explosion results in a two-fold expansion of a deuterium cluster measuring 100 Å within $\leqslant 20$ fs at an electron temperature of 1 keV. The analysis shows [57, 83] that large clusters expand more slowly than small ones. Large clusters are on the whole preferable for laser excitation because they withstand disintegration longer when heated by a laser pulse and can therefore acquire more energy from it. Expansion affects cluster dynamics since its electron temperature decreases in accordance with relationship (6.3). At the same time, an alternative mechanism of electron cooling deserves to be considered. It is associated with the energy transfer from hot electrons to cold ions in the course of collisional thermalization [53 – 58].

6.2.2 Generation of X-ray emission and neutrons. The interaction between a cluster beam and femtosecond high-intensity laser pulses is used to create an effective and a compact source of X-ray emission [84 – 92, 487 – 490]. As noted in Section 6.1, absorption of laser radiation by clusters leads to the appearance of heterogeneous hot plasma composed of multiply charged ions and electrons captured by them [53 – 59]. Further development of the plasma after cessation of the laser pulse is accompanied by the formation of excited multiply charged ions and other excited states that begin then to emit shortwave photons. It should be noted that the ability to emit shortwave radiation is inherent in any hot plasma [56], while a characteristic feature of the plasma under consideration is the high rate of processes proceeding in it, with the duration of its early evolution stages being shorter than the time of photon emission. This predetermines the specificity of radiative processes. The excitation develops at the initial stages of plasma evolution, whereas photons are formed at subsequent stages. Nevertheless, the plasma maintains a highly efficient conversion of the laser pulse energy into X-ray energy that ranges from one to several percent [53 – 59, 478].

Similar processes occur in the plasma being considered, when it is used as a source of neutrons [56 – 59, 93 – 97]. In this case, a beam of deuterium clusters is irradiated by a laser pulse. The high electric potential of the plasma being formed at each cluster creates active ions as this plasma flies apart under the action of the self-consistent cluster field. The energy of such ions amounts to several dozen kiloelectron-volts, and collisions of fast deuterium ions at the next stage of plasma evolution, when it becomes homogeneous following the bouncing apart of the clusters, may ignite a thermonuclear fusion reaction with the participation of these ions. Such a scheme cannot be used to build a thermonuclear reactor because the Lawson criterion for the plasma parameters proves to be four or five orders of magnitude smaller than its threshold value for a self-supporting thermonuclear reaction. For all that, this scheme is suitable for the construction of a source of neutrons using a beam of deuterium clusters or deuterium-containing molecules [56, 59, 93 – 97].

High-energy ions were first utilized to produce D – D-fusion neutrons in the work [93]. Figure 20a displays the layout of the experiment. Large deuterium clusters formed in a gasdynamic jet in the course of gas outflow from a nozzle. A superhigh-power ($\geqslant 10^{16}$ W cm^{-2}) ultrashort (35 ps) laser pulse with an energy of 120 mJ (at the pulse repetition frequency of 10 Hz) was focused on the jet containing deuterium clusters and rapidly heated them. The clusters then exploded and gave rise to ions with an energy of several kiloelectron-volts. This process resulted in the formation of a plasma filament with a diameter approximately equal to the laser focal diameter (around 200 μm) and a length roughly identical to the width of the deuterium cluster jet ($\cong$ 2 mm). Fast deuterium ions that flew away from exploding clusters may interact with the ions ejected from other clusters present in the plasma. At a high energy of the ions (in excess of several kiloelectron-volts), there was a high probability of D – D fusion. A good indicator of this process was that one of the channels of the D – D fusion reaction $D + D \rightarrow {}^3He + n$, in which the neutrons formed had an energy of 2.45 MeV.

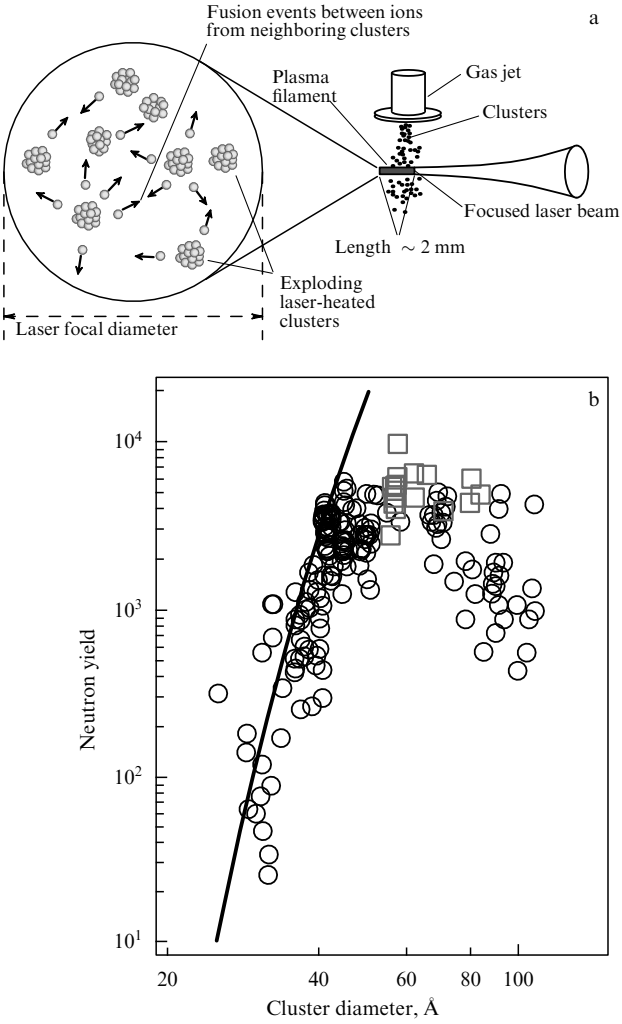

Figure 20. (a) Experimental configuration for the synthesis of deuterium clusters [93]. (b) Neutron yield plotted versus the mean diameter of the deuterium clusters. The gas pressure above the nozzle is 55 atm. Squares denote maximum neutron yields obtained by varying the distance between the nozzle and the excitation zone. The solid line portrays the expected dependence [94].

A combination of scintillators with a photomultiplier was employed to detect neutrons in the work under consideration. The neutron energy was determined by time-of-flight measurements. It was found that the neutrons' time of flight was 46 ns per meter, which corresponded to the neutron energy of 2.45 MeV and the reaction yield of 1×10^4 neutrons per pulse [93, 94] (see Fig. 20b). Such neutron generation efficiency (about 10^5 neutrons per 1 J of the laser energy) is comparable to neutron yields at large-scale production units (see, for instance, the paper [93] and references cited therein).

It is worthwhile noting that the generation of neutrons during the excitation of clusters by superhigh-power ultrashort laser pulses has recently attracted the attention of many researchers (see, for example, the works [59, 95–97] and references cited therein). There is reason to expect that a combination of cluster beams and superhigh-power ultrashort laser pulses will make it possible to create compact sources of X-rays and neutrons.

To summarize, the results reviewed in this section and Section 5 indicate that the excitation of clusters by superhigh-power ultrashort laser pulses and that by high-velocity collisions with a surface have much in common. In particular, the energy depositions to the clusters in these two mechanisms are comparable, as are cluster excitation rates ($\sim 10^{13}-10^{14}$ s^{-1}) and decay lifetimes ($\sim 10^{-13}$ s). In either case, the excitation is accompanied by the emission of charged particle (electrons and ions), cluster fragmentation, light emission, a nuclear fusion reaction, and a generation of neutrons. At the same time, cluster excitation by laser pulses probably permits one to realize a larger specific energy deposition per particle [59] and obtain a larger volume of denser cluster plasma than in the case of cluster impact on the solid surface. This method is preferred for producing high-temperature cluster plasma and generating X-rays and neutrons.

7. Conclusions

The available results of research provide an insight into the mechanisms of scattering of van der Waals clusters from a solid surface at moderate (thermal) collision velocities and into many processes associated with cluster impact on a solid surface at supersonic and hypersonic velocities. Even the very first experiments on the interaction between clusters and surfaces showed that clusters are largely scattered within the incidence plane, unlike monomers scattered outside it. Under certain conditions, a cluster beam may even be focused as it is reflected from the surface. Of primary importance for cluster scattering is the cluster size, velocity, angle of incidence upon the surface, and surface temperature. Three major scattering channels have been identified, through which low-energy clusters interact with a solid surface: (1) scattering of monomers from the surface due to the adsorption–desorption process; (2) scattering of small fragments from a cluster sliding over the surface as a result of cluster evaporation, and (3) scattering of big fragments survived after collisions through large tangential angles. The fraction of clusters surviving after collisions grows with increasing cluster size, angle of incidence, and surface temperature, while it decreases as the normal component of the incidence velocity increases.

Experimental and theoretical studies of collisions between water clusters and solid surfaces demonstrated that cluster ionization and charge separation are the probable processes. At the same time, quite a different mechanism of charge formation and separation upon collisions of water clusters and clusters of other polar molecules with a solid surface was proposed. The results of many earlier experiments on water cluster ionization allow an alternative explanation. This emphasizes the necessity of further studies for a deeper insight into the nature of charge formation and separation that occur as water clusters impact on a surface.

Investigations into the collisions of high-energy clusters with a solid surface revealed a number of extreme processes in clusters and a collision zone that cannot proceed under ordinary thermal conditions. They include electron emission, cluster fragmentation, breaking of chemical bonds, initiation of chemical reactions in clusters, generation of microshock waves, nuclear fusion and generation of neutrons, light emission, and bombardment of the surface. All these processes are conditioned by the strong and rapid heating of clusters in their impact on the surface that leads to the generation of a microshock wave within the cluster and in the collision zone during a very short span of time $\leqslant 1$ ps. Many of the listed processes and the results of their studies

are of great interest in the context of cluster application to the solution of many theoretical and practical problems. The fundamental aspects of the employment of high-energy clusters and cluster ions include, for example, the delivery of nuclear matter into a thermonuclear reactor, investigations into the interaction of high-energy particles with the materials of spacecrafts and other objects, and collisions of meteorites with Earth and other planets. The practical value of the available data is determined by their relevance to technological applications of clusters in such fields as microelectronics, film deposition, the formation of nanostructures, surface treatment, and the production of new materials.

Comparison of the results obtained in studies on cluster excitation by superhigh-power ultrashort laser pulses and by collisions with a surface indicates that these two approaches have much in common. Specifically, the energy depositions to the clusters are comparable, as are their excitation rates and decay lifetimes. In either case, the excitation is accompanied by the emission of charged particle (electrons and ions), cluster fragmentation, light emission, a nuclear fusion reaction, and the generation of neutrons. At the same time, cluster excitation by laser pulses probably permits us to realize a larger specific energy deposition to a particle [59] and to obtain a larger volume of denser cluster plasma than in the case of cluster impact on the surface. There is one more important feature characterizing cluster excitation by these two methods. In the case of laser excitation, the energy is deposited to a cluster largely through the electron subsystem, whereas in the case of impact-induced excitation the cluster acquires energy via the nuclear subsystem. For this reason, the cluster–surface collision allows for a 'smoother' excitation regime to be realized than laser irradiation does. Cluster impact on a surface makes it possible to attain nonequilibrium conditions where ion temperature is higher than electron temperature ($T_i > T_e$), as opposed to nonequilibrium conditions ($T_e > T_i$) produced by laser-induced cluster excitation. It is a distinctive feature of cluster excitation that distinguishes between the two methods. As shown in Ref. [108], conditions $T_i > T_e$ (or $T_e = 0$) provide for a substantial increase in the nuclear fusion rate. Of interest in this context is the combined excitation of clusters by superhigh-power ultrashort laser pulses and by collisions with a solid surface (or between themselves in counterpropagating beams).

In conclusion, one more remark is in order. New sources for the production of previously unknown materials may appear if researchers manage to develop methods for the synthesis of clusters in volumetric amounts, so that they retain their structure [1, 154, 168]. In-depth and extensive studies of cluster beams currently in progress give reason to believe that new interesting and important data necessary for explaining their behavior and better understanding physical mechanisms of cluster excitation will be obtained in the near future [491, 492]. This will doubtlessly promote both the use of cluster beams in research and their practical implementation.

The author expresses his thanks to V N Lokhman, E A Nikolaeva, and A N Petin for technical assistance. Profound gratitudes are due to the reviewer for valuable comments. The work was partly supported by the Russian Foundation for Basic Research (grant No. 03-02-17067).

References

1. Pauly H *Atom, Molecule, and Cluster Beams* Vol. 2 *Cluster Beams, Fast and Slow Beams, Accessory Equipment, and Applications* (New York: Springer, 2000)
2. Scoles G (Ed.) *Atomic and Molecular Beam Methods* Vol. 1 (New York: Oxford Univ. Press, 1988)
3. Scoles G (Ed.) *Atomic and Molecular Beam Methods* Vol. 2 (New York: Oxford Univ. Press, 1992)
4. Petrov Yu I *Klastery i Malye Chastitsy* (Clusters and Small Particles) (Moscow: Nauka, 1986)
5. Jena P, Rao B K, Khanna S N (Eds) *Physics and Chemistry of Small Clusters* (NATO ASI Ser., Ser. B, Vol. 158) (New York: Plenum Press, 1987)
6. Jena P, Khanna S N, Rao B K (Eds) *Physics and Chemistry of Finite Systems*: *From Clusters to Crystals* (NATO ASI Ser., Ser. C, No. 374) (Dordrecht: Kluwer Acad. Publ., 1992)
7. Jortner J, Pullman A, Pullman B (Eds) *Large Finite Systems*: *Proc. of the Twentieth Jerusalem Symp. on Quantum Chemistry and Biochemistry, Jerusalem, Israel, May 11–14, 1987* (The Jerusalem Symp. on Quantum Chemistry and Biochemistry, Vol. 20) (Dordrecht: D. Reidel, 1987)
8. Vostrikov A A, Rebrov A K (Eds) *Fizika Klasterov* Sbornik Nauchnykh Trudov (Cluster Physics. Collected Works) (Novosibirsk: Nauka, 1987)
9. Sugano S, Nishina Y, Ohnishi S (Eds) *Microclusters*: *Proc. of the First NEC Symp., Hakone and Kawasaki, Japan, October 20–23, 1986* (Springer Ser. in Materials Science, Vol. 4) (Berlin: Springer-Verlag, 1987)
10. Takagi T *Ionized-Cluster Beam Deposition and Epitaxy* (Park Ridge, NJ: Noyes Publ., 1988)
11. Benedek G, Martin T P, Pacchioni G (Eds) *Elemental and Molecular Clusters*: *Proc. of the 13th Intern. School, Erice, Italy, July 1–15, 1987* (Springer Ser. in Materials Science, Vol. 6) (Berlin: Springer-Verlag, 1988)
12. Aleksandrov M L, Kusner Yu S *Gazodinamicheskie Molekulyarnye, Ionnye i Klastirovannye Puchki* (Gasdynamic Molecular, Ionic, and Cluster Beams) (Ed.-in-Chief E P Velikhov) (Leningrad: Nauka, 1989)
13. Bernstein E R (Ed.) *Atomic and Molecular Clusters* (Studies in Physical and Theoretical Chemistry, Vol. 68) (Amsterdam: Elsevier, 1990)
14. Billups W E, Giufolini M A (Eds) *Buckminsterfullerenes* (New York: VCH, 1993)
15. Haberland H (Ed.) *Clusters of Atoms and Molecules*: *Theory, Experiment, and Clusters of Atoms* (Springer Ser. in Chemical Physics, Vol. 52) (Heidelberg: Springer-Verlag, 1994)
16. Klabunde K J *Free Atoms, Clusters, and Nanoscale Particles* (San Diego: Academic Press, 1994)
17. Kondow T, Kaya K, Terasaki A (Eds) *Structures and Dynamics of Clusters*: *Proc. of the Yamada XLIII Conf. on Structures and Dynamics of Clusters, May 10–13, 1995, Shimoda, Shizuoka, Japan* (Frontiers Science Ser., No. 16) (Tokyo: Universal Academy Press, 1996)
18. Martin T P (Ed.) *Large Clusters of Atoms and Molecules* (NATO ASI Ser., Ser. E, No. 313) (Dordrecht: Kluwer Acad. Publ., 1996)
19. Yoshimura S, Chang R P H (Eds) *Supercarbon*: *Synthesis, Properties, and Applications* (Springer Ser. in Materials Science, Vol. 33) (Heidelberg: Springer, 1998)
20. Hirsch A (Ed.) *Fullerenes and Related Structures* (Topics in Current Chemistry, Vol. 199) (Heidelberg: Springer-Verlag, 1999)
21. Smirnov B M *Clusters and Small Particles*: *in Gases and Plasmas* (New York: Springer, 2000)
22. Campargue R (Ed.) *Atomic and Molecular Beams*: *the State of the Art 2000* (Berlin: Springer, 2001)
23. Lakhno V D *Klastery v Fizike, Khimii, Biologii* (Clusters in Physics, Chemistry, Biology) (Izhevsk: RKhD, 2001)
24. Hagena O F "Cluster beams from nozzle sources", in *Molecular Beams and Low Density Gasdynamics* (Gasdynamics, Vol. 4, Ed. P P Wegener) (New York: M. Dekker, 1974) p. 93
25. Morokhov I D et al. *Usp. Fiz. Nauk* **133** 653 (1981) [*Sov. Phys. Usp.* **24** 295 (1981)]
26. Miller R E *J. Phys. Chem.* **90** 3301 (1986)

27. Becker E W *Z. Phys. D* **3** 101 (1986)
28. Hagena O F *Z. Phys. D* **4** 291 (1987)
29. Miller D E "Free jet sources", in *Atomic and Molecular Beam Methods* Vol. 1 (Ed. G Scoles) (New York: Oxford Univ. Press, 1988) p. 14
30. Kappes M, Leutwyler S "Molecular beams of clusters", in *Atomic and Molecular Beam Methods* Vol. 1 (Ed. G Scoles) (New York: Oxford Univ. Press, 1988) p. 380
31. Huisken F *Adv. Chem. Phys.* **81** 63 (1992)
32. Smirnov B M *Usp. Fiz. Nauk* **162** (1) 119 (1992) [*Sov. Phys. Usp.* **35** 37 (1992)]
33. Miller R E "Infrared laser spectroscopy", in *Atomic and Molecular Beam Methods* Vol. 2 (Ed. G Scoles) (New York: Oxford Univ. Press, 1992) p. 192
34. Eletskiĭ A V, Smirnov B M *Usp. Fiz. Nauk* **163** (2) 33 (1993) [*Phys. Usp.* **36** 202 (1993)]
35. Buck U *J. Phys. Chem.* **98** 5190 (1994)
36. Buck U, in *Advances in Atomic, Molecular, and Optical Physics* Vol. 35 (Eds B Bederson, H Walther) (Amsterdam: Elsevier, 1995) p. 121
37. Eletskiĭ A V, Smirnov B M *Usp. Fiz. Nauk* **165** 977 (1995) [*Phys. Usp.* **38** 935 (1995)]
38. Alivisatos A P *J. Phys. Chem.* **100** 13226 (1996)
39. Bacic Z, Miller R E *J. Phys. Chem.* **100** 12945 (1996)
40. Castleman A W (Jr), Bowen K H (Jr) *J. Phys. Chem.* **100** 12911 (1996)
41. Gspann J, in *Large Clusters of Atoms and Molecules* (NATO ASI Ser., Ser. E, No. 313, Ed. T P Martin) (Dordrecht: Kluwer Acad. Publ., 1996)
42. Kohler B et al. *Adv. Chem. Phys.* **101** 83 (1997)
43. Eletskiĭ A V *Usp. Fiz. Nauk* **167** 945 (1997) [*Phys. Usp.* **40** 899 (1997)]
44. Smirnov B M *Usp. Fiz. Nauk* **167** 1169 (1997) [*Phys. Usp.* **40** 1117 (1997)]
45. Valbusa U "Molecular beams in high-energy physics: beam targets", in *Atomic and Molecular Beam Methods* Vol. 1 (Ed. G Scoles) (New York: Oxford Univ. Press, 1988) p. 438
46. Christen W, Even U *J. Phys. Chem. A* **102** 9420 (1998)
47. Herschbach D *Rev. Mod. Phys.* **71** S411 (1999)
48. Smalley R E *Rev. Mod. Phys.* **69** 723 (1998); *Usp. Fiz. Nauk* **168** 323 (1998)
49. Curl R F *Rev. Mod. Phys.* **69** 691 (1997); *Usp. Fiz. Nauk* **168** 331 (1998)
50. Kroto H W *Rev. Mod. Phys.* **69** 703 (1997); *Usp. Fiz. Nauk* **168** 343 (1998)
51. Eletskiĭ A V *Usp. Fiz. Nauk* **170** 113 (2000) [*Phys. Usp.* **43** 111 (2000)]
52. Rakov E G *Usp. Khim.* **69** 41 (2000) [*Russ. Chem. Rev.* **69** 35 (2000)]
53. Smirnov B M *Usp. Fiz. Nauk* **170** 495 (2000) [*Phys. Usp.* **43** 453 (2000)]
54. Kraĭnov V P, Smirnov M B *Usp. Fiz. Nauk* **170** 969 (2000) [*Phys. Usp.* **43** 901 (2000)]
55. Krainov V P, Smirnov M B *Phys. Rep.* **370** 237 (2002)
56. Smirnov B M *Usp. Fiz. Nauk* **173** 609 (2003) [*Phys. Usp.* **46** 589 (2003)]
57. Ditmire T et al. *Phys. Rev. A* **53** 3379 (1996)
58. Ditmire T et al. *Phys. Rev. A* **57** 369 (1998)
59. Zweiback J et al. *Phys. Plasmas* **9** 3108 (2002)
60. Eletskiĭ A V *Usp. Fiz. Nauk* **174** 1191 (2004) [*Phys. Usp.* **47** 1119 (2004)]
61. Kwon Y et al. *J. Chem. Phys.* **113** 6469 (2000)
62. Northby J A *J. Chem. Phys.* **115** 10065 (2001)
63. Callegari C et al. *J. Chem. Phys.* **115** 10090 (2001)
64. Stienkemeier F, Vilesov A F *J. Chem. Phys.* **115** 10119 (2001)
65. Toennies J P, Vilesov A F, Whaley K B *Phys. Today* **54** (2) 31 (2001)
66. Dalfovo F, Stringari S *J. Chem. Phys.* **115** 10078 (2001)
67. Dalfovo F et al. *Rev. Mod. Phys.* **71** 463 (1999)
68. Lugovoj E et al. "Spectroscopy of single molecules and clusters inside superfluid helium droplets", in *Atomic and Molecular Beams: the State of the Art 2000* (Ed. R Campargue) (Berlin: Springer, 2001) p. 755
69. Makarov G N *Usp. Fiz. Nauk* **174** 225 (2004) [*Phys. Usp.* **47** 217 (2004)]
70. Kapitza P L *Zh. Eksp. Teor. Fiz.* **11** 1, 581 (1941)
71. Pi M, Mayol R, Barranco M *Phys. Rev. Lett.* **82** 3093 (1999)
72. Pörtner N, Toennies J P, Vilesov A F *J. Chem. Phys.* **117** 6054 (2002)
73. Chin S A, Krotscheck E *Phys. Rev. B* **52** 10405 (1995)
74. Sindzingre P, Klein M L, Ceperley D M *Phys. Rev. Lett.* **63** 1601 (1989)
75. Casas M et al. *Z. Phys. D* **35** 67 (1995)
76. Rama Krishna M V, Whaley K B *J. Chem. Phys.* **93** 746 (1990)
77. Ditmire T et al. *Nature* **386** 54 (1997)
78. Last I, Jortner J *J. Phys. Chem. A* **102** 9655 (1998)
79. Springate E et al. *Phys. Rev. A* **61** 044101 (2000)
80. Auguste T et al. *J. Quant. Spectrosc. Radiat. Transf.* **71** 147 (2001)
81. Skobelev I Yu et al. *Zh. Eksp. Teor. Fiz.* **121** 88 (2002) [*JETP* **94** 73 (2002)]
82. Maltsev A, Ditmire T *Phys. Rev. Lett.* **90** 053002 (2003)
83. Parra E et al. *J. Opt. Soc. Am. B* **20** 118 (2003)
84. McPherson A et al. *Nature* **370** 631 (1994)
85. Dobosz S et al. *Phys. Rev. A* **56** R2526 (1997)
86. Ditmire T et al. *Appl. Phys. Lett.* **71** 166 (1997)
87. Stenz C et al. *Kvantovaya Elektron.* **30** 721 (2000) [*Quantum Electron.* **30** 721 (2000)]
88. Junkel-Vives G C et al. *J. Quant. Spectrosc. Radiat. Transf.* **71** 417 (2001)
89. Skobelev I Yu et al. *Zh. Eksp. Teor. Fiz.* **121** 1124 (2002) [*JETP* **94** 966 (2002)]
90. Magunov A I et al. *Laser Part. Beams* **21** 73 (2003)
91. Fukuda Y et al. *Pis'ma Zh. Eksp. Teor. Fiz.* **78** 146 (2003) [*JETP Lett.* **78** 115 (2003)]
92. Ivanova E P, Ivanov A L *Zh. Eksp. Teor. Fiz.* **127** 957 (2005) [*JETP* **100** 844 (2005)]
93. Ditmire T et al. *Nature* **398** 489 (1999)
94. Zweiback J et al. *Phys. Rev. Lett.* **84** 2634 (2000)
95. Zweiback J et al. *Phys. Rev. Lett.* **85** 3640 (2000)
96. Last I, Jortner J *J. Phys. Chem. A* **106** 10877 (2002)
97. Madison K W *J. Opt. Soc. Am. B* **20** 113 (2003)
98. Campbell E E B et al. *Phys. Rev. Lett.* **70** 263 (1993)
99. Campbell E E B et al. *CR Phys.* **3** 341 (2002)
100. Beuhler R J, Friedlander G, Friedman L *Phys. Rev. Lett.* **63** 1292 (1989)
101. Pool R *Science* **245** 1448 (1989)
102. Leonas V B *Usp. Fiz. Nauk* **160** (11) 135 (1990) [*Sov. Phys. Usp.* **33** 956 (1990)]
103. Beuhler R J et al. *J. Phys. Chem.* **94** 7665 (1990)
104. Beuhler R J et al. *Phys. Rev. Lett.* **67** 473 (1991)
105. Bae Y K, Lorents D C, Young S E *Phys. Rev. A* **44** R4091 (1991)
106. Vandenbosch R et al. *Phys. Rev. Lett.* **67** 3567 (1991)
107. Vandenbosch R et al. *Nucl. Instrum. Meth. B* **88** 116 (1994)
108. Fortov V E et al. *Int. J. Impact Eng.* **17** 323 (1995)
109. Velikodnyi V Yu, Bityurin V A *Teplofiz. Vys. Temp.* **41** 347 (2003) [*High Temp.* **41** 295 (2003)]
110. John P M St, Beck R D, Whetten R L *Phys. Rev. Lett.* **69** 1467 (1992)
111. Beauregard J N, Mayne H R *Surf. Sci. Lett.* **280** L253 (1993)
112. Beauregard J N, Mayne H R *J. Chem. Phys.* **99** 6667 (1993)
113. Mair C et al. *J. Chem. Phys.* **111** 2770 (1999)
114. Christen W, Even U *Eur. Phys. J. D* **9** 29 (1999)
115. Yasumatsu H et al. *J. Chem. Phys.* **105** 9509 (1996)
116. Yasumatsu H, Terasaki A, Kondow T *J. Chem. Phys.* **106** 3806 (1997)
117. Yasumatsu H et al. *Surf. Rev. Lett.* **3** 901 (1996)
118. Schek I et al. *Chem. Phys. Lett.* **257** 273 (1996)
119. Schek I et al. *J. Chem. Phys.* **101** 8596 (1994)
120. Raz T et al. *J. Chem. Phys.* **101** 8606 (1994)
121. Raz T, Levine R D *Chem. Phys. Lett.* **226** 47 (1994)
122. Raz T, Levine R D *J. Am. Chem. Soc.* **116** 11167 (1994)
123. Raz T, Levine R D *J. Phys. Chem.* **99** 13713 (1995)
124. Raz T, Levine R D *J. Phys. Chem.* **99** 7495 (1995)
125. Raz T, Levine R D *Chem. Phys. Lett.* **246** 405 (1995)
126. Gupta M, Walters E A, Blais N C *J. Chem. Phys.* **104** 100 (1996)
127. Qi L, Sinnott S B *J. Phys. Chem. B* **101** 6883 (1997)
128. Kornweitz H, Raz T, Levine R D *J. Phys. Chem. A* **103** 10179 (1999)
129. Nguyen T-N V et al. *J. Chem. Phys.* **119** 7451 (2003)
130. Takagi T, Yamada I, Sasaki A *J. Vac. Sci. Technol.* **12** 1128 (1975)
131. Yamada I, Usui H, Takagi T *J. Phys. Chem.* **91** 2463 (1987)
132. Yamada I, Inokawa H, Takagi T *J. Appl. Phys.* **56** 2746 (1984)
133. Takagi T et al. *Thin Solid Films* **126** 149 (1985)

134. Takaoka G H, Yamada I, Takagi T *J. Vac. Sci. Technol. A* **3** 2665 (1985)
135. Yamada I et al. *J. Vac. Sci. Technol. A* **4** 722 (1986)
136. Takagi T *Vacuum* **36** 27 (1986)
137. Usui H, Yamada I, Takagi T *J. Vac. Sci. Technol. A* **4** 52 (1986)
138. Takagi T *Pure Appl. Chem.* **60** 781 (1988)
139. Sosnowski M, Yamada I *Nucl. Instrum. Meth. B* **46** 397 (1990)
140. Huq S E, McMahon R A, Ahmed H *Semicond. Sci. Technol.* **5** 771 (1990)
141. Takaoka G H, Ishikawa J, Takagi T *J. Vac. Sci. Technol. A* **8** 840 (1990)
142. Yamada I, Takaoka G H *Jpn. J. Appl. Phys.* **32** 2121 (1993)
143. Cleveland C L, Landman U *Science* **257** 355 (1992)
144. Haberland H, Insepov Z, Moseler M *Phys. Rev. B* **51** 11061 (1995)
145. Kraft J et al. *Surf. Coat. Technol.* **158–159** 131 (2002)
146. Haberland H et al. *Surf. Rev. Lett.* **3** 887 (1996)
147. Haberland H et al. *Nucl. Instr. Meth. B* **80–81** 1320 (1993)
148. Haberland H et al. *J. Vac. Sci. Technol. A* **12** 2925 (1994)
149. Cheng H-P, Landman U *J. Phys. Chem.* **98** 3527 (1994)
150. Bromann K et al. *Surf. Sci.* **377–379** 1051 (1997)
151. Palmer R E, Pratontep S, Boyen H-G *Nature Mater.* **2** 443 (2003)
152. Fuchs G et al. *Phys. Rev. B* **44** 3926 (1991)
153. Mélinon P et al. *Int. J. Mod. Phys. B* **9** 339 (1995)
154. Perez A et al. *J. Phys. D*: *Appl. Phys.* **30** 709 (1997)
155. Mélinon P et al. *Phys. Rev. B* **58** 16481 (1998)
156. Mélinon P et al. *CR Phys.* **3** 273 (2002)
157. Mélinon P et al. *J. Chem. Phys.* **107** 10278 (1997)
158. Perez A et al. *Mater. Trans.* **42** 1460 (2001)
159. Gaudry M et al. *Phys. Rev. B* **67** 155409 (2003)
160. Jena P et al. *MRS Symp. Proc.* **206** 3 (1991)
161. Khanna S N, Jena P *Phys. Rev. Lett.* **69** 1664 (1992)
162. de Heer W A, Milani P, Chtelain A *Phys. Rev. Lett.* **65** 488 (1990)
163. Khanna S N, Linderoth S *Phys. Rev. Lett.* **67** 742 (1991)
164. Wiel R *Z. Phys D* **34** 47 (1993)
165. Harbich W, Fedrigo S, Buttet J *Chem. Phys. Lett.* **195** 613 (1992)
166. Harbich W et al. *J. Chem. Phys.* **96** 8104 (1992)
167. Jena P, Khanna S N, Rao B K *Surf. Rev. Lett.* **3** 993 (1996)
168. Rao B K, Khanna S N, Jena P *J. Cluster Sci.* **10** 477 (1999)
169. Haberland H et al. *J. Vac. Sci. Technol. A* **10** 3266 (1992)
170. Orloff J *Rev. Sci. Instrum.* **64** 1105 (1993)
171. Haberland H et al., in *Beam Processing of Advanced Materials*: *Proc. of the Second Intern. Conf., Cleveland, Ohio, USA, 1995* (Eds J Singh, J Mazumder, S M Copley) (Materials Park, OH: ASM Intern., 1996) p. 1
172. Gspann J, in *Physics and Chemistry of Finite Systems*: *From Clusters to Crystals* Vol. 2 (NATO ASI Ser., Ser. C, No. 374, Eds P Jena, S N Khanna, B K Rao) (Dordrecht: Kluwer Acad. Publ., 1992) p. 1115
173. Gspann J *Z. Phys. D* **20** 421 (1991)
174. Henkes P R W, Klingelhöfer R *J. Phys.* (Paris) **50** 159 (1989)
175. Henkes P R W, Klingelhöfer R *Vacuum* **39** 541 (1989)
176. Gspann J *Microelectron. Eng.* **27** 517 (1995)
177. Gspann J, in *Large Clusters of Atoms and Molecules* (NATO ASI Ser., Ser. E, No. 313, Ed. T P Martin) (Dordrecht: Kluwer Acad. Publ., 1996) p. 443
178. von Blanckenhagen P, Gruber A, Gspann J *Nucl. Instrum. Meth. B* **122** 322 (1997)
179. Gruber A, Gspann J *J. Vac. Sci. Technol. B* **15** 2362 (1997)
180. Gruber A, Gspann J, Hoffmann H *Appl. Phys. A* **68** 197 (1999)
181. Rattunde O et al. *J. Appl. Phys.* **90** 3226 (2001)
182. Bromann K et al. *Science* **274** 956 (1996)
183. Akizuki M et al. *Surf. Rev. Lett.* **3** 891 (1996)
184. Qiang Y et al. *Surf. Coat. Technol.* **100–101** 27 (1998)
185. Henkes P R W, Krevet B *J. Vac. Sci. Technol. A* **13** 2133 (1995)
186. Yamaguchi Y, Gspann J *Eur. Phys. J. D* **16** 103 (2001)
187. Yamaguchi Y, Gspann J, Inaba T *Eur. Phys. J. D* **24** 315 (2003)
188. Vostrikov A A, Dubov D Yu, Predtechenskii M R *Zh. Tekh. Fiz.* **56** 1393 (1986) [*Sov. Phys. Tech. Phys.* **31** 821 (1986)]
189. Vostrikov A A, Dubov D Yu, Predtechenskii M R *Zh. Tekh. Fiz.* **57** 760 (1987) [*Sov. Phys. Tech. Phys.* **32** 459 (1987)]
190. Vostrikov A A, Dubov D Yu, Predtechenskiy M R *Chem. Phys. Lett.* **139** 124 (1987)
191. Vostrikov A A, Dubov D Yu, Predtechenskii M R *Zh. Tekh. Fiz.* **58** 1897 (1988) [*Sov. Phys. Tech. Phys.* **33** 1153 (1988)]
192. Vostrikov A A, Dubov D Yu, Predtechenskii M R, in *Fizika Klasterov* (Cluster Physics) (Eds A A Vostrikov, A K Rebrov) (Novosibirsk: Nauka, 1987) p. 65
193. Vostrikov A A, Dubov D Yu *Z. Phys. D* **20** 61 (1991)
194. Vostrikov A A et al. *Z. Phys. D* **40** 542 (1997)
195. Gebhardt C R, Schröder H, Kompa K-L *Nature* **400** 544 (1999)
196. Andersson P U, Pettersson J B C *Z. Phys. D* **41** 57 (1997)
197. Andersson P U, Pettersson J B C *J. Phys. Chem. B* **102** 7428 (1998)
198. Even U et al. *Phys. Rev. Lett.* **56** 965 (1986)
199. De Lange P J, Renkema P J, Kommandeur J *J. Phys. Chem.* **92** 5749 (1988)
200. Yeretzian C, Hansen K, Whetten R L *Science* **260** 652 (1993)
201. Leisner T et al. *Z. Phys. D* **20** 127 (1991)
202. Amrein A, Simpson R, Hackett P *J. Chem. Phys.* **95** 1781 (1991)
203. Yeretzian C, Whetten R L *Z. Phys. D* **24** 199 (1992)
204. Campbell E E B, Ulmer G, Hertel I V *Phys. Rev. Lett.* **67** 1986 (1991)
205. John P M St, Whetten R L *Chem. Phys. Lett.* **196** 330 (1992)
206. John P M St, Yeretzian C, Whetten R L *J. Phys. Chem.* **96** 9100 (1992)
207. Hendell E, Even U *J. Chem. Phys.* **103** 9045 (1995)
208. Töglhofer K et al. *J. Chem. Phys.* **99** 8254 (1993)
209. Töglhofer K et al. *Nucl. Instrum. Meth. B* **88** 44 (1994)
210. Baudin K et al. *Nucl. Instrum. Meth. B* **117** 47 (1996)
211. Billebaud A et al. *Nucl. Instrum. Meth. B* **112** 79 (1996)
212. Aumayr F et al. *Int. J. Mass Spectr. Ion Proc.* **163** (3) 9L (1997)
213. Aumayr F et al. *Int. J. Mass Spectr. Ion Proc.* **174** 317 (1998)
214. Winter H P et al. *Phys. Rev. A* **56** 3007 (1997)
215. Fallavier M *Nucl. Instrum. Meth. B* **112** 72 (1996)
216. Hendell E et al. *Phys. Rev. Lett.* **75** 2670 (1995)
217. Christen W et al. *Int. J. Mass Spectr. Ion Proc.* **174** 35 (1998)
218. Christen W, Even U *Eur. Phys. J. D* **24** 283 (2003)
219. Farizon B et al. *Int. J. Mass Spectr. Ion Proc.* **164** 225 (1997)
220. Ehlich R, Westerburg M, Campbell E E B *J. Chem. Phys.* **104** 1900 (1996)
221. Ouaskit S et al. *Int. J. Mass Spectr. Ion Proc.* **139** 141 (1994)
222. LeBrun T et al. *Phys. Rev. Lett.* **72** 3965 (1994)
223. Farizon B et al. *Nucl. Instrum. Meth. B* **88** 86 (1994)
224. Hvelplund P et al. *Phys. Rev. Lett.* **69** 1915 (1992)
225. Mazuy B et al. *Nucl. Instrum. Meth. B* **28** 497 (1987)
226. Raz T, Even U, Levine R D *J. Chem. Phys.* **103** 5394 (1995)
227. Raz T, Levine R D *J. Chem. Phys.* **105** 8097 (1996)
228. Raz T, Levine R D *Chem. Phys.* **213** 263 (1996)
229. Lifshitz C, Louage F *J. Phys. Chem.* **93** 5633 (1989)
230. Wei S, Tzeng W B, Castleman A W (Jr) *J. Chem. Phys.* **92** 332 (1990)
231. Echt O et al. *J. Chem. Phys.* **82** 4076 (1985)
232. Wei S, Tzeng W B, Castleman A W (Jr) *J. Chem. Phys.* **93** 2506 (1990)
233. Beck R D et al. *Chem. Phys. Lett.* **187** 122 (1991)
234. Beck R D et al. *J. Phys. Chem.* **95** 8402 (1991)
235. Mowrey R C et al. *J. Phys. Chem.* **95** 7138 (1991)
236. Even U, Schek I, Jortner J *Chem. Phys. Lett.* **202** 303 (1993)
237. Schek I, Jortner J *J. Chem. Phys.* **104** 4337 (1996)
238. Gross A, Levine R D *J. Phys. Chem. A* **107** 9567 (2003)
239. Mandrich M L, Reents W D (Jr), Bondebey V E, in *Atomic and Molecular Clusters* (Ed. E R Bernstein) (Amsterdam: Elsevier, 1990)
240. de Heer W A *Rev. Mod. Phys.* **65** 611 (1993) p. 69
241. Haberland H, in *Clusters of Atoms and Molecules*: *Theory, Experiment, and Clusters of Atoms* (Springer Ser. in Chemical Physics, Vol. 52, Ed. H Haberland) (Heidelberg: Springer-Verlag, 1994) p. 207
242. Pauly H "High-energy beam sources", in *Atomic and Molecular Beam Methods* Vol. 1 (Ed. G Scoles) (New York: Oxford Univ. Press, 1988) p. 124
243. Sattler K, Mühlbach J, Recknagel E *Phys. Rev. Lett.* **45** 821 (1980)
244. Krätschmer W et al. *Nature* **347** 354 (1990)
245. Bergmann W et al. *Z. Phys. D* **3** 183 (1986)
246. Michalopoulos D L et al. *J. Phys. Chem.* **86** 3914 (1982)
247. Milani P, de Heer W A *Rev. Sci. Instrum.* **61** 1835 (1990)
248. Bhaskar N D et al. *Phys. Rev. B* **36** 4418 (1987)
249. Ehbrecht M et al. *Chem. Phys. Lett.* **214** 34 (1993)
250. Ehbrecht M, Huisken F *Phys. Rev. B* **59** 2975 (1999)

251. Aman C, Holmlid L *J. Phys. D: Appl. Phys.* **24** 1049 (1991)
252. Rutzen M et al. *Z. Phys. D* **38** 89 (1996)
253. Gough T E et al. *J. Chem. Phys.* **83** 4958 (1985)
254. Vach H *Phys. Rev. B* **59** 13413 (1999)
255. Vach H *J. Chem. Phys.* **111** 3536 (1999)
256. Thomas J M *Michael Faraday and the Royal Institution: the Genius of Man and Place* (Bristol: A. Hilger, 1991)
257. Aitken J *Collected Scientific Papers of John Aitken* (Ed. C G Knott) (Cambridge: The Univ. Press, 1923)
258. Wilson J G *The Principles of Cloud-Chamber Technique* (Cambridge: Univ. Press, 1951)
259. Kantrowitz A, Grey J *Rev. Sci. Instrum.* **22** 328 (1951)
260. Kistiakowsky G B, Slichter W P *Rev. Sci. Instrum.* **22** 333 (1951)
261. Becker E W, Bier K, Henkes W *Z. Phys.* **146** 333 (1956)
262. Oswatitsch K *Z. Angew. Math. Mech.* **22** 1 (1942)
263. Bentley P G *Nature* **190** 432 (1961)
264. Henkes W *Z. Naturforsch. A* **16** 842 (1961)
265. Hagena O F, Obert W *J. Chem. Phys.* **56** 1793 (1972)
266. Hagena O F *Surf. Sci.* **106** 101 (1981)
267. Hagena O F *Rev. Sci. Instrum.* **63** 2374 (1992)
268. Smirnov B M *Usp. Fiz. Nauk* **164** 665 (1994) [*Phys. Usp.* **37** 621 (1994)]
269. Wörmer J et al. *Chem. Phys. Lett.* **159** 321 (1989)
270. Farges J et al. *J. Chem. Phys.* **84** 3491 (1986)
271. Abraham O et al. *Phys. Fluids* **24** 1017 (1981)
272. Miller D R, Fineman M A, Murphy H R, in *Rarefied Gas Dynamics: 13th Intern. Symp., Novosibirsk, 1982* Vol. 2 (Eds O M Belotserkovskii et al.) (New York: Plenum Press, 1985) p. 923
273. Murphy H R, Miller D R *J. Phys. Chem.* **88** 4474 (1984)
274. Kappes M et al. *Z. Phys. D* **5** 359 (1987)
275. Schlag E W, Selzle H L *J. Chem. Soc., Faraday Trans.* **86** 2511 (1990)
276. Gough T E, Knight D G, Scoles G *Chem. Phys. Lett.* **97** 155 (1983)
277. Boesiger J, Leutwyler S *Z. Phys. Chem.* **154** 31 (1987)
278. Kappes M M, Kunz R W, Schumacher E *Chem. Phys. Lett.* **91** 413 (1982)
279. Dietz T G et al. *J. Chem. Phys.* **74** 6511 (1981)
280. Powers D E et al. *J. Phys. Chem.* **86** 2556 (1982)
281. Hopkins J B et al. *J. Chem. Phys.* **78** 1627 (1983)
282. Smalley R E *Laser Chem.* **2** 167 (1983)
283. Gole J L, English J H, Bondybey V E *J. Phys. Chem.* **86** 2560 (1982)
284. Rohlfing E A, Cox D M, Kaldor A *Chem. Phys. Lett.* **99** 161 (1983)
285. Richtsmeier S C et al. *J. Chem. Phys.* **82** 3659 (1985)
286. Kroto H W et al. *Nature* **318** 162 (1985)
287. Liu Y et al. *J. Chem. Phys.* **85** 7434 (1986)
288. Yang S H et al. *Chem. Phys. Lett.* **139** 233 (1987)
289. de Heer W A, Milani P, Chtelain A *Phys. Rev. Lett.* **63** 2834 (1989)
290. Heath J R et al. *J. Chem. Phys.* **83** 5520 (1985)
291. Pellarin M et al. *Chem. Phys. Lett.* **224** 338 (1994)
292. O'Brien S C et al. *J. Chem. Phys.* **84** 4074 (1986)
293. Zhang Q L et al. *J. Phys. Chem.* **90** 525 (1986)
294. Pellarin M et al. *Chem. Phys. Lett.* **277** 96 (1997)
295. Downer M C, Fork R L, Shank C V *J. Opt. Soc. Am. B* **2** 595 (1985)
296. Cox D M et al. *J. Phys. Chem.* **92** 421 (1988)
297. Brucat P J et al. *J. Chem. Phys.* **84** 3078 (1986)
298. Becker E W, Klingelhöfer R, Lohse P *Z. Naturforsch. A* **17** 432 (1962)
299. Bauchert J, Hagena O F *Z. Naturforsch. A* **20** 1135 (1965)
300. Henkes W *Z. Naturforsch. A* **17** 786 (1962)
301. Greene F T, Milne T A *J. Chem. Phys.* **39** 3150 (1963)
302. Hagena O F, Henkes P R W *Z. Naturforsch. A* **20** 1344 (1965)
303. Jortner J *Ber. Bunsen-Gesell. Phys. Chem.* **88** 188 (1984)
304. Muntz E P *Phys. Fluids* **5** 80 (1962)
305. Coe D et al., in *Rarefied Gas Dynamics: Proc. of the 11th Intern. Symp., Cannes, France, July 3–8, 1978* Vol. 2 (Ed. R Campargue) (Paris: Commissariat a l'Energie Atomique, 1979) p. 907
306. Levy D H, Wharton L, Smalley R E, in *Chemical and Biochemical Applications of Lasers* Vol. 11 (Ed. C B Moore) (New York: Academic Press, 1977) p. 1
307. Levy D H *Annu. Rev. Phys. Chem.* **31** 197 (1980)
308. Amirav A, Even U, Jortner J *Chem. Phys.* **51** 31 (1980)
309. Hefter U, Bergmann K "Spectroscopic detection methods", in *Atomic and Molecular Beam Methods* Vol. 2 (Ed. G Scoles) (New York: Oxford Univ. Press, 1992) p. 193
310. Holland R J et al. *J. Chem. Phys.* **88** 7952 (1988)
311. Messiah A *Quantum Mechanics* Vol. 2 (Amsterdam: Interscience Publ., 1962)
312. Kittel C *Introduction to Solid State Physics* 5th ed. (New York: Willey, 1976)
313. Farges J, Raoult B, Torchet G *J. Chem. Phys.* **59** 3454 (1973)
314. Farges J et al. *Surf. Sci.* **106** 95 (1981)
315. Kim S S, Stein G D *Rev. Sci. Instrum.* **53** 838 (1982)
316. Torchet G et al., in *The Chemical Physics of Atomic and Molecular Clusters* (Proc. of the Intern. School of Physics "Enrico Fermi", Course 107, Ed. G Scoles) (Amsterdam: North-Holland, 1990) p. 413
317. Kovalenko S I et al. *Fiz. Nizk. Temp.* **24** 481 (1998) [*Low Temp. Phys.* **24** 364 (1998)]
318. Lee J W, Stein G D *Surf. Sci.* **156** 112 (1985)
319. Lee J W, Stein G D *J. Phys. Chem.* **91** 2450 (1987)
320. Farges J et al. *J. Chem. Phys.* **78** 5067 (1983)
321. Torchet G, de Feraudy M-F, Loreaux Y *J. Mol. Struct.* **485–486** 261 (1999)
322. Stein G D, Wegener P P *J. Chem. Phys.* **46** 3685 (1967)
323. Newton R G *Scattering Theory of Waves and Particles* (New York: McGraw-Hill, 1966)
324. Kerker M *The Scattering of Light, and Other Electromagnetic Radiation* (New York: Academic Press, 1969)
325. Abraham O, Kim S-S, Stein G D *J. Chem. Phys.* **75** 402 (1981)
326. Ditmire T et al. *J. Phys. B: At. Mol. Opt. Phys.* **31** 2825 (1998)
327. Smith R A, Ditmire T, Tisch J W G *Rev. Sci. Instrum.* **69** 3798 (1998)
328. Karnbach R et al. *Rev. Sci. Instrum.* **64** 2838 (1993)
329. Buck U, Krohne R *J. Chem. Phys.* **105** 5408 (1996)
330. Lewerenz M, Schilling B, Toennies J P *Chem. Phys. Lett.* **206** 381 (1993)
331. Lewerenz M, Schilling B, Toennies J P *J. Chem. Phys.* **102** 8191 (1995)
332. Lokhman V N, Makarov G N *Chem. Phys. Lett.* **398** 453 (2004)
333. Lokhman V N, Makarov G N *Zh. Eksp. Teor. Fiz.* **127** 570 (2005) [*JETP* **100** 505 (2005)]
334. Gough T E, Miller R E, Scoles G *Appl. Phys. Lett.* **30** 338 (1977)
335. Gough T E, Miller R E, Scoles G *J. Mol. Spectrosc.* **72** 124 (1978)
336. Apatin V M et al. *Appl. Phys. B* **29** 273 (1982)
337. Apatin V M, Makarov G N *Zh. Eksp. Teor. Fiz.* **84** 15 (1983) [*Sov. Phys. JETP* **57** 8 (1983)]
338. Zen M "Accommodation, accumulation, and other detection methods", in *Atomic and Molecular Beam Methods* Vol. 1 (Ed. G Scoles) (New York: Oxford Univ. Press, 1988) p. 254
339. Ambartzumian R V et al. *Appl. Phys. B* **22** 409 (1980)
340. Makarov G N *Usp. Fiz. Nauk* **173** 913 (2003) [*Phys. Usp.* **46** 889 (2003)]
341. Makarov G N *Usp. Fiz. Nauk* **175** 41 (2005) [*Phys. Usp.* **48** 37 (2005)]
342. Becker E W, Klingelhofer R, Mayer H *Z. Naturforsch. A* **23** 274 (1968)
343. Becker E W, Gspann J, Krieg G *Entropie* **30** 59 (1969)
344. Krieg G, Doctoral Thesis (Karlsruhe, Germany: Univ. of Karlsruhe, 1970)
345. Gspann J, Krieg G, in *Rarefied Gas Dynamics* (Ed. C G Cercignani) (New York: Academic Press, 1972)
346. Mayer H, Doctoral Thesis (Karlsruhe, Germany: Univ. of Karlsruhe, 1972)
347. Gspann J, Krieg G *J. Chem. Phys.* **61** 4037 (1974)
348. Goodman F O *Surf. Sci.* **26** 327 (1971)
349. Smith J N (Jr) *Surf. Sci.* **34** 613 (1973)
350. Gspann J, Körting K *J. Chem. Phys.* **59** 4726 (1973)
351. Farges J et al. *Ber. Bunsen-Gesell. Phys. Chem.* **88** 211 (1984)
352. Farges J et al. *Surf. Sci.* **106** 95 (1981)
353. Xu G-Q, Bernasek S L, Tully J C *J. Chem. Phys.* **88** 3376 (1988)
354. Xu G-Q et al. *J. Chem. Phys.* **90** 3831 (1989)
355. Beauregard J N, Mayne H R *Chem. Phys. Lett.* **173** 189 (1990)
356. Gentry W R "Low-energy pulsed beam sources", in *Atomic and Molecular Beam Methods* Vol. 1 (Ed. G Scoles) (New York: Oxford Univ. Press, 1988) p. 54
357. Châtelet M et al. *Chem. Phys. Lett.* **196** 563 (1992)
358. Vach H et al. *J. Chem. Phys.* **100** 8526 (1994)
359. Vach H et al. *J. Chem. Phys.* **103** 1972 (1995)
360. De Martino A et al. *J. Chem. Phys.* **105** 7828 (1996)

361. Benslimane M et al. *Chem. Phys. Lett.* **237** 323 (1995)
362. Pradère F et al. *Rev. Sci. Instrum.* **65** 161 (1994)
363. Andersson P U et al. *Chem. Phys. Lett.* **279** 100 (1997)
364. Svanberg M, Marković N, Pettersson J B C *Chem. Phys.* **220** 137 (1997)
365. Marković N, Pettersson J B C *J. Chem. Phys.* **100** 3911 (1994)
366. Pettersson J B C, Marković N *Chem. Phys. Lett.* **201** 421 (1993)
367. Head-Gordon M et al. *J. Chem. Phys.* **94** 1516 (1991)
368. Tomsic A, Marković N, Pettersson J B C *Chem. Phys. Lett.* **329** 200 (2000)
369. Svanberg M, Marković N, Pettersson J B C *Chem. Phys.* **201** 473 (1995)
370. Tomsic A et al. *J. Chem. Phys.* **115** 10509 (2001)
371. Dreyfuss D, Wachman H Y *J. Chem. Phys.* **76** 2031 (1982)
372. Mironov S G et al. *Surf. Sci.* **106** 212 (1981)
373. Dreyfuss D, Wachman H Y, in *Rarefied Gas Dynamics, 12th Intern. Symp., Charlottesville, VA, USA, July 7 – 11, 1980, Technical Papers* Pt. 1 (Progress in Astronautics and Aeronautics, Vol. 74, Ed. S S Fisher) (New York: American Institute of Astronautics and Aeronautics, 1981) p. 183
374. Eisenberg D, Kauzmann W *The Structure and Properties of Water* (New York: Oxford Univ. Press, 1969)
375. Christen W et al. *Ber. Bunsen-Gesell. Phys. Chem.* **96** 1197 (1992)
376. Lee G H et al. *Z. Phys. D* **20** 9 (1991)
377. Nimlos M E, Ellison G B *J. Phys. Chem.* **90** 2574 (1986)
378. Tomsic A et al. *J. Chem. Phys.* **119** 4916 (2003)
379. Knight B, Goodall D M, Greenhow R C *J. Chem. Soc., Faraday Trans. 2* **75** 841 (1979)
380. Cheng H-P, Landman U *Science* **260** 1304 (1993)
381. Fort E et al. *Eur. Phys. J. D* **14** 71 (2001)
382. Fort E et al. *J. Chem. Phys.* **110** 2579 (1999)
383. Fort E et al. *Eur. Phys. J. D* **7** 229 (1999)
384. Baragiola R A *Nucl. Instrum. Meth. B* **88** 35 (1994)
385. Jacquet D, Le Beyec Y *Nucl. Instrum. Meth. B* **193** 227 (2002)
386. Abroyan I A, Eremeev M A, Petrov N N *Usp. Fiz. Nauk* **92** 105 (1967) [*Sov. Phys. Usp.* **10** 332 (1967)]
387. Arifov U F et al. *Zh. Tech. Fiz.* **43** (1) 184 (1973)
388. Hangstrum H D, in *Inelastic Ion-Surface Collisions* (Eds N H Tolk et al.) (New York: Academic Press, 1977)
389. Hofer W O, in *Sputtering by Particle Bombardment* Vol. 3 (Topics in Applied Physics, Vol. 64, Eds R Behrisch, K Witmaack) (Berlin: Springer-Verlag, 1991) p. 15
390. Baragiola R A et al. *Surf. Sci.* **90** 240 (1979)
391. Dvooght J et al., in *Particle Induced Electron Emission I* (Springer Tracts in Modern Physics, Vol. 122, Eds G Hohler, E A Niekisch) (Berlin: Springer-Verlag, 1991)
392. Yu M L, in *Sputtering by Particle Bombardment* Vol. 3 (Topics in Applied Physics, Vol. 64, Eds R Behrisch, K Witmaack) (Berlin: Springer-Verlag, 1991) p. 91
393. Hasselkamp D et al., in *Particle Induced Electron Emission II* (Springer Tracts in Modern Physics, Vol. 123, Ed. G Hohler) (Berlin: Springer-Verlag, 1992)
394. Baragiola R A *Nucl. Instrum. Meth. B* **78** 223 (1993)
395. Parilis E S, Kishinevskii L M *Fiz. Tverd. Tela* **61** 1219 (1961)
396. Rösler M et al., in *Particle Induced Electron Emission I* (Springer Tracts in Modern Physics, Vol. 122, Eds G Hohler, E A Niekisch) (Berlin: Springer-Verlag, 1991)
397. Kennedy E T *Phys. Scripta* **T95** 32 (2001)
398. Aumayr F, Winter H P *Comments At. Mol. Phys.* **29** 275 (1994)
399. Stock G *Chem. Phys. Lett.* **224** 131 (1994)
400. Robinson P J, Holbrook K A *Unimolecular Reactions* (London: Wiley-Interscience, 1972) [Translated into Russian (Moscow: Mir, 1975)]
401. Hagstrum H D *Phys. Rev.* **96** 325, 336 (1954)
402. Schou J *Phys. Rev. B* **22** 2141 (1980)
403. Hasselkamp D, in *Particle Induced Electron Emission II* (Springer Tracts in Modern Physics, Vol. 123, Ed. G Hohler) (Berlin: Springer-Verlag, 1992) p. 149
404. Lakits G, Aumayr F, Winter H *Rev. Sci. Instrum.* **60** 3151 (1989)
405. Töglhofer K, Aumayr F, Winter H *Surf. Sci.* **281** 143 (1993)
406. Eder H et al. *Rev. Sci. Instrum.* **68** 165 (1997)
407. Lakits G et al. *Phys. Rev. A* **42** 5780 (1990)
408. Kirson Z et al. *Surf. Sci.* **151** 531 (1985)
409. Levy D H, in *Photoselective Chemistry* Pt. 1 (Advances in Chemical Physics, Vol. 47, Eds J Jortner, R D Levine, S A Rice) (New York: Wiley, 1981)
410. Mints R I, Mil'man I I, Kryuk B I *Usp. Fiz. Nauk* **119** 749 (1976) [*Sov. Phys. Usp.* **19** 697 (1976)]
411. Herring C, Nichols M H *Rev. Mod. Phys.* **21** 185 (1949)
412. Wang L-S et al. *Chem. Phys. Lett.* **182** 5 (1991)
413. Foltin M et al. *J. Chem. Phys.* **98** 9624 (1993)
414. Leisner T et al. *Chem. Phys. Lett.* **148** 386 (1988)
415. Klots C E *J. Phys. Chem.* **92** 5864 (1988)
416. Landman U, Scharf D, Jortner J *Phys. Rev. Lett.* **54** 1860 (1985)
417. O'Brien S C et al. *J. Chem. Phys.* **88** 220 (1988)
418. Scheier P et al. *Phys. Rev. Lett.* **77** 2654 (1996)
419. Beck R D et al. *Chem. Phys. Lett.* **257** 557 (1996)
420. Beck R D et al. *J. Chem. Phys.* **104** 3638 (1996)
421. Amar F G, Perera L *Z. Phys. D* **20** 173 (1991)
422. Papanikolas J M, Maslen P E, Parson R *J. Chem. Phys.* **102** 2452 (1995)
423. Gerber R B, Amirav A *J. Phys. Chem.* **90** 4483 (1986)
424. Rettner C T, Michelsen H A, Auerbach D J *Chem. Phys.* **175** 157 (1993)
425. Rettner C T et al. *J. Phys. Chem.* **100** 13021 (1996)
426. Gross A et al. *Chem. Phys. Lett.* **354** 395 (2002)
427. Beuhler R, Friedman L *Chem. Rev.* **86** 521 (1986)
428. Hanley L (Ed.) "Polyatomic ion-surface interactions" *Int. J. Mass Spectr. Ion Proc.* **174** (1 – 3) (1998)
429. Even U et al. *Comments At. Mol. Phys.* (D1) 1 (1999)
430. *Focus* (June) 57 – 59 (1995)
431. Zel'dovich Ya B, Raizer Yu P *Fizika Udarnykh Voln i Vysokotemperaturnykh Gidrodinamicheskikh Yavlenii* (Physics of Shock Waves and High-Temperature Hydrodynamic Phenomena) (Moscow: Nauka, 1966) [Translated into English (Mineola, NY: Dover Publ., 2002)]
432. Ross M *J. Chem. Phys.* **71** 1567 (1979)
433. Landau L D, Lifshitz E M *Gidrodinamika* (Fluid Mechanics) (Moscow: Nauka, 1986) [Translated into English (Oxford: Pergamon Press, 1987)]
434. Eisenberg J M, Greiner W *Nuclear Theory* Vol. 1 *Nuclear Models* (Amsterdam: North-Holland, 1987)
435. Fleischmann M, Pons S *J. Electroanalyt. Chem.* **261** 301 (1989)
436. Jones S E et al. *Nature* **338** 737 (1989)
437. Koonin S E, Nauenberg M *Nature* **339** 690 (1989)
438. Leggett A J, Baym G *Phys. Rev. Lett.* **63** 191 (1989)
439. Arzhannikov A V, Kezerashvili G Ya, Kruglyakov É P *Usp. Fiz. Nauk* **169** 699 (1999) [*Phys. Usp.* **42** 615 (1999)]
440. Winterberg F *Z. Naturforsch. A* **19** 231 (1964)
441. Manzon B M *Usp. Fiz. Nauk* **134** 611 (1981) [*Sov. Phys. Usp.* **24** 662 (1981)]
442. Cecil F E, McNeil J A *Phys. Rev. Lett.* **64** 2210 (1990)
443. Amato I *Science* **254** 515 (1991)
444. Lo D H, Petrasso R D, Wenzel K W *Phys. Rev. Lett.* **68** 2107 (1992)
445. Amato I *Science* **256** 178 (1992)
446. Carraro C et al. *Phys. Rev. A* **42** 1379 (1990)
447. Shirokov Yu M, Yudin N P *Yadernaya Fizika* (Nuclear Physics) (Moscow: Nauka, 1980) [Translated into English (Moscow: Mir Publ., 1982)]
448. Fallavier M et al. *Phys. Rev. Lett.* **65** 621 (1990)
449. Fallavier M et al. *Phys. Rev. Lett.* **70** 1022 (1993)
450. Fallavier M et al. *Nucl. Instrum. Meth. B* **88** 122 (1994)
451. Echenique P M, Manson J R, Ritchie R H *Phys. Rev. Lett.* **64** 1413 (1990)
452. Beuhler R J, Friedlander G, Friedman L *Phys. Rev. Lett.* **68** 2108 (1992)
453. Shapiro M H, Tombrello T A *Phys. Rev. Lett.* **65** 92 (1990)
454. Vostrikov A A, Dubov D Yu, Agarkov A A *Pis'ma Zh. Eksp. Teor. Fiz.* **63** 915 (1996) [*JETP Lett.* **63** 963 (1996)]
455. Agarkov A A et al. *Eur. Phys. J. D* **9** 331 (1999)
456. Vostrikov A A, Dubov D Yu, Agarkov A A *Teplofiz. Vys. Temp.* **39** 26 (2001) [*High Temp.* **39** 22 (2001)]
457. Frenzel U et al. *Z. Phys. D* **40** 108 (1997)
458. Frenzel U, Roggenkamp A, Kreisle D *Chem. Phys. Lett.* **240** 109 (1995)

459. Smirnov B M *Usp. Fiz. Nauk* **163** (7) 51 (1993) [*Phys. Usp.* **36** 592 (1993)]
460. Luizova L A, Smirnov B M, Khakhaev A D *Dokl. Akad. Nauk SSSR* **309** 1359 (1989) [*Sov. Phys. Dokl.* **34** 1086 (1989)]
461. Luizova L A et al. *Teplofiz. Vys. Temp.* **28** 897 (1990) [*High Temp.* **28** 674 (1990)]
462. Faraday M *The Chemical History of a Candle* (New York: Crowell, 1957)
463. Weber B, Scholl R *J. Illum. Eng. Soc.* (Summer) 93 (1992)
464. Scholl R, in *Physics and Chemistry of Finite Systems*: *From Clusters to Crystals* Vol. 2 (NATO ASI Ser., Ser. C, No. 374, Eds P Jena, S N Khanna, B K Rao) (Dordrecht: Kluwer Acad. Publ., 1992) p. 1275
465. Weber B, Scholl R *J. Appl. Phys.* **74** 607 (1993)
466. Scholl R, Notour G, in *Phenomena in Ionized Gases* (AIP Conf. Proc., Vol. 363, Eds K H Becker, W E Carr, E E Kunhardt) (Woodbury, NY: AIP, 1996) p. 373
467. Bar-Ziv E, Weiss S *J. Chem. Phys.* **64** 2412 (1976)
468. Levine R D, Bernstein R B *Molecular Reaction Dynamics and Chemical Reactivity* (New York: Oxford Univ. Press, 1987)
469. Cho M-H et al. *J. Appl. Phys.* **85** 2909 (1999)
470. Huisken F, Kohn B, Paillard V *Appl. Phys. Lett.* **74** 3776 (1999)
471. Diederich L et al. *Appl. Phys. Lett.* **75** 2662 (1999)
472. Cich M et al. *Appl. Phys. Lett.* **73** 2116 (1998)
473. Gleiter H *Nanostruct. Mater.* **6** 3 (1995)
474. Perry M D, Mourou G *Science* **264** 917 (1994)
475. Kryukov P G *Kvantovaya Elektron.* **31** 95 (2001) [*Quantum Electron.* **31** 95 (2001)]
476. Shao Y L et al. *Phys. Rev. Lett.* **77** 3343 (1996)
477. Hansen J P, Sørevik T, Madsen L B *Phys. Rev. A* **68** 031401(R) (2003)
478. Smirnov M B et al. *Zh. Eksp. Teor. Fiz.* **125** 1283 (2004) [*JETP* **98** 1123 (2004)]
479. Norreys P A et al. *Plasma Phys. Control. Fusion* **40** 175 (1998)
480. Andreev A V, Gordienko V M, Savel'ev A B *Kvantovaya Elektron.* **31** 941 (2001) [*Quantum Electron.* **31** 941 (2001)]
481. Belyaev V S et al. *Zh. Eksp. Teor. Fiz.* **125** 1295 (2004) [*JETP* **98** 1133 (2004)]
482. Junkel-Vives G C et al. *Phys. Rev. A* **66** 033204 (2002)
483. Magunov A I et al. *Pis'ma Zh. Eksp. Teor. Fiz.* **74** 412 (2001) [*JETP Lett.* **74** 375 (2001)]
484. Chichkov B N et al. *Phys. Rev. A* **50** 2691 (1994)
485. Lezius M et al. *Phys. Rev. Lett.* **80** 261 (1998)
486. Hutchinson H *Science* **280** 693 (1998)
487. McPherson A et al. *Phys. Rev. Lett.* **72** 1810 (1994)
488. Ditmire T et al. *Phys. Rev. Lett.* **75** 3122 (1995)
489. Dobosz S et al. *Pis'ma Zh. Eksp. Teor. Fiz.* **68** 454 (1998) [*JETP Lett.* **68** 485 (1998)]
490. Skobelev I Yu et al. *Zh. Eksp. Teor. Fiz.* **121** 88 (2002) [*JETP* **94** 73 (2002)]
491. Wabnitz H et al. *Nature* **420** 482 (2002)
492. Kapteyn H C, Ditmire T *Nature* **420** 467 (2002)